DOCTORAL THESIS

Title	Development of mucus permeating nanoparticles-based drug delivery systems
Presented by	Sejin Oh
Centre	IQS School of Engineering
Department	Bioengineering
Directed by	Dr. Salvador Borrós Gómez

SIN PRISA, PERO SIN PAUSA

Slowly but surely

천천히 그러나 확실하게

Abstract

Mucus penetrating nanoparticle-based delivery systems of macromolecular drugs are currently receiving increasing attention in both academic and industrial research. Synthetic delivery systems provide highly suitable and tunable platform for the delivery of the macromolecules. However, a highly viscoelastic and adhesive mucus layer generally traps and rapidly removes most foreign substance from the mucosal surfaces, thereby limiting effectiveness of these nanocarriers. This Thesis is addressed to the development of engineering DNA delivery systems capable of high stability and transfection efficiency with low toxicity, and quickly crossing the mucus layer. Moreover, this Thesis is focused on design and development of methods and techniques in vitro in order to select more efficient delivery systems.

A simple and efficient method, based on the use of the quartz crystal microbalance with dissipation (QCM-D) technique, is developed and evaluated the interaction of the polymers and nanoparticles with the mucin layer, resulting in the development of nanoparticle-based delivery systems to mucosal tissue. This highly sensitive technique also offers to evaluate the two opposing properties, needed for the design of efficient mucous permeation systems: mucoadhesion vs mucus penetration.

Poly(β-amino ester)s (PBAEs) are currently considered of great interest as biodegradable polymeric carriers of DNA delivery, but they present limited stability in physiological conditions and the inability to penetrate the mucus layer. In this Thesis, we describe a novel surface-modified formulation of DNA delivery systems consisting of PBAE/DNA complexes and the coating agents, including: i) sugars (sucrose, trehalose or mannitol), ii) unmodified chitosan with a 22 kDa (CS) and a with a 60-120 kDa (CSM), iii) chitosan-thioglycolic acid (CS-TGA), and iv) poly(acrylic acid)-bromelain (PAA-BRO) conjugates. All novel formulations formed with different amounts of the coating agents are evaluated the physicochemical properties. The influence of coating agents on transfection efficiency and cytotoxicity is evaluated in COS-7 cells. Particle diffusion through porcine intestinal mucus (PImucus) is assessed by either rotating silicone tube technique or multiple particle tracking (MPT). The results highlight the superior stability, transfection efficiency and mucus permeability of the novel nanoparticle-based drug delivery systems. The effect of the amount of coating agents is also discussed.

Resumen

Existe un interés creciente, tanto en el mundo académico como en la investigación industrial en el desarrollo de sistemas de liberación de fármacos macromoleculares (proteínas, péptidos, oligonucleótidos) capaces de atravesar la mucosa. En este sentido, la utilización de vectores sintéticos para la liberación de dichas macromoléculas, permite disponer de una plataforma versátil y altamente eficiente. Sin embargo, la capa de mucosa con propiedades adhesivas y altamente viscoelástica, tiene una elevada capacidad de atrapar y eliminar cualquier sustancia extraña que quede adherida sobre su superficie, limitando, de forma evidente, la eficacia de cualquier tratamiento

Esta Tesis se centra en el desarrollo de sistemas de liberación de ADN, diseñados a medida, que presentan una elevada estabilidad y eficacia de transfección con un nivel muy bajo de toxicidad y muy importante en el contexto de la tesis, una capacidad de permeación a través de la mucosa. Además la tesis también se centra en el diseño y el desarrollo de métodos y técnicas in vitro que ayuden a una mejor selección de sistemas eficientes de liberación a través de la mucosa.

Así se ha desarrollado un método simple y eficiente, basado en la utilización de una microbalanza de cuarzo con disipación (QCM-D). Este método ha permitido evaluar la interacción de polímeros y nanopartículas con una capa de mucina. Los resultados obtenidos con el método desarrollado han permitido diseñar sistemas de nanopartículas con un mayor potencial de permeación a través de la mucosa. Esta técnica de alta sensibilidad también ha ofrecido la posibilidad de evaluar las dos propiedades opuestas, el conocimiento de las cuales es necesario para un correcto diseño de sistemas cpaços de cruzar la mucosa: mucoadhesió vs mucopenetració.

Los Poly (β-amino ester)s (PBAEs) se han propuesto como sistemas biodegradables capaces de formar nanopartículas, por complejación con ADN, que presentan una elevada capacidad de transfección. Sin embargo, muestran problemas de estabilidad en condiciones fisiológicas y son incapaces de atravesar la capa de mucosa. En esta tesis se describe una nueva solución en la preparación de las formulaciones de los nanocomplejos basada en la utilización de recubrimientos que estabilizan las nanopartículas y aumentan su permeabilidad. Los recubrimeintos propuestos inclutyen: i) azúcares (sucrosa, trhalosa y manitol), ii) quitosano sin modificar de 22 KDa y con 60-120 kDa, iii) quitosano modificado con ácido tioglicólico y iv) ácido poliacrílico-bromelaina. Todas las nuevas formulaciones se han evaluado con diferentes cantidades de recubrimiento. Se han determinado sus propiedades fisicoquímicas y su eficacia de

transcripción y citotoxicidad frente a células COS-7. Se ha estudiado La difusión de las partículas a través de la mucosa gástrica de cerdo utilizando diferentes técnicas como el tubo rotatorio de silicona o el múltiple particle tracking (MPT).

Los resultados obtenidos han mostrado superior estabilidad, eficacia de transfección y permeabilidad sobre la mucosa de las nuevas formulaciones diseñadas.

Resum

Existeix un interès creixent, tant en el món acadèmic com en la recerca industrial en el desenvolupament de sistemes d'alliberament de fàrmacs macromoleculars (proteïnes, pèptids, oligonucleotids) capaços de travessar la mucosa. En aquest sentit, la utilització de vectors sintètics per a l'alliberament de les esmentades macromolècules, permet disposar d'una plataforma versàtil i altament eficient. Tanmateix, la capa de mucosa amb propietats adhesives i altament viscoelàstica, té una elevada capacitat d'atrapar i eliminar qualsevol substància estranya que quedi adherida sobre la seva superfície, limitant, de forma evident, la eficàcia de qualsevol tractament

Aquesta Tesi es centra en el desenvolupament de sistemes d'alliberament de DNA, dissenyats a mida, que presenten una elevada estabilitat i eficàcia de transfecció amb un nivell molt baix de toxicitat i molt important en el context de la tesi, una capacitat de permeació a través de la mucosa. A més la tesi també es centra en el disseny i el desenvolupament de mètodes i tècniques in vitro que ajudin a una millor selecció de sistemes eficients d'alliberament a través de la mucosa.

Així s'ha desenvolupat un mètode simple i eficient, basat en la utilització de una microbalança de quartz amb dissipació (QCM-D). Aquest mètode ha permès avaluar la interacció de polímers i nanopartícules amb una capa de mucina. Els resultats obtinguts amb el mètode desenvolupat han permés dissenyar sistemes de nanopartícules amb un potencial més gran de permeació a través de la mucosa. Aquesta tècnica d'alta sensibilitat també ha ofert la possibilitat d'avaluar las dos propietats oposades, el coneixement de les quals és necessari per un correcte disseny de sistemes cpaços de creuar la mucosa: mucoadhesió vs mucopenetració.

Los Poly(β-amino ester)s (PBAEs) s'han proposat com a sistemes biodegradables capaços de formar nanopartícules, per complexació amb DNA, que presenten una elevada capacitat de transfecció. Tanmateix, mostren problemes d'estabilitat en condicions fisiològiques i són incapaços de travessar la capa de mucosa. En aquesta tesi es descriu una nova solució en la preparació de les formulacions dels nanocomplejos basada en la utilització de recobriments que estabilitzen les nanopartícules i augmenten la seva permeabilitat. Els recubrimeintos proposats inclutyen: i) sucres (sucroses, trhalosa i manitol), ii) quitosà sense modificar de 22 KDa i amb 60-120 kDa, iii) quitosan modificat amb àcid tioglicolidoi i iv) acid poliacrílic-bromelaina. Totes les noves formulacions s'han avaluat amb diferents quantitat de recobriment. S'han determinat les seves propietats fisicoquímiques i la seva eficàcia de transfecció i citotoxicitat en front de cèl.lules COS-7.

S'ha estudiat La difusió de las partícules a través de la mucosa gàstrica de porc utilitzant diferents tècniques com el tub rotatori de silicona o el *multiple particle tracking* (MPT).

Els resultats obtinguts han mostrat la superior estabilitat, eficàcia de transfecció i permeabilitat sobre la mucosa de las noves formulacions dissenyades.

Table of Contents

Glossary

BRO	Bromelain
COS-7	African green monkey kidney fibroblast cell line
CS	Chitosan with a 22 kDa
CSM	Chitosan with a 60-120 kDa
CPGM	Commercially available porcine gastric mucin
CT	Chitosan-thioglycolic acid
CV track	Cervicovaginal track
D	Dissipation
DLS	Dynamic light scattering
DMSO	Dimethyl sulfoxide
EDAC	Ethyl(dimethylaminopropyl)carbodiimide
EDTA	Ethylenediaminetetraacetic acid
f	Frequency
FBS	Fetal bovine serum
GI track	Gastrointestinal track
HA	Hyaluronic acid
HA-SH	Thiolated hyaluronic acid
^{1}H-NMR	Proton nuclear magnetic resonance
m	Mass
Mnt	Mannitol
MTS	3-(4,5-dimethylthiazol-2-yl)-5-3-carboxymethoxyphenyl)-2-(4-sulfophynyl)-2H-tetrazolium
NaAc	Sodium Acetate
NHS	N-hydroxysuccinimide
NPGM	Native porcine gastric mucin
PAA	Poly(acrylic acid)
PAH	Poly(allylamine hydrochloride)
PBS	Phosphate-buffered saline
PBAEs	Poly(β-amino ester)s
PEG	Polyethylene glycol
PEI	Polyethylenimine
pGFP	Green fluorescent protein plasmid
PGM	Porcine gastric mucin
PLL	Poly(L-lysine)
QCM-D	Quartz crystal microbalance with dissipation
R	Arginine-terminated poly(β-amino ester)s
rhDNase	Recombinant human DNase

RT	Room temperature
SIF	Simulated intestinal fluid without pancreatin
Suc	Sucrose
TAE	Tris-acetate-EDTA
TC	Thiolated chitosan
TCL	Thiolated chitosan with low content of free thiol groups
TCM	Thiolated chitosan with medium content of free thiol groups
TCH	Thiolated chitosan with high content of free thiol groups
TGA	Thioglycolic acid
Tre	Trehalose

AIM AND OUTLINE OF THIS THESIS

Introduction

The development of engineering nanoparticles-based delivery systems for macromolecular drugs, such as peptides, proteins and nucleic acids (DNA and RNA), to mucosal tissue has attracted increasing interest. Drug delivery technologies have been extensively investigated, in the last few decades, for improvement of therapeutic efficacy. It is well defined that drug delivery systems must possess a number of desirable features for therapy, including: i) sustained and controlled release of drugs locally (Langer 1998; Farokhad and Langer 2006), ii) deep tissue penetration due to the nanomeric size (Dawson *et al.*, 2003 and 2004; Prego *et al.*, 2005; Mackay *et al.*, 2005), iii) cellular uptake and sub-cellular trafficking (Medina-Kauwe *et al.*, 2005; Lai *et al.*, 2007), iv) protection of cargo therapeutics from degradation and removal in the mucus (Allemann *et al.*, 1998; Panyam and Labhasetwar *et al.*, 2003) and v) penetration through the mucus barrier, which has been a key for achieving therapeutic efficacy in target tissue or cells (Lai *et al.*, 2009).

Mucosal membranes cover natural body cavities such as the eye, gastrointestinal (GI) track, lung airway, nasal/pharyngeal region, and female reproductive track. Besides, it servers many functions in those locations, among which are lubrication for the passage of objects, maintenance of a hydrated layer over the epithelium, a barrier to foreign substances (Allen 1981; Neutra and Forstner 1987). In the GI track, for example, the majority of administered particles does not adhere or transport through the mucus layer, but undergo direct transit through the GI track (Galindo-Rodriguez *et al.*, 2005). Thus, research has largely focused on minimizing the fraction of therapeutics undergoing direct transit and fecal elimination by improving their association to mucus.

According to this consideration, the concept of mucoadhesion, as a new strategy for drug delivery systems, was introduced by the pioneering work of several research groups in pharmaceutical technology in the early 1980 (Nagai 1985; Peppas and Buri 1985). Since then the use of mucoadhesive polymers was considered in drug delivery applications due to their ability to prolong residence time of the drug at mucosal surface, thus increasing drug absorption (Maggi *et al.*, 1994; Mortazavi and Samrt 1994; Caramella *et al.*, 1994). Later, it was discovered that some mucoadhesive polymers, such as polyacrylic acid and chitosan, possess multifunctional properties, and can modulate the permeability of the epithelial tissues by partially opening the tight junctions (Borchard *et al.*, 1996; Schipper *et al.*, 1997). In addition, these systems can also adhere to specific sites of the body leading to greater bioavailability (Peppas *et al.*, 2000; Ahn *et al.*, 2002; Chowdary and Srinivasa 2004). The ability of mucoadhesion depends on the structure of mucosal membranes, the properties of mucus gels, and the physicochemical properties of mucoadhesive polymers (Boddupalli *et al.*, 2010; Shaikh *et al.*, 2011). One of the most popular mucoadhesive polymers is a poly(acrylic acid) (Rowe *et al.*, 2006). Mechanisms of

mucoadhesion are largely attributed to a combination of H-bonding and molecular entanglements of this polymer with mucus glycoproteins (Park and Robinson 1985). Additionally, the cationic polymer chitosan has a well-known mucoadhesive nature (Sogias *et al.*, 2008; Bravo-Osuna *et al.*, 2014), by the establishment of electrostatic interactions between their primary amino groups and sialic acid/sulfonic acid groups of the mucus (Gaserod *et al.*, 1998). Moreover, it was demonstrated that chitosan can enhance the absorption of hydrophilic molecules by promoting a structural reorganisation of the tight junction-associated proteins (Jung *et al.*, 2000). However, current mucoadhesive polymers provide only a weak adhesion for the localization of delivery systems to mucosal tissue, thus still required to enhance mucoadhesion.

Fortunately, these mucoadhesive polymers can be improved by modifying their chemical structure. In the late 1990s, Bernkop-Schnürch and coworkers firstly proposed the concept of thiolated polymers, designated as thiomers, showing the potential of mucoadhesion through chemical modification (Bernkop-Schnürch *et al.*, 1999). They proposed the use of thiol groups in polymers to increase mucoadhesion. They showed that polycarbophil-cystein conjugates exhibited high mucoadhesion due to the formation of covalent bonds with cysteine-rich domains of glycoproteins in the mucus layer (Kast *et al.*, 2003). These covalent bonds are supposedly stronger than non-covalent bonds such as ionic interactions. To date, numerous thiomers have been developed, e.g. chitosan-thioglycolic acid conjugates, and applied for the novel mucoadhesive drug delivery systems as drug carriers capable of prolonging residence time of drug in body via effective adhesion to the mucus layer (Bernkop-Schnürch 2005; Andrew *et al.*, 2009; Serra *et al.*, 2009).

In spite of their advantages described above, the mucoadhesive drug delivery systems have limitations. The critical shortcoming of the mucoadhesive systems is that their transit time is limited to the physiological turnover rate of the mucus layer (Galindo-Rodriguez *et al.*, 2005). In other words, these systems are trapped in mucus layers via steric or adhesive forces, and then rapidly eliminated by mucus clearance mechanisms over time scale that ranges from seconds in the eyes (Greaves and Wilson 1993) to a few hours in the GI track, lung airways and female reproductive tract (Lehr *et al.*, 1991; Kieweg *et al.*, 2004; Galindo-Rodriguez *et al.*, 2005; Ali and Pearson 2007). Furthermore, mucoadhesive systems are fully immobilized in the luminal mucus gel are therefore unable to penetrate the mucus layer and reach the underlying epithelia. Thus, mucoadhesive systems are inefficient for applications that require intracellular delivery of drugs for gene therapy and/or sustained drug release over longer duration than the time scale of mucus renewal (Lai *et al.*, 2009). To overcome this issue, the concept of mucus-penetrating nanoparticles technology capable of overcoming the mucus barrier was pioneered, and there has been designed and developed the novel drug delivery systems using this technique (Scheme 1.1) (Lai *et al.*, 2009; Hanes 2009).
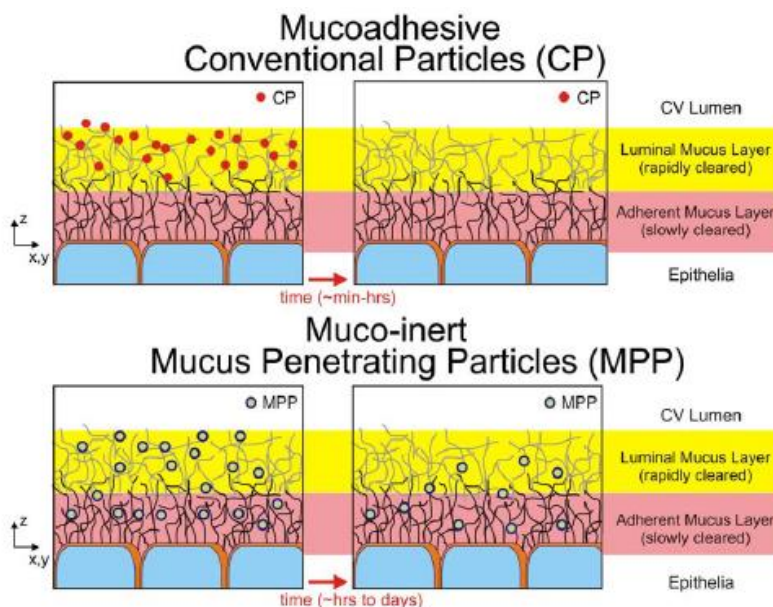
Scheme 1.1. Schematic illustration of the fate of mucus-penetrating particles (MPP) and conventional (mucoadhesive) particles (CP) administered to a mucosal surface. MPP readily penetrate the luminal mucus layer (LML) and enter the underlying adherent mucus layer (AML). In contrast, CP are largely immobilized in the LML. Because MPP can enter the AML and thus are in closer proximity to the cells, cells will be exposed to a greater dose of drug released from MPP compared to drug released from CP. As the LML layer is cleared, CP are removed along with the LML whereas MPP are retained in the AML, leading to prolonged residence time for MPP at the mucosal surface. Thus, at long times, there is almost no drug dosing to cells with CP, whereas MPP, because they are retained longer, will continue to release drug to cells. Since MPP can penetrate both the LML and AML, a fraction may reach and bind to the underlying epithelia and thus further improve drug delivery (Lai *et al.*, 2009).

It should be noted that Hanes and coworkers proposed the effectiveness of nanoparticles for drug delivery to mucosal sites that relies on the ability of these particles to cross mucosal barrier (Hanes *et al.*, 2004). The primary component of mucus is high molecular weight mucin glycoproteins exhibiting cysteine-rich subunits, which are connected with each other via disulfide bonds (Scheme 1.2) (Cone 2008). This stable three-dimensional network (the so-called adherent mucus layer) forms a thick layer on surfaces, ranging from 0.05 µm in ocular surface to 640 µm in the large intestine (Khanvilkar *et al.*, 2001; Strugala *et al.*, 2003; Bansil and Turner 2006), and gives rise to a highly viscoelastic gel, which significantly impedes the transport rates of nanoparticles for drug delivery (Sanders *et al.*, 2000; Olmsted *et al.*, 2001). The work by Knowles and Boucher supported that most foreign particles, including many benificial drugs, were traped by mucus via steric or adhesive forces and rapidly removed via mucus clearance (Knowles and Boucher 2002). Accordingly, the nanoparticles must be suitable adhesive, small (nanomeric) and smooth enough for mucosal drug delivery systems. In order to achieve the desired nanoparticles characteristics, the combination of both mucosadhesive and mucus penetrating properties of delivery systems

has been required. Since then, considerable attention has been focused on the development of both type of novel nanoparticle delivery systems that can transport through the mucus layer, based on using the several different strategies (e.g. size-dependent and surface change, surface-modification, mucolytic agents, etc) as described below. Thus, it has been a main challenge to develop and optimize the strategies for the novel drug delivery systems to mucosal tissue.
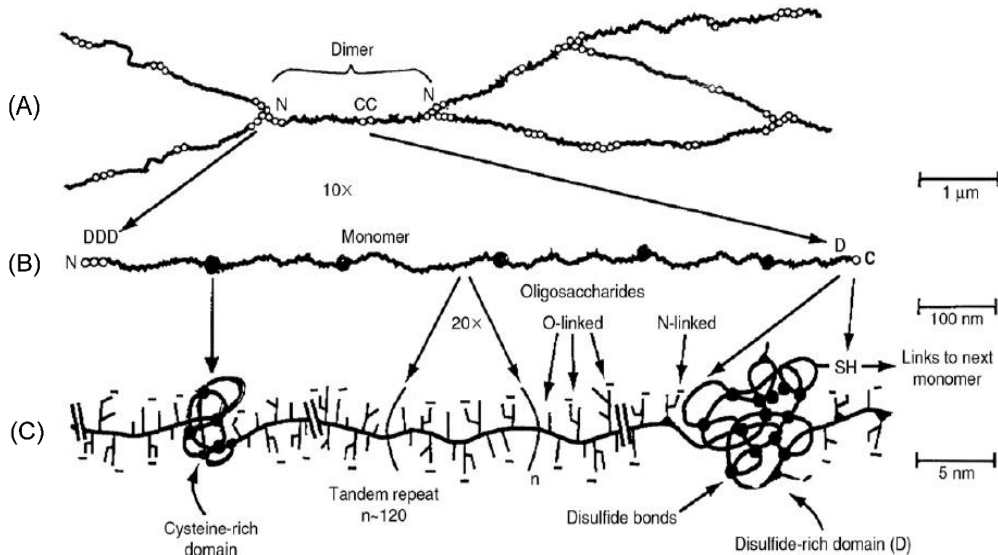
Scheme 1.2. Major biochemical features of gel-forming mucins. (A) Mucin monomers are cross-linked end-to-end via disulfide bonds between disulfide-rich domains (labeled "D") near the amino- and carboxyl-termini. (B) Interspersed along each fiber are "naked" globular protein regions, with small exposed hydrophobic patches, stabilized by multiple disulfide bonds. (C) Individual mucin fibers are densely glycosylated with *O*- and *N*-linked glycans, most of which are negatively charged with sialic acids or sulfate groups (Cone 2009).

According to this issue, there is a growing appreciation that an understanding of fundamental interaction of nanoscale objects with biological barriers will play a central role in nanomedicine (Lundqvist *et al.*, 2008). Due to the special biological role, mucus significantly limits the drug delivery across biological barriers (Lopez-Vidriero 1989). To gain insight into particle transport mechanisms through mucus, it was focused on understanding the physicochemical properties (i.e. size and surface charge) that govern the rapid transport of specific viruses, which have evolved over thousands of years to infect mucosal tissues (Cone 1999). It was demonstrated the size dependent diffusion of macromolecules (proteins) and particulate systems (viruses) through the mucus gel layer. The study suggested that small molecules diffuse rapidly through mucus barrier, while large molecules become trapped due to steric hindrance (Cone 1999; Sanders *et al.*, 2000; Olmsted *et al.*, 2001). For example, small

viruses up to 55 nm showed to diffuse in mucus as rapidly as in water, while a larger virus, 180 nm herpes simplex virus, was nearly completely inhibited, proposing that the mucus mesh spacing is approximately 20-180 nm. On the other hand, Dowson et al. demonstrated that that neutrally charged hydrophobic particles, regardless of surface chemistry (COOH or PEG), with 200- and 500- nm in size moved faster in mucus than anionic but otherwise similar particles, suggesting charge may be an important parameter in governing transport rates of nanoparticles in mucus (Dawson *et al.*, 2003 and 2004).

Later, Lai and colleagues found that large nanoparticles, 200 and 500 nm in diameter, if properly coated, can transport much more rapidly than 100 nm nanoparticles in physiological human cervicovaginal track (CV) mucus (Lai *et al.*, 2007). The faster transport of the large particles is contrary to the expectation described above that smaller particle should move faster in mucus as well as mucus mesh spacing. These results suggested that the coating modification may be an important factor for mucus penetration. This finding strongly encouraged the commercial development of new nanoparticle-based drug delivery systems for the CV track and potentially other mucosal surfaces, because drug delivery kinetic and loading efficiency are vastly improved as particle size increases. In parallel, Lai et al. have developed the mucus-penetrating particles technology by mimicking the essential surface properties of viruses that allow them to avoid mucoadhesion, resulting in great promise in mucosal drug delivery (Lai *et al.*, 2009). According to a hypothesis first proposed by Cone et al., they suggested that an equal density of positive and negative charges, a net neutral surface, may facilitate efficient mucus transport by allowing the viruses to avoid electrostatic adhesive interactions.

Last but not least, understanding the biochemical basis of the viscoelastic properties of mucus, which can be manipulated by mucolytic agents, has important consequences to the development and selection of potential therapeutic strategies (Lai *et al.*, 2009). Mucolytic agents currently used clinically to reduce mucus viscosity and increase mucociliary clearance rates may be important adjuvants to delivery for macromolecular drugs (Mrsny *et al.*, 1996; Ferrari *et al.*, 2001; Dawson *et al.*, 2003; Decramen *et al.*, 2005). For example, cystic fibrosis patients often need to inhale specific mucolytic for enzymatic cleavage of mucus constituents to facilitate mucus clearance from lungs by coughing. Commonly used mucolytic agents are recombinant human DNase (rhDNase) (Shak *et al.*, 1990; Ulmer *et al.*, 1996) and N-acetylcysteine (NAC) (Henke *et al.*, 2007). Recently, Suk and coworkers reported that the gene carriers with NAC or NAC + rhDNase transfer genes more effectively into the cells (Suk *et al.*, 2011). Yet, there has been no cure to date, a challenge widely attributed to inefficient mucosal delivery for biopharmaceutics. In the case of mucosal delivery of DNA-based drugs in particular, the development of the strategies allowing delivery systems to cross the mucus layer and consequently be taken up by epithelial cell will certainly lead to improvement in non-viral gene therapy (EU-project FP7). The surface-modification technique has been generally

applied as non-viral vectors for gene therapy. Especially, the surface-modification of delivery vehicles with polyethylene glycol (PEG), or PEGylation, has shown promise as a method to improve the stability and in vivo performance of various delivery systems for macromolecular drugs (Sanders *et al.*, 2002; Ogris *et al.*, 2003; Lenter *et al.*, 2004; Mishra *et al.*, 2004; Pun *et al.*, 2004; Sun *et al.*, 2005; Zahr *et al.*, 2005). In addition, the surface-modification technique has been shown to enhance particle transport through mucus (Suh *et al.*, 2007; Lai *et al.*, 2007; Tang *et al.*, 2009; Cu *et al.*, 2009; Boylan *et al.*, 2011; Ensign *et al.*, 2012; Suk *et al.*, 2014; Mastorakos *et al.*, 2015). Nevertheless, gene therapy has by far not reached its full potential owing to the lack of enabling delivery technologies. Thus, it will be a great challenge to develop and optimize the novel technologies for delivery systems of biopharmaceutics to mucosal tissue. These novel delivery systems must be evaluated by precise and accurate methods and techniques in vitro in order to select the best mucosal delivery systems for in vivo test. Therefore, the design and development of methods and techniques will be a promising approach to achieve the challenge described above.

Aim and scope of this Thesis

A main objective of this Thesis is to develop and optimize a nanotechnology-based strategy for solving the major limitation of crossing the mucus layer and thus enabling the efficient delivery of macromolecules, especially DNA-based drugs. Additionally, it is aimed to develop an in vitro method utilizing a quartz crystal microbalance with dissipation (QCM-D) technique in order to evaluate the interaction between the novel nanoparticulate drug delivery systems and mucins, thus allowing for selecting the best candidates for in vivo testing. The aims of this Thesis are briefly described below:

- To establish and develop a QCM-D method as an in vitro model with mucins.

- To compare and evaluate two sources of mucin; native porcine gastric mucin (NPGM) vs commercially available porcine gastric mucin (CPGM).

- To evaluate the interaction between mucoadhesive polymers and NPGM

- To assess the interaction of mucoadhesive and mucus penetrating nanoparticles with NPGM

- To prepare and characterize the polymers or conjugates described as follows: oligopeptide-terminated poly(β-amino ester)s (PBAEs), the mixtures of PBAE with trehalose (TreR), sucrose (SucR) and mannitol (MntR), chitosan-thioglycolic acid (CS-TGA) and poly(acrylic acid)-bromelain (PAA-BRO) conjugates.

- To investigate the effect of experimental conditions such as ionic strength of medium, incubation time and temperature on stability and transfection efficiency of the conventional PBAE/DNA complexes nanoparticles.

- To develop and optimize a novel surface-modified formulation of PBAE/DNA nanoparticles with coating agents (e.g. Tre, Suc, Mnt, chitosan (CS), CS-TGA and PAA-BRO)

- To evaluate the physicochemical properties (e.g. size, surface charge and agarose gel electrophoretic mobility).

- To investigate the influence of coating on stability, transfection efficiency and cytotoxicity of all the testing nanoparticles.

- To study the effect of the coating agents, especially CS-TGA and PAA-BRO, on mucus penetration.

Structure of the Thesis

This Thesis consists of four Chapters followed by a summary of the conclusions drawn from the whole work.

Chapter 1 is a general introduction of the Thesis which includes its aims and organization.

Chapter 2 describes the development of an efficient and simple method, based on the use of quartz crystal microbalance with dissipation, to evaluate the mucoadhesive characteristics of mucoadhesive polymers as well as the permeability of thiolated chitosan-based complexes into the mucin layer. This technique allows an initial screening of the novel nanocarriers to select the best efficient drug delivery systems.

Chapter 3 presents a novel gene delivery system with enhanced stability and transfection efficiency. Trehalose, sucrose, mannitol, and chitosan are employed as modification agents to prepare the novel carrier by two different strategies using surface modification technique consisting in coating and blending. For example, sugar was added after-the so-called coating- or before-the so-called blending- the polymerization of poly(β-amino ester)s.

In Chapter 4, it is focused on a simple surface-modified formulation of functionalized nanocarriers capable of permeating the mucus gel layer and efficient gene delivery with low toxicity. Biodegradable poly(β-amino ester)s/DNA are prepared with either thiolated chitosan or poly(acrylic acid)-bromelain conjugates, which are employed as disulfide breaking agents or mucolytic agents, respectively.

References

Ahn, J.S.; Choi, H.K.; Chun, M.K.; Ryu, J.M.; Jung, J.H.; Kim, Y.U.; Cho, C.S. *Biomaterials* **2002**, *23,* 1411-1416.

Ali, M.S.; Pearson, J.P. *Laryngoscope* **2007**, *117*, 932–938.

Allemann, E.; Leroux, J.C.; Gurny, R. *Adv. Drug Deliv. Rev.* **1998**, *34*, 171–189.

Allen A. *Structure and function of gastrointestinal mucus*. In: *Physiology of the gastroenterology tract*, 1st edn. New York, NY: Raven Press; **1981**. p. 617– 639.

Andrew, G.P.; Laverty, T.P.; Jones, D.S. *Eur. J. Pharm. Biopharm.* **2009**, *71*, 505-518.

Bansil, R.; Turner, B.S. *Curr. Opin. Colloid. Interface Sci.* **2006**, *11*, 164-170.

Bernkop-Schnürch, A.; Schwarz, A.; Steininger, S. *Pharm. Res.* **1999**, *16*, 876–881.

Bernkop-Schnürch, A. *Drug Discov.Today: Technol.* **2005**, *2*, 83–87.

Bernkop-Schnürch, A. *Adv. Drug Deliv. Rev.* **2005**, *57*, 1569-1585.

Boddupalli, B.M.; Mohammed, Z.N.; Nath, R.A.; Banji, D. *J. Adv. Pharm. Technol. Res.* **2010**,*1,* 381–387.

Borchard, G.; Luessen, H.L.; deBoer, A.G.; Verhoef, *I.C;,* Lehr, C.M.; Junginger, H.E. *J. Control Release* **1996**, *39*, 131-138.

Bravo-Osuna, I.; Vauthier, C.; Farabollini, A.; Palmieri, G.F.; Ponchel, G. *Biomaterials* **2007**, *28*, 2233-2243.

Breunig, M.; Bauer, S.; Goepferich, A. *Eur. J. Pharm. Biopharm.* **2008**, *68*, 112–128.

Caramella, C.; Bonferoni, MC.; Rossi, S.; Ferrari, F. *Eur J. Pharm. Biopharm.* **1994**, *40,* 213–217.

Chowdary, K.P.R.; Srinivasa, Y. *Biol. Pharm. Bull.* **2004**, 27, 1717–1724.

Cone, R.A. *Mucus. In Mucosal Immunology*; 2nd edn; Orga PL, edn. Academic Press:San Diego, **1999**; 43–64.

Cone, R.A. *Adv. Drug Deliv. Rev.* **2009,** *61*, 75–85.

Cu, Y.; Saltzman, W.M. *Mol. Pharm.* **2009**, *6*, 173–181.

Dawson, M.; Wirtz, D.; Hanes, J. *J. Biol. Chem.* **2003**, *278*, 50393–50401.

Dawson, M.; Krauland, E.; Wirtz, D.; Hanes, J. *Biotechnol. Prog.* **2004**, *20*, 851–857.

Ehrhardt, C.; Fiegel, J.; Fuchs, S.; Abu-Dahab, R.; Schaefer, U.F.; Hanes, J.; Lehr, C.M. *J. Aerosol. Med.* **2002**, *15*, 131-139.

Ensign, L.M.; Cone, R.; Hanes, J. *Adv. Drug Deliv. Rev.* **2012**, *64*, 557-570.

Ensign, L.M.; Tang, B.C.; Wang, Y.Y.; Tse, T.A.; Hoen, T.; Cone, R.; Hanes, *J. Sci. Transl. Med.* **2012**, *4,* 138ra79.

Farokhzad, O.C.; Langer, R. *Adv. Drug Deliv. Rev.* **2006**, *58*, 1456–1459.

Ferrari, S.; Kitson, C.; Farley, R.; Steel, R.; Marriott, C.; Parkins, D.A.; Scarpa, M.; Wainwright, B.; Evans, M.J.; Colledge, W.H.; Geddes, D.M.; Alton, E.W. *Gene Ther.* **2001**, *8*, 1380–1386

Galindo-Rodriguez, S.A.; Allemann, E.; Fessi, H.; Doelker, E. *Crit. Rev. Ther. Drug Carr. Syst.* **2005**, *22*, 419–464.

Garcia-Contreras, L.; Hickey, A.J. *Adv. Drug Deliv. Rev.* **2002**, *54,*1491–1504.

Gaserod, O.; Jolliffe, I.G.; Hampson, F.C.; Dettmar, P.W.; Skjak-Braek, G. *Int. J. Pharm.* **1998**,*175*, 237–246

Greaves, J.L.; Wilson, .CG. *Adv. Drug Deliv. Rev.* **1993**, *11*, 349–383.

Hanes, J.; Dawson, M.; Har-el, Y.; Suh, J.; Fiegel, J. *Gene therapy in the lung*. In *Pharmaceutical Inhalation Aerosol Technology*, 2nd edn.; Marcel Dekker Inc.: New York, **2004**, pp 489-539.

Hanes, R. . *Adv. Drug Deliv. Rev.***2009**, *61*, 73-74.

Heller, J. Hoffman, A.S. *Drug delivery systems*. In: *Biomaterials science*, 2nd edn. San Diego, California: Elsevier Academic Press; **2004**. pp. 639.

Henke, M.O.; Ratjen, F. *Paediatr. Respir. Rev.* **2007**, *8*, 24–29.

Jung, T.; Kamm, W.; Breitenbach, A.; Kaiserling, E.; Xiao, J.X.; Kissel, T. *Eur. J. Pharm. Biopharm.* **2000**, *50*,147–60.

Kieweg, S.L.; Geonnotti, A.R.; Katz, D.F. *J. Pharm. Sci.* **2004**, *93*, 2941–2952.

Kast, C.E.; Guggi, D.; Langoth, N.; Bernkop-Schnürch, A. *Pharm. Res.***2003**, *20*, 931–936.

Khanvilkar, K.; Donovan, M. D.; Flanagan, D. R. *Adv. Drug Deliv. Rev.* **2001**, *48*, 173-193.

Kim, A.J.; Boylan, N.J.; Suk, J.S.; Hwangbo, M.; Yu, T.; Schuster, B.S.; et al. *Angew. Chem. Int. Ed.* **2013**, 52, 3985–3988.

Knowles, M.R.; Boucher, R.C. *J. Clin. Invest.* **2002**,*109*, 571–577.

Lai, S.K.; O'Hanlon, D.E.; Harrold, S.; Man, S.T.; Wang, Y.Y.; Cone, R.; Hanes, J. *Proc. Natl. Acad. Sci. U.S.A.* 2**007**, *104*, 1482-1487.

Lai, S.K.; Hida, K.; Man, S.T.; Chen, C.; Machamer, C.; Schroer, T.A.; Hanes, J. *Biomaterials* **2007**, *28*, 2876-2884.

Lai, S.K.; Wang, Y.Y.; Wirtz, D.; Hanes, J. *Adv. Drug Deliv. Rev.* **2009**, *61*, 86–100.

Lai, S.K.; Wang, Y.Y.; Hanes, J. *Adv. Drug Deliv. Rev.* **2009**, *61,* 158–171.

Lai, S.K.; Wang, Cone, R.; Wirtz, D.; Hanes, J. *PloS. ONE.* **2009**; *4*, e4294.

Langer, R. *Nature* **1998**, *392*, 5–10.

Leitner, V.M.; Walker, G.F.; Bernkop-Schnu¨rch, A. *Eur. J. Pharm. Biopharm*. **2003**, *56*, 207–214.

Lehr, C.M.; Bouwstra, J.A.; Kok, W. *et al. Pharm. Res.* **1992**, *9*, 547–553.

MacKay, J.A.; Deen, D.F.; Szoka, J.F.C. *Brain Res.* **2005,** *1035*, 139–153.
Maggi, L.; Carena, E.; Torre, M.L.; Giunchedi, P.; Conte, U. *STP Pharma. Sci.* **1994**, *4*, 343–348.

Mastorakos, P.; de Silva, A.L.; Chisholm, J.; Song, E.; Choi, W.K.; Boyle, M.P.; Morales, M.M.; Hanes, J.; Suk, J.S. *PANS* **2015**, *112*, 8720-8725.

Mrsny, R.; Daugherty, A.; Short, S.; Widmer, R.; Siegel, M.; Keller, G. *J. Drug Target.* **1996**, *4*, 233–243

Medina-Kauwe, L.K.; Xie, J.; Hamm-Alvarez, S. *Gene Ther.* **2005**, *12*, 1734–1751.

Mortazavi, S.A.; Smart, J.D. *J. Control Release* 1**994**, *31*, 207–212.

Nagai, T. *J. Control Release* **1985**, *2*, 121-34
Nance, E.A.; Woodworth, G.F.; Sailor, K.A.; Shih, T.Y.; Xu, Q.; Swaminathan, G.; Xiang, D.;

Eberhart, C.; Hanes, J. *Sci. Transl. Med.* **2012**, *4*, 149ra19.

Neutra, M.; Forstner, J. *Gastrointestinal mucus: synthesis, secretion, and function*. In: Johnson, L., editor. *Physiology of the gastrointestinal tract*, 2nd edn. New York, NY Raven Press; **1987**. Chapter 34.

Lundqvist, M.; Stigler, J.; Elia, G.; Lynch, I.; Cedervall, T.; Dawson, K.A. *Proc. Natl. Acad. Sci. U.S.A.* **2008**, *105*, 14265–14270.

Lopez-Vidriero, M.T. *Respiration* **1989**, *55*, 28-32.

Olmsted, S.S.; Padgett, J.L.; Yudin, A.I.; Whaley, K.J.; Moench, T.R. et al. *Biophys. J.* **2001**, *81*, 1930-1937.

Ozturk, E.; Eroqlu, M.; Ozdemir, N.; Denkbas, E.B. *Adv. Exp. Med. Biol.* **2004**, *553*, 231-242.

Panyam, J.; Labhasetwar,. V. *Drug Deliv. Rev.* **2003**, *55*, 329–347.

Peppas, N.A.; Buri. P.; *J. Control Release* **1985**, *2*, 257-275.

Peppas, N.A.; Little, M.D.; Huang, Y. *Bioadhesive controlled release systems* in: Wise, D.L.; Brannon-Peppas, L.; Klibanov, A.M.; Langer, R.L.; Mikos, A.G.; Peppas, N.A.; Trantolo, D.J.; Wnek, G.E.; Yaszemski, M.J. (Eds.), *Handbook of Pharmaceutical Controlled Release Technology*, Dekker, New York, **2000**, pp. 255–269.

Park, H., and Robinson, J. *J. Controlled Release* **1985**, *2*, 47–57.

Prego, C.; Garcia, M.; Torres, D.; Alonso, M.J. *J. Control. Release* **2005**, 101, 151–162

Rowe, R.C.; Sheskey, P.J.; Owen, S. Handbook of Pharmaceutical Excipients, 5th edn., The Pharmaceutical Press and the American Pharmacists Association, London, UK, **2006**.

Sanders, N.N.; De Smedt, S.C.; Rompaey, E.; Simoens, P.; de Baets, F. et al. *Am. J. Respir. Crit. Care Med.* **2000**, *162*, 1905-1911.

Seisenberger, G.; Ried, M.U.; Endress, T.; Buning, H.; Hallek, M.; Brauchle, C. *Science* **2001**, *294*, 1929–1932.

Serra, L.; Doménech, J.; Peppas, N.A. *Eur. J. Pharm. Biopharm.* **2009**, *71*, 519–528.

Schipper, N.G.M.; Olsson, S.; Hoogstraate, J.A.; de Boer, A.G.; Varum, K.M.; Artursson, P. *Pharm. Res.* **1997**, *14*, 923-929.

Shaikh, R.; Raj, T.R.; Garland, M.J.; Woolfson, A.D.; Donnelly, R.F. *J. Pharm. Bioallied. Sci.* **2011**, *3*, 89-100.

Shak, S.; Capon, D.J.; Hellmiss, R.; Marsters, S.A.; Baker, C.L. *Proc. Natl. Acad. Sci.* **1990**, *87*, 9188–9192.

Sogias, I.A.; Williams, A.C.; Khutoryanskiy, V.V. *Biomacromolecules* **2008**, *9*, 1837–1842.

Strugala, V.; Allen, A.; Dettmar, PW.; Pearson, J.P. *Proc. Nutr. Soc.* **2003**, *62,:*237–243.

Suk JS, Boylan, N.; Trehan, K.; Tang, B.C.; Schneider, C.S.; Lin, J.M.; Boyle, M.P.; Zeitlin, P.L.; Lai, S.K. Cooper, M.J.; Hanes, J. *Mol. Ther.* **2011**, *19*, 1981–1989.

Suk, J.S.; Lai, S.K.; Boylan, N.J.; Dawson, M.R.; Boyle, M.P.; Hanes, J. *Nanomedicine (Lond)* **2011**, *6*, 365–375.

Suh, J.; Wirtz, D.; Hanes, J. *Proc. Natl. Acad. Sci. U.S.A.* **2003,** *100*, 3878–3882.

Tang, B.C.; Dawson, M.D.; Lai, S.K.; Wang, Y.Y.; Suk, J.S.; Yang, M.; Zeitlin, P.; Boyle, M.P.; Fu, J.; Hanes, J. *PNAS* **2009,** *160*, 19268-19273.

Ulmer, J.S.; Herzka, A.; Toy, K.J.; Baker, D.L.; Dodge, A.H.; Sinicropi, D.; Shak, S.; Lazarus, R.A. *Proc. Natl. Acad. Sci.* **1996**, *93*, 8225–8229

Welsher, K.; Yang, H. *Nat. Nanotechnol.* **2014**, *9*, 198–203.

DEVELOPMENT OF A QCM-D TECHNIQUE FOR STUDING THE INTERACTIONS OF POLYMERS/PARTICLES WITH MUCIN

2.1.   Introduction

As explained earlier, the development of the mucosal drug delivery systems has been of great interest as drug carriers capable of adhering and rapidly penetrating through the mucus layer. The recent advanced in techniques for nanoparticle diffusional kinetics through the mucus have resulted in this development of the novel delivery systems for biopharmaceutics. In this Chapter, therefore, the utilizing of a quartz crystal microbalance with dissipation (QCM-D) technique for evaluating the interaction of nanoparticles with mucin is highlighted.

As mentioned in the previous Chapter, mucus plays a key role of the defence mechanism from nanoparticulate drug delivery systems because it covers and protects the body by lubricating, trapping and removing foreign particles. Thus, it is important to note the properties of mucus that need to be overcome in mucosal drug delivery application. The ability of mucus to function as an effective lubricant and selective diffusional barrier is critically dependent on adherent mucus layer and the biochemical interactions between mucus constituents, including mainly of water (up to 95% weight) lipids, inorganic salts, and glycoproteins called mucins (Allen *et al.*, 1981; Cone 1999; Thornton and Sheehan 2004). In particular, mucins are the most important components determining viscoelastic gel-like properties of mucus. Mucins consist of large macromolecular monomers with a protein backbone with one or more heavily glycosylated domains, rich in serine and threonine residues which serve as anchoring points for the oligosaccharide side chains (Bansil and Turner, 2006; Cone *et al.*, 2009). The oligosaccharide chains have sugar residues such as galactose, fructose, N-acetylglucosamine, N-acetylgalactosamine and sialic acid. At pH > 3, both sialic acid and sulphated sugars are fully ionized and this confers a net negative charge to the molecules (Marriott and Gregory 1990). Due to their importance the relevance for mucoadhesion and mucus permeability, interaction of mucins has been considerably studied to a variety of surfaces and by applying different techniques (Svensson and Arnebrant 2010). Therefore, it will be a great challenge to design and develop methods and techniques in vitro in order to evaluate the interaction between the polymers or nanoparticles and mucin. A profound knowledge about methods and techniques allowing a precise and accurate evaluation of interactions between particles and mucin/mucus is consequently substantial for the design and development of more efficient drug delivery systems (Grießinger *et al.*, 2015). Regarding this issue, different methods and techniques including, QCM-D, multiple particle tracking (MPT), transwell diffusion system, and rotating silicone tube technique are utilized by various research groups to assess the behaviour of drug delivery systems in the mucus.

In this Chapter, we have focused and developed a simple and efficient method, based on the use of the QCM-D monitoring, to elucidate the relationship of polymers or particles with mucin/mucus. The results will be further compared with those obtained by different methods

and techniques described above, and they may help to better understand and select promising drug delivery systems in vitro screening. Moreover, the developed QCM-D method could give insight on the mechanisms of two opposing properties of mucoadhesion and mucus penetration of the engineering nanoparticles.
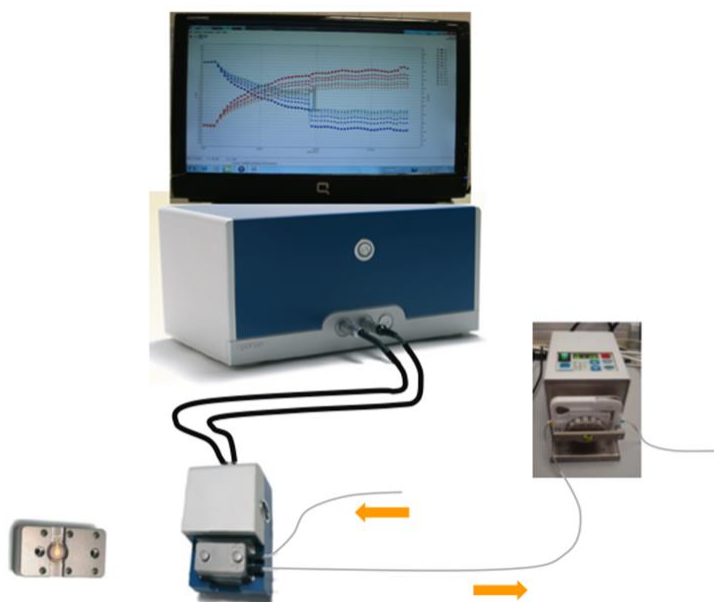
Scheme 2.1. Scheme of the QCM-D instrument and the different part used in the protocol described in detail 2.3.4

The QCM-D is a high sensitive and versatile instrument for real-time study of the dynamic behaviors of a layer on the crystal surface (O'Sullivan and Guilbault, 1999; Marx *et al.*, 2003; Halthur *et al.*, 2010). QCM-D technique provides information of both the mass and structural changes occurring to the layer by simultaneous measurements of the frequency (*f*) and dissipation factor (*D*) (Scheme. 2.1) (Rodahl *et al.*, 1996; Hook *et al.*, 1998; Lu *et al.*, 2013; Barrantes *et al.*, 2014). From these changes it is possible to calculate the mass/thickness of the adsorbed layer and also its viscoelastic properties (Rodahl *et al.*, 1997; Voinova *et al.*, 2002; Molino *et al.*, 2006; Xu *et al.*, 2013). Therefore, QCM-D is a powerful technique to evaluate interactions or reaction on various surfaces.

This technique can be adapted to study the interaction of polymers and nanoparticles with mucin. In detail, the QCM-D instrument is able to measure two things.

First, the variation in quartz crystal resonance frequency (Δf), which is related with the mass uptake and release at the sensor surface, can be measured. There are different approaches both for rigid (Sauerbrey equation) and flexible films to correlate the variation in *f*

with the mass change (Rodahl *et al.*, 1995). Thus, the instrument can be calibrated for calculating the mass absorbed on the sensor. Changes in mass on the quartz surface related to changes in f of the oscillating crystal according to the Sauerbrey relation (equation 2.1) (Rodahl *et al.*, 1995). The constant C represents the mass sensitivity (17.7 ng/cm·Hz for a 5 MHz sensor). The Sauerbrey relation is valid for rigid.

$$\Delta m = -C \cdot \Delta f \qquad\qquad\qquad\qquad \text{(equation 2.1)}$$

Secondly, the energy dissipation (ΔD), which is related with the structure and viscoelasticity of the non-rigid or viscoelastic film like mucins, can be determined. Briefly, QCM-D measures the dissipation of energy by the system, which is the part of accumulated energy lost at each oscillation, after switching off the exciting electric field (Fredriksson *et al.*, 1998; Voinova *et al.*, 1999 and 2002). *D* is defined as:

$$D = E_{Dissipated}2\pi E_{stored} \qquad\qquad\qquad \text{(equation 2.2)}$$

When the film is rigid, the oscillation decays very slowly. When the viscoelasticity of the film increases (for instance in a hydrogel water absorption) the decay is much faster (Scheme 2.2).
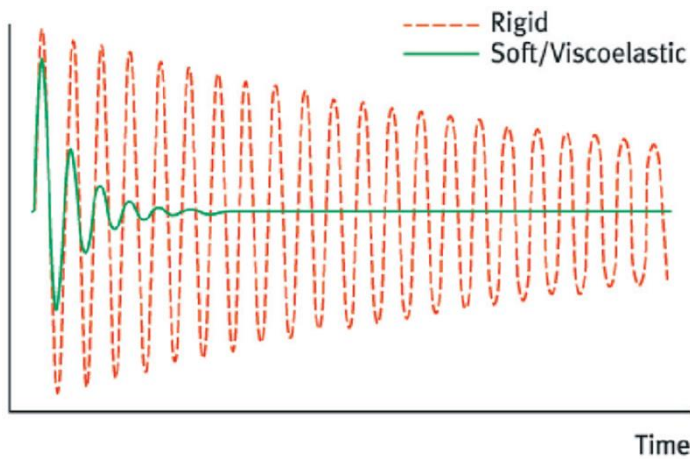
Scheme 2.2. Scheme of the different dissipation signal generated by a rigid (red) and soft (green) molecular layer on the sensor crystal (adopted from Q-Sense basic training 2006).

Moreover, sequential multi-frequency measurement (the frequencies corresponding to the harmonic frequencies of the crystal) is carried out in order to record the different overtones of the oscillating system. It is important to point out that each overtone has a specific penetration depth, and they are measuring the behaviour at different depths of the attached film (Lens *et al.*, 2003). The sensor´s overtones have higher *f*, so the penetration depth

(sensitivity range) will be smaller as shown in Scheme 2.3. This means that, as measurements are at different depths of the deposited film, they can be used to record the film response in several points at the same time. It is the maximum recording distance. For a 5 MHz crystal in water, the maximum penetration depth is is δ ≈ 250 nm. This characteristic may offer how the polymers and the nanoparticles interact with the mucin film. If the samples are adsorbed on the mucin film surface, the overtones response would be similar. However, a penetration that affects the whole mucin would lead to different overtones behaviour.
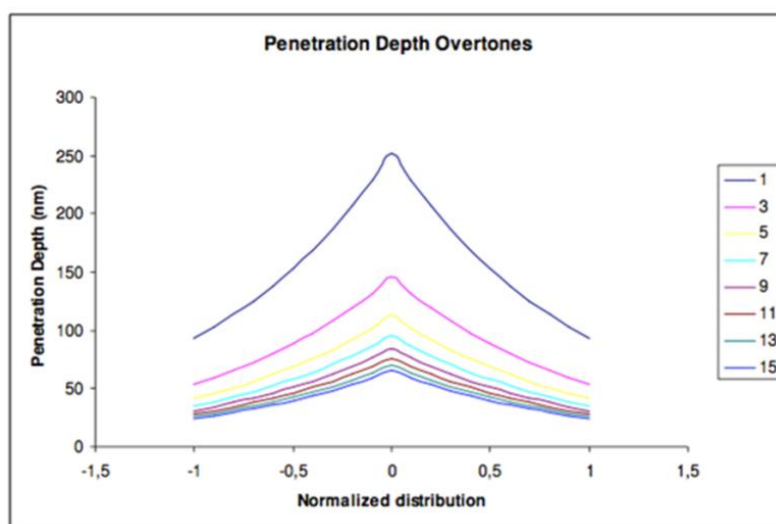
Scheme 2.3. Scheme of viscous penetration depth as function of overtone (adapted from Q-Sense basic training 2006).

There are numerous publications that illustrated the interaction, especially adsorption, of particles with mucin using QCM-D. However, so far, no studies evaluating the permeation of particles through the mucin layer has been conducted. According to their interrelationship, it should be noted that the particles, when interact with the mucin, modify its viscoelasticity, resulting in that the monitoring of changes in *D* with behavior of overtones gives insights about the nature of this interaction.

Chayed and Winnik studied the interaction between mucin (bovine submaxillary mucin, a sigma preparation that is unlikely to be native) and mucoadhesive polymers-based nanoparticles by means of QCM-D, and demonstrated that QCM-D was a promising technique for studying the mucoadhesive properties (Chayed and Winnik 2007). Sandberg et al. reported that adsorption of porcine gastric mucin (PGM) was proven a useful route for the biomaterials of highly surface-passivating mucin coating, suggesting that pre-adsorbed mucins could provide favorable support for adsorbing host components (Sandber *et al.*, 2008).

Later, Pedersen et al. showed QCM-D can be used as a screening method of biodurability of toxic nanoparticles (Pedersen *et al.*, 2009). They suggested that the interaction of nanoparticles with PGM could be a good model to understand the impact of nanoparticles in the body. Recently, it was reported that the interrelation for the mucoadhesive mechanism using QCM-D is affected by the complexation between particles and mucin. As a result, QCM-D technique may be useful for analysing the behaviour of the drug carriers into the mucin layer (Mazzarino *et al.*, 2013). It should be stated that, as far as we know, all the experiments described in literature have been carried out using commercially available porcine gastric mucin (CPGM), and no comparison with mucins with different origins has been reported yet.

Commercially available porcine gastric mucin (CPGM) has been widely used for mucus-relevant investigation because it is simple and inexpensive to purchase. However, Kocevar-Nared *et al.* (Kocervar-Nared *et al.*, 1997) compared the rheological properties of CPGM obtained from Sigma Aldrich (Type II) and isolated native porcine gastric mucus. It was demonstrated that the usage of rehydrated CPGM for the preparation of *in vitro* membranes is limited because CPGM is isolated after enzymatic hydrolysis treatment that can affect its primary structure. After this study, several groups have reported the differences in the gel behaviour (rheology) within native gastric mucus and mucin (NPGM) (Pearson *et al.*, 2000; Taylor *et al.*, 2004, 2005). Here we evaluate how the differences in structure can affect the ability of the different mucins to interact with the described mucoadhesive polymers. Thereafter, we will evaluate the interaction of polymers and particles with the NPGM.

2.2.   Aim and scope of this Chapter

The first objective of this Chapter is to develop an *in vitro* method, based on the use of the QCM-D technique, to evaluate the mucoadhesive properties of cationic polymers; chitosan, thiolated chitosan (TC), and poly(allylamine hydrochloride) (PAH), and anionic polymers; hyaluronic acid (HA) and thiolated hyaluronic acid (HA-SH). Positively charged chitosan polymer forms polyelectrolyte complexes with negative charged mucins, whereas negatively charged HA polymers have mucoadhesive properties due to hydrogen bonding with the mucus layer. Both chitosan and HA exhibit excellent mucoadhesive properties (Ludwig, 2005; Andrew *et al.*, 2009; Woertz *et al.*, 2013). Recently, it has been shown that polymers with thiol groups provide much higher adhesive properties (Kast and Bernkop-Schnürch 2001; Grabovac *et al.*, 2005; Wang *et al.*, 2012), resulting from covalent bonds with cysteine-rich subdomains of mucins, than polymers generally considered to be mucoadhesive. PAH composed of a large number of primary amine groups and can also improve mucoadhesion (Thomson *et al.*, 2009) via electrostatic interactions between negative charges on the mucin

and positively charged amino groups on the polymer.

Here, two types of mucin have been used: native porcine gastric mucin (NPGM) and commercially available porcine gastric mucin (CPGM). We will compare the mechanism of the interaction between polymers and either NPGM or CPGM layers. Thus, it is proposed to use the QCM-D protocol developed to study the behaviour of the different mucins and their interaction with the different polymers analysed.

The second objective of this Chapter is to understand in vitro screening using the QCM-D technique to assess the combination properties between mucoadhesion of thiolated polymers with the different amount of the thiol groups. The advantages related to mucoadhesive drug delivery systems include improved drug bioavailability, reduced administration frequency, besides to permit the modification of mucosa permeability (Chowdary *et al.*, 2004, Khutoryanskiy *et al.*, 2011, Mazzariono *et al.*, 2014). Among several promising mucoadhesive polymers, thiolated chitosan is currently considered of great interest as a potential carrier for the drug delivery applications due to biocompatibility, biodegradability and low toxicity (Bernkop-Schnürch 2003; Lee *et al.*, 2007). Positively charged amino groups of the polymer allow for electrostatic interactions with negatively charged nucleic acids to form stable complexes (Mao *et al.*, 2010; Park *et al.*, 2013). In this study we would like to evaluate the interaction between mucoadhesive systems and mucin, and to examine how these characteristics impart the physicochemical properties of the produced polymers/ nanoparticles in order to selectively systematically modify the nanocarriers. Moreover, the combination properties of mucoadhesion and mucus permeation of nanoparticles are assessed.

The QCM-D experiments are conducted at pH 4 or 6.8 to evaluate the interaction of thiolated chitosan polymers, with low (TCL), medium (TCM) and high (TCH) contents of free thiol groups, with NPGM. TCL, which showed relatively higher permeability, was chosen for further DNA carriers. Here we describe a formulation of a novel carrier comprised by positively charged TCL, and negatively charged both DNA and degradable oligopeptide-modified poly(β-amino ester)s (PBAEs), which were employed in order to approach for tuning particle size and surface charge of complexes. PBAEs will be described in detail in Chapter 3. The results show the adsorption of thiolated chitosan polymers and nanoparticles with NPGM as well as the permeation, which can be characterized by measuring at multiple frequencies and applying a viscoelastic model (e.g. the so called Voigt model) incorporated in Q-Sense software QTools.

Simultaneously, it is to elucidate the interrelationship between the nanoparticles, which are obtained by 4 different strategies; slippery surface, proteolytic enzyme, thiomer and SNEDDS, and NPGM for a profound study of both mucoadhesive and mucus permeating drug delivery systems. A set of different nanoparticles, coming from different EU-project FP7

ALEXANDER partners, is monitored using the method described above. The results show the QCM technique is well suited for measuring adsorption of nanoparticles with NPGM. On the other hand, this technique may give insight into the particle permeability through the mucin layer.

To accomplish these aims the following steps will be developed:

- To develop the QCM-D method of the viscoelastic model with NPGM and CPGM on the surface of gold-sensor.

- To evaluate the interaction of the mucoadhesive polymers; chitosan, thiolated chitosan (TC), and polyallylamine hydrochloride (PAH), hyaluronic acid (HA) and thiolated hyaluronic acid (HA-SH), with NPGM and CPGM at pH 4 and compare the mechanism of this interaction for studying the effect of mucin origins.

- To assess the combination properties of mucoadhesive and mucus permeability of thiolated chitosan polymers, with low (TCL), medium (TCM) and high (TCH) contents of free thiol groups, with NPGM at pH 4 or 6.8.

- To formulate the novel nanoparticles comprising thiolated chitosan and poly(β-amino esters) and the developed nanoparticles with NPGM at pH 4 or 6.8.

- To evaluate mucoadhesive and mucus permeation properties of the developed particles with NPGM at pH 4 or 6.8.using the QCM-D technique.

- To investigate interrelation between the novel particles, obtained by different strategies, and NPGM at pH 4 in order to select the best candidate for further studies.

2.3. Experimental section

2.3.1. Materials

Commercially available porcine gastric mucin (CPGM, Type III) containing 0.5-1.5% bound sialic acid was purchased from Sigma Aldrich. All chemicals were purchased from Sigma Aldrich and used as received, unless otherwise mentioned. All reagents were analytical grade and used without further purification. The samples tested here were supplied by

different FP 7 Alexander European Project Partners. The preparation of negative oligopeptide-terminated poly(β-amino ester)s (PBAEs) (e.g. D and E polymers) was described in detail in 4.3.2.

Thiolated chitosans with a low, medium and high content of thiol groups were referred to as TCL, TCM and TCH, respectively.

2.3.2. Mucin purification

The procedure of purification of native porcine gastric mucin (NPGM) was described in a previous paper in detail by Fogg et al. (Fogg *et al.*, 1996). Briefly, the mucus gel, from freshly slaughtered pig stomach, was scraped from the mucosal surface of the gastric fundus using a glass microscope slide. The mucin was purified by equilibrium density gradient centrifugation in CsCl (1.42 g/mL starting density). The final NPGM sample has been freeze-dried and kept at -20 $^{\circ}$C until use.

2.3.3. Sample preparation

Two buffer solutions were prepared depending on the type of mucin used: For NPGM, the citric acid/phosphate buffer was prepared by mixing a solution of 0.1 M citric acid and 0.2 M disodium hydrogen phosphate. NPGM was dissolved in 150 mM buffer with gentle stirring at least for 1 h at room temperature. For CPGM, succinate/phosphate buffer was obtained from a mixture solution of 0.01 M H_3PO_4/succinic acid and 0.01 M Na_3PO_4/sodium succinate dibasic. CPGM was dissolved in 30 mM NaCl buffer and left under stirring for 1 h at room temperature. A buffer solution was prepared to optimal isoionic conditions with mucin at appropriated concentrations of NaCl (Wiecinski *et al.*, 2009 and Celli *et al.*, 2007).

2.3.4. QCM-D experiments

Polymer interaction assays were performed using a Q-Sense E1 instrument (Q-Sense AB, Gothenburg, Sweden) with a window module. The QCM-D sensors used here were the piezoelectric AT-cut quartz crystals with gold electrodes on both sides with a fundamental frequency of 4.95 MHz (QSX301, Q-Sense AB). All experiments were conducted at 37.0 ± 0.1 ºC using a flow rate of 0.11 mL/min in a flow mode, and the 3rd, 5th, 7th, 9th, 11th, and 13th overtones were recorded. For each type of surface the experiments were run twice and the results are presented as mean values ± standard deviation from the mean. All sample solutions were degassed before measurement to avoid bubble formation. The procedure of the surface modification followed different steps described below (Lu *et al.*, 2013):

1) Prior to the PGM layer deposition, buffer was injected into the flow cell to allow a stable baseline.
2) After stabilization of the signals, PGM (25 mg/L in buffer) was introduced to the crystal until both Δf and ΔD stabilized.
3) Rinsing with buffer for approximately 10 min to remove unbound mucin.
4) After establishing a mucin layer, sample solutions (100 mg/L in buffer) were introduced to the measurement cell for approximately 60 min.
5) Finally, unbound polymers or particles were removed by rinsing with buffer for 10 min.

The principle of the QCM-D technique is illustrated in Scheme 2.4.
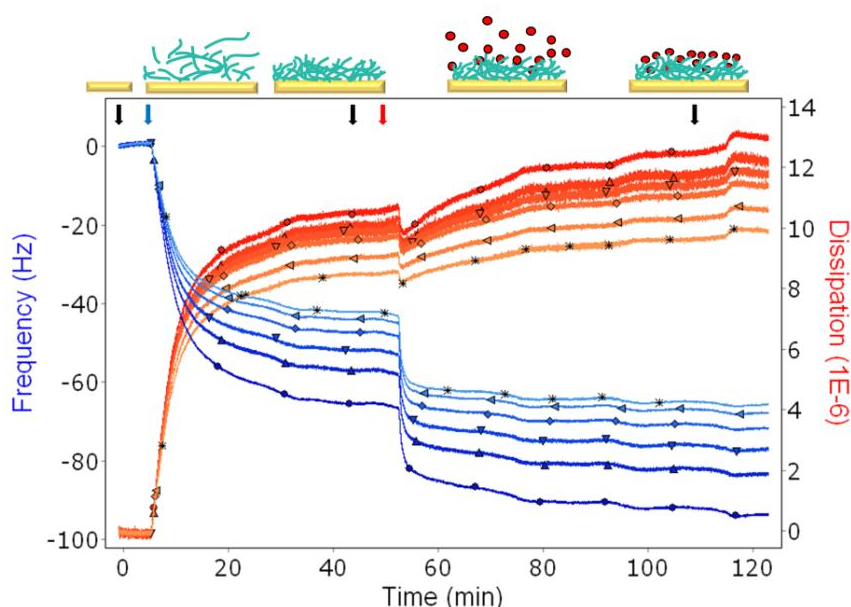
Scheme 2.4. Scheme of the experiment described in the protocol. Blue and red arrows indicate the addition of mucin and sample solutions, respectively. Black arrow indicates the introduction of buffer solution. Gold bar, cyan line, red circle with black coating indicate the crystal gold-coated sensor, mucins and samples, respectively.

2.3.5. Preparation QCM-D sensor

Gold-coated QCM-D sensors were cleaned prior to use or re-use by immersion in 1:1:5 mixture of H_2O_2 (30%), NH_3 (25%) and Milli-Q water for 10 min at 75 ºC, followed by rinsing with Milli-Q water, dried with nitrogen, rinsing with ethanol (≥ 99%), and dried with nitrogen. This cleaning procedure was repeated at least three times. The procedure followed a standard of protocol supplied by Q-Sense.

2.3.6. QCM-D data analysis

The Δf and ΔD results were evaluated with the software QTools 3 data analysis so-called Voigt model for viscoelastic representation (Q-Sense AB, Sweden) (Rodahl *et al.*, 1995). Changes in interaction, viscosity and shear modulus of the layer of particles with NPGM were calculated as follows, respectively:

1) ΔParticles Interaction (PI) = Thickness of the total layer – Thickness of the NPGM layer
2) ΔViscosity = Viscosity of the total layer – Viscosity of the NPGM layer
3) ΔShear modulus = Shear modulus of the total layer – Shear modulus of the NPGM layer

The fixed parameters were the solvent density as 1000 kg/m^3, the solvent viscosity as 0.00071 Pas, and the mucin layer density, which was set to theoretical value of 1050 kg/m3 (Celli *et al.*, 2007), and the range of them were set to get a good fit between 0.001 and 0.01 kg/ms, 10000 and 1 E^8 Pa, and 1 E^{-10} and 1 E^{-6} m, respectively. The QTools software was used to numerically fit the measured changes in *f* and *D*, which were recorded with 6 overtones. From this fitting the values for the thickness, viscosity, and shear modulus of mucin layer and polymer layer were obtained.

2.3.7. Preparation of TC/PBAE complexes

Thiolated chitosan:PBAE complexes were prepared by mixing and positively charged thiolated chitosan and negatively charged PBAE. In brief, thiolated chitosan (TC, 2 mg/ml) was dissolved in 10 mM phosphate buffer (pH 6.2). Anionic PBAE stock solutions (100 mg/ml in DMSO) were diluted in same buffer used for TC solution at appropriated concentrations to obtain the desired complexes. To form complexes, 100 µl of TC solution was added to 100 µl of PBAE solution, and vigorously mixed with vortex for a few seconds and incubated at room temperature for 20 min.

2.3.8. Formulation of complexes of polymers with DNA

For the DNA complexes, polymers:DNA complexes were formulated by mixing polymer and pGFP (plasmid green fluorescent protein) in a weight ratio of 150:1. The preparation of diluted polymer solutions was described above. All polymer solutions were filtered through a 0.2 µm membrane. 85 µl of DNA (0.06 mg/ml in phosphate buffer) was added to 100 µl of PBAE, and mixed with vortex. 100 µl of positively charged TC solution was added to negatively charged mixture solutions, mixed vigorously with vortex and incubated at room temperature for 20 min.

2.3.9. Dynamic light scattering

Dynamic light scattering (DLS) was used to characterize the unmodified and thiolated chitosan-based complexes. The particle size, polydispersity index and zeta potential of the resulting complexes diluted in simulated intestinal fluid without pancreatin (SIF) at pH 6.8 to a final concentration of 0.25 mg/ml, by DLS using a Zetasizer Nano ZS (Malvern Instruments, Ltd., UK) at 25 ºC. Each experiment was carried out in triplicate and the mean result was reported.

2.4.   Results and discussion

2.4.1. Study of mucin origin at pH 4

It was pointed out previously that the rheological behaviour of commercially available porcine gastric mucin (CPGM) was more like a dilute polymer solution rather than the viscoelastic gel of native porcine gastric mucin (NPGM). In spite of this inconsistency, CPGM is still widely used for mucus-relevant investigations. In this 2.4.1, we will evaluate and compare the viscoelastic behaviours of polymers with either NPGM or CPGM. This study was carried out at pH 4 because PGM is very nearly a critical gel at pH 4 (Celli *et al.*, 2007).

2.4.1.1. Characterization of NPGM and CPGM

The mucins were characterised by determining the viscosity of a 5% solution in PBS and by elution profiles on sepharose 2B gel filtration. The NPGM had a viscosity between 2.5 and 4 (10^{-3}) Pas whereas the CPGM had a viscosity 1-1.5 (10^{-3}) Pas. On gel filtration the NPGM was 70-80% excluded whereas the CPGM was only about 10% excluded, indicating little evidence of polymeric mucins in the CPGM. This is almost certainly as a result of

proteolysis during isolation. In addition, the NPGM forms a gel at 50 mg/ml, but the CPGM will not.

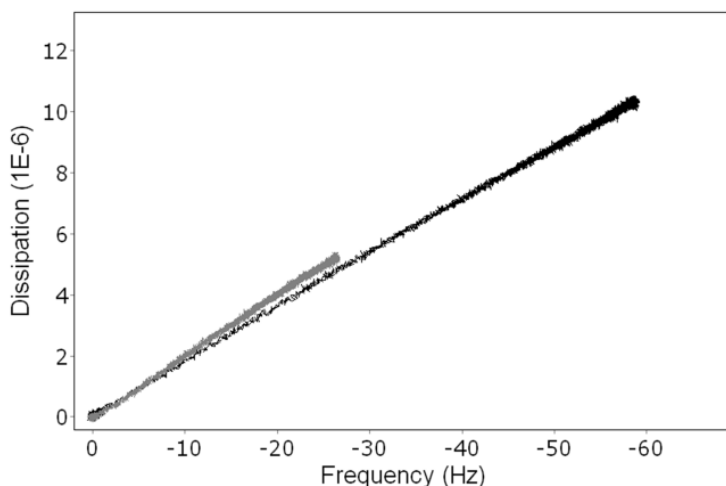### 2.4.1.2. Adsorption of NPGM and CPGM

As described before, the main aim of this Chapter was to investigate the use of the QCM-D technique for studying the mucoadhesive polymers adsorption to mucin-modified sensors. In the first step, we have developed a method based on either NPGM or CPGM immobilized gold-coated crystals for *in vitro* mucoadhesive assessment by QCM-D measurements in order to study the effect of mucin origin. Generally, changes in *f* are qualitatively related to mass change in the system, either adsorption (negative shift) or desorption (positive shift) (Wang *et al.*, 2014). Conversely, changes in *D* are qualitatively related to mechanical properties of the system becoming more viscous (increase) or more stiff (decrease). The experiments were conducted at pH 4 in buffer solutions of appropriate ionic strength for different mucins, and it was performed as follows. Initially, buffer solutions were added for 5 min to be a stable surface of crystal, and then approximately 5 mL of mucin solutions were switched and injected into the crystal. The sensor was rinsed with buffer to remove unmodified mucin. The adsorption of a 25 mg/L of NPGM solution in citric acid/phosphate buffer (150 mM NaCl) and that of CPGM solution in succinate/phosphate buffer (30 mM NaCl) are presented in Fig. 2.1A and 2.1B, respectively.

When the mucin solutions were introduced in the flow module, the adsorbed mucin films (either NPGM or CPGM) resulted in an immediate decrease in *f*, indicating a mass increase, and an increase in *D*, indicating that the adsorbed mucin films are a soft layer, not a rigid one ($D \geq 1$). After rinsing, in order to remove the unbounded PGM solutions, there were changes in *f* and *D*. These results support that both NPGM and CPGM films at pH 4 were effectively formed on the gold-coated QCM-D surface, and the system of a PGM-coated QCM-D sensor is easily reproducible and can be manipulated. This model system was used for the evaluation of mucoadhesive polymer interactions with mucin. It was also observed that the changes in *f* and *D* were larger when NPGM was added than CPGM. This is the first indication that the adsorbed NPGM layer was larger and it forms faster than the adsorbed CPGM layer.
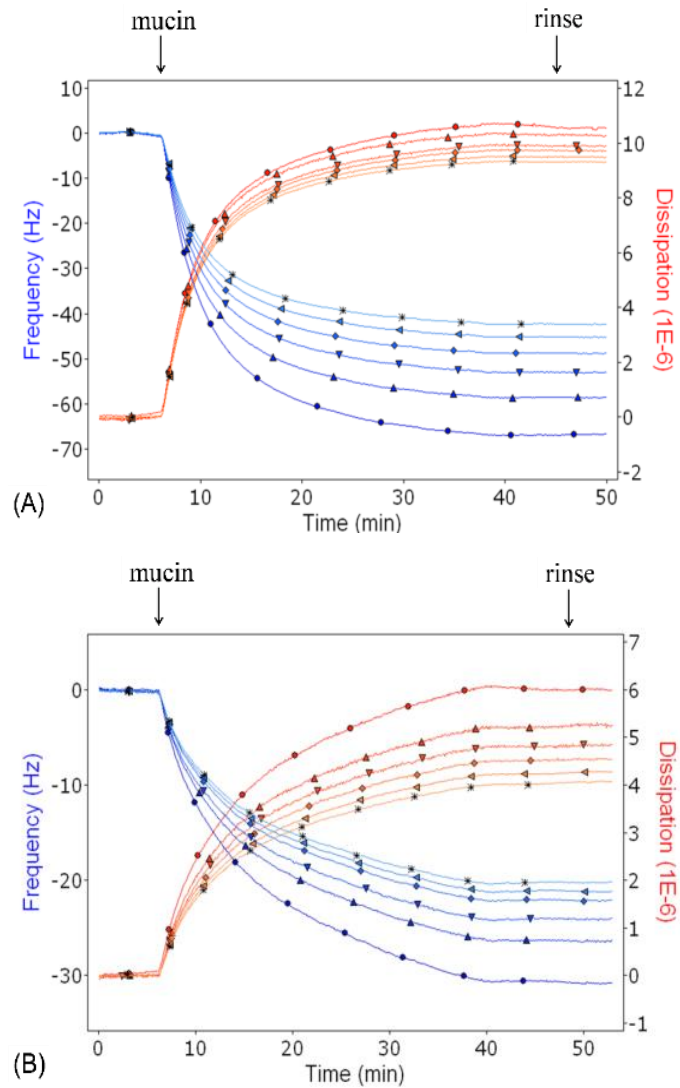
Fig. 2.1. Frequency and dissipation changes with time, blue line and red line, respectively, for QCM-D monitoring of mucin adsorption on gold-coated sensor at pH 4: (A) NPGM and (B) CPGM. The 3rd (●), 5th (▲), 7th (▼), 9th (♦), 11th (◄), and 13th (✸) overtones are shown

The value of the ratio between the changes in *D* vs. *f* ($\Delta D/\Delta f$) gives qualitative information regarding the viscoelasticity (Feiler *et al.*, 2007). Fig. 2.2 compares the $\Delta D/\Delta f$ plot for adsorption of NPGM and CPGM onto gold-coated sensor taken from Figs. 2.1A and 1B, respectively. The slope of $\Delta D/\Delta f$ plot for CPGM adsorption was slightly higher than that for NPGM adsorption, indicating that the CPGM film is relatively less rigid than NPGM film. After the addition of mucins for 40 min, however, changes in frequency and dissipation of NPGM (5th overtone) are twice lager than those of CPGM. These results further support the idea of the higher capability of the NPGM layer to swell in comparison with the CPGM layer.

Fig. 2.2. Representative change of dissipation vs. frequency (5th overtone) obtained of the adsorption of NPGM (lower) and CPGM (upper) onto the gold-coated surface.

It was studied viscoelastic properties such as viscosity or shear modulus correlating with thickness of mucin layer. As the results are obtained for the soft layer of mucin film, these values were calculated by using Voigt model instead of Sauerbrey model. Table 2.1 shows thickness, viscosity, and shear modulus of NPGM film compared to those of CPGM film. The thickness values of NPGM film and CPGM film are 16.2 and 8.6 nm, respectively. The thickness value of CPGM film onto the gold surface is in agreement with that obtained by Wiecinski and colleagues (Wiecinski *et al.*, 2009). NPGM film was formed for the first time in our study and was twice thicker than CPGM film. There were observed higher viscosity and shear modulus values for the film of NPGM compared to that of CPGM. In other words, the thicker films have higher viscosity and shear modulus values.

Table 2.1. Mean values ± deviation for the properties of the NPGM and CPGM layers, before rinsing obtained by using Voigt model. The results shown represent the mean values obtained from two independent measurements and the error values (±) are the deviation from the mean.

	Thickness (nm)	Viscosity (10^{-3}) (Pas)	Shear modulus (10^{3}) (Pa)
NPGM	16.2 ± 0.6	1.46 ± 0.07	92.6 ± 9.8
CPGM	8.6 ± 0.1	1.22 ± 0.02	66.2 ± 4.5

### 2.4.1.3. Interaction of polymers with the layer of mucins

The cationic and anionic polymers selected enhanced the mucoadhesive behaviour as a result of non-covalent interactions (ionic interaction or hydrogen bonds) with the mucus layer (Ludwig, 2005; Andrew *et al.*, 2009; Woertz *et al.*, 2013). The thiolated polymers selected are also beneficial to mucoadhesion due to disulfide bonds (Kast and Bernkop-Schnürch 2001; Grabovac *et al.*, 2005; Wang *et al.*, 2012). Poly(allylamine hydrochloride) (PAH) is a weak cationic polyelectrolyte and exhibits less mucoadhesion than chitosans, thus it was chosen for this study for comparison of its mucoadhesive behaviour with those of chitosans. All polymers were kindly supplied by Croma GmbH. (Austria).

In order to study the interaction between polymers and NPGM, the adsorption of 5 mucoadhesive polymers described above on the NPGM layer was carried out using QCM-D. All mucoadhesive experiments with the polymers were performed when the mucins layer was completely established on the surface of the QCM-D sensor. All results of the adsorbed mucin layers on the gold surface are in full agreement with those shown in Fig. 2.1. Here, we focused on explaining and interpreting the interaction of the polymers with mucins. There were changes detected in *f* and *D* to all 6 overtones, which cover different depths into the sample materials. It is often informative to compare the results for many overtones, which show the sample response. For the liquid-like layer, the film will not couple perfectly to the oscillation sensor surface. As a result, there will be spread of overtones since they will sense differently into the sample materials and displays different perspectives of the materials (Feiler *et al.*, 2007). The lower overtones will sense a large volume (mass uptake) due to the large penetration depth compared to higher overtones.

In Fig. 2.3, the results corresponding to the interaction of cationic charged polymers for 25 mg/L of NPGM solution at pH 4 are presented. Fig. 2.3A shows that introduction of chitosan resulted in a large decrease in *f* and a large increase in *D* accompanied with spreading of overtones for *f* and *D*, indicating a significant increase in mass and viscoelasticity. These results confirm previous results on the mucoadhesive properties of chitosan and can be explained due to an ability of the highly positive charged chitosan to improve molecular attraction forces by electrostatic interaction with negatively charged mucin. Interestingly, a small decrease in *D* accompanied without spreading of overtones was observed within the first few minute upon the addition of chitosan, indicating that chitosan permeated somewhat into the mucin film. This finding has important implications in assessing polymers-mucin interactions. Similar trends of changes in *f* and *D* for thiolated chitosan (TC) polymer were shown in Fig. 2.3B. However, changes in *f* and *D* were much larger for TC than those for chitosan, indicating higher adsorption of chitosan-SH onto the NPGM film. This is in accordance with the results described in the literature (Bernkop-Schnürch, 2005) for the significantly improved mucoadhesion enhancing properties of thiolated chitosan polymers in

comparison to unmodified chitosan polymers. Fig. 2.3C exhibits the adsorption of poly(allylamine hydrochloride) (PAH) onto NPGM, as seen by the decrease in f shift. Unlike the results observed for chitosan and chitosan-SH, the addition of PAH induced decreases in both f and D, indicating an increase in mass but a decrease in viscoelasticity. The smallest decrease in f was obtained for the adsorption of PAH onto NPGM in comparison with those of chitosan and TC, indicating relatively poor mucoadhesive characteristic of PAH. This may be due to the weak ionic interaction with mucin. As reported in literature (Choi and Rubner 2005) the pKa of PAH is approximately 8, meaning that PAH will be fully ionized at low pH values (lower than pH 6). However, PAH has identical polymer backbones and differs only in the ionic side groups (Mihai *et al.*, 2011), was chosen as model weak polymer for this study. In all cases, after rinsing with buffer, there were observed small decreases in f and increases in D. These results suggest that the interaction of these cationic polymers with NPGM film clearly modifies the capability of the mucin to absorb water.
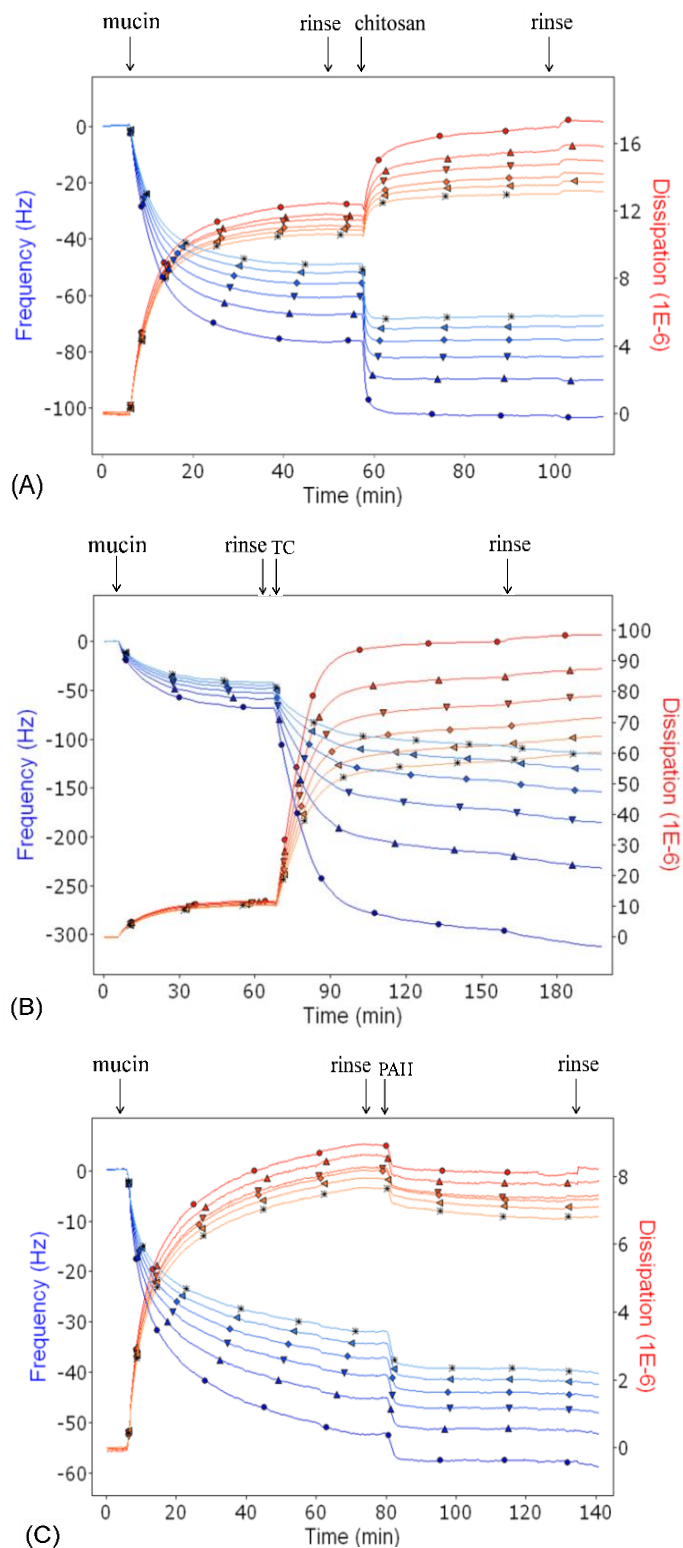
Fig. 2.3. Changes in frequency (Δf) and dissipation (ΔD) with time, blue line and red line, respectively, were recorded with QCM-D for interactions between NPGM with (A) chitosan, (B) TC, and (C) PAH. The 3rd (●), 5th (▲), 7th (▼), 9th (♦), 11th (◄), and 13th (✶) overtones are shown.

Regarding the anionic polymers, as mentioned in 2.2, the mucoadhesive properties of hyaluronic acid (HA) and its derivatives have been attributed to its ability to establish hydrogen bonding and electrostatic interaction with mucin. Figs. 2.4A and 2.4B show the adsorption of anionic polymers of hyaluronic acid (HA) and thiolated hyaluronic acid (HA-SH) onto the NPGM film at pH 4, respectively, which followed the same procedure describe above. Introduction of HA produced a negligible change in *f*, indicating a slight change in mass. However, a reduction of *D* shift and less spreading of overtones were simultaneously obtained in the first few minutes, indicating a conformational change. This effect can be explained by slight interaction with the mucin film due to the electrostatic repulsion with the negatively charged polymers. These results agree with those obtained by Sigurdsson *et al.* (Sigurdsson *et al.*, 2006) who reported the limited interaction of HA with mucin in the range of pH 4.0-8.2. This fact may be related to the low pKa of the polymer (~3.2), at the considered pH values, the molecule is ionized, which can lead to repulsive electrostatic interaction with the also negatively charged mucin (isoelectric point around 2-3). The addition of HA-SH resulted in similar trends for HA. After the addition of HA-SH, however, small differences were observed in the second changes in *f* and *D* within 10 min. Moreover, a slight difference in behaviour of the adsorbed HA film was also observed when rinsing with buffer, indicating a greater water adsorption. These findings suggest that the viscoelastic properties of the adsorbed thiolated HA film was not significantly altered in comparison with HA, but water uptake was. According to these results, the QCM-D technique could be also regarded as an alternative to detect negligible interaction between polymers and mucin.
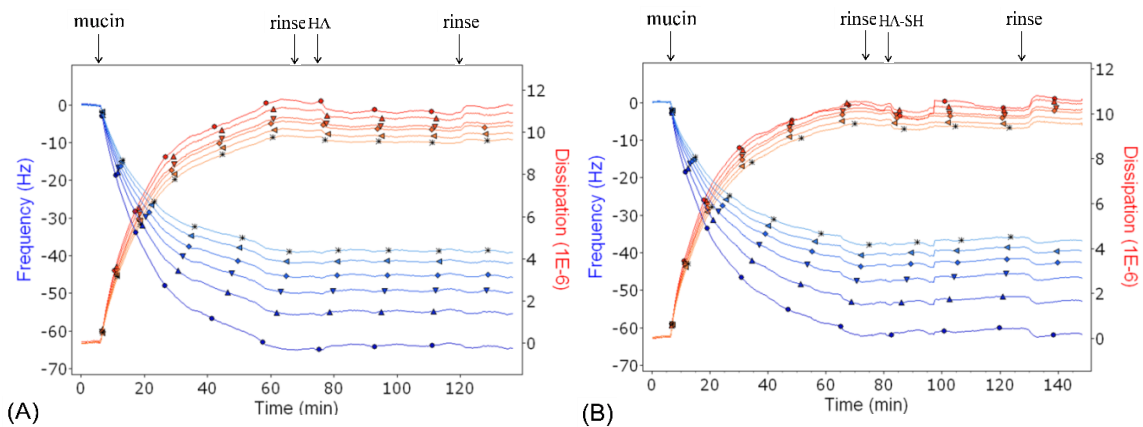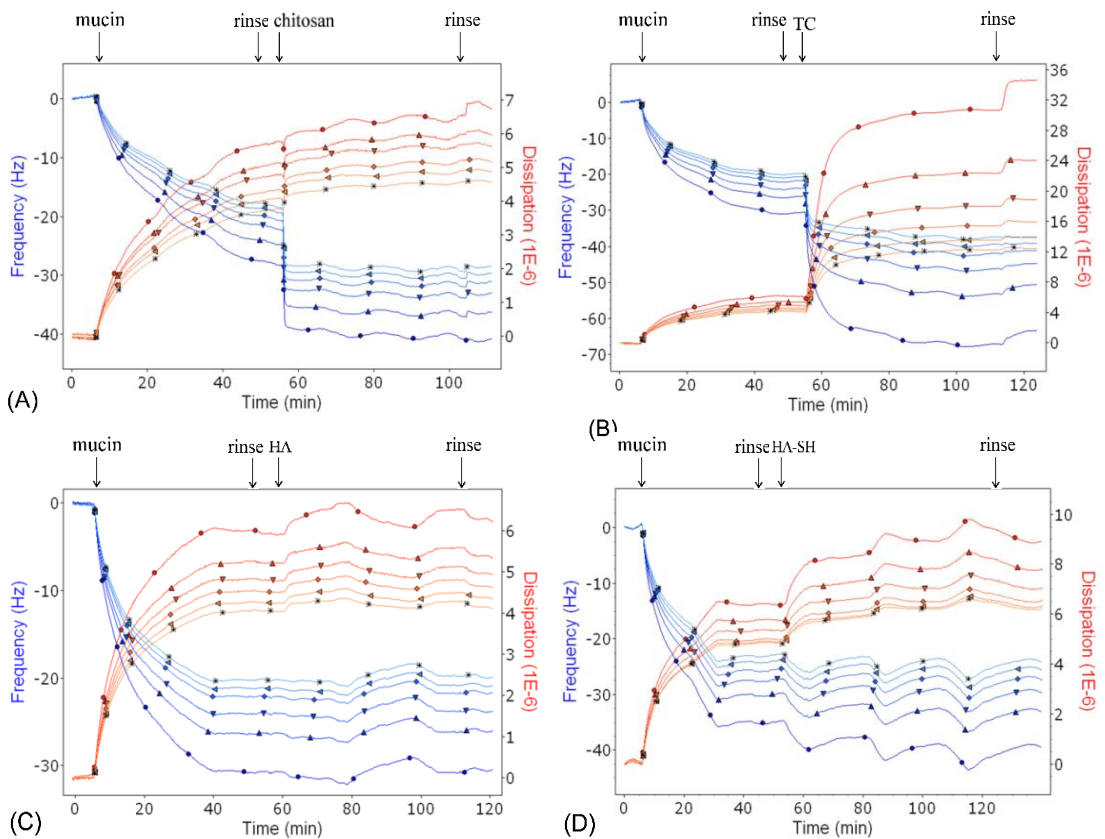

Fig. 2.4. Changes in frequency (Δf) and dissipation (ΔD) with time, blue line and red line, respectively, were recorded with QCM-D for interactions between NPGM with (A) HA and (B) HA-SH. The 3rd (●), 5th (▲), 7th (▼), 9th (◆), 11th (◄), and 13th (✶) overtones are shown.

In order to compare the effect of mucin origin using the QCM-D technique, the interaction of polymers with CPGM at pH 4 are shown in Fig. 2.5. 100 mg/L of polymer solution was followed by 25 mg/L of CPGM solution on the QCM-D sensor and rinsed with buffer. Similar trends of the interaction of chitosan, TC, and HA with CPGM film were detected with those shown for NPGM in Figs. 2.3A and B, and 2.4A, respectively. However, changes in *f* and *D* during the interaction of both chitosan and TC with CPGM (Figs. 2.5A and 2.5B) were approximately 3 times smaller than those with NPGM (Figs. 2.3A and 2.3B), indicating that the polymers layer on the CPGM is adsorbed in a less viscous conformation. These findings suggest that the viscoelastic behaviour of CPGM is not similar to that of NPGM. This is in accordance with the different rheological behaviour reported for both mucins (Kocevar-Nard *et al.*, 1997). Furthermore, this is clearly supported by the results obtained for the interaction of HA-SH with CPGM (Fig. 2.5D) compared to those with NPGM (Fig. 2.4B). Introduction of HA-SH progressively produced a large negative *f* and a positive *D* with CPGM film, while there were negligible changes in *f* and *D* observed for the interaction of HA-SH with NPGM. This may be because the film of HA-SH with CPGM is more hydrated than those with NPGM. According to the overall results, NPGM was chosen for further studies.

Fig. 2.5. Changes in frequency (Δ*f*) and dissipation (Δ*D*) versus time curves, blue line and red line, respectively, were recorded with QCM-D for interactions between CPGM with (A) chitosan, (B) chitosan-SH, (C) HA, and (D) HA-SH. The 3rd (●), 5th (▲), 7th (▼), 9th (◆), 11th (◄), and 13th (✶) overtones are shown

2.4.2. Study of the interaction between samples and NPGM at pH 4 or 6.8

In the previous section, we have developed the method of NPGM immobilized gold-coated crystal for mucoadhesive assessment, which was carried out at pH 4, by QCM-D measurement. To further investigate the interaction between complexes and NPGM, the adsorption of NPGM onto gold-coated sensor was firstly evaluated for two different pH values of the buffer solutions: pH 4 and pH 6.8, which was chosen for this study under the working in the gastrointestinal (GI) track conditions. The preparation of 25 mg/L NPGM solution at pH 4 was followed as described in 2.4.1.2 and that at pH 6.8 was conducted by the same method for pH 4.

2.4.2.1. Adsorption of NPGM

The experiments were performed in citric acid/phosphate pH 4 or 6.8 buffer (150 mM NaCl). In brief, prior to adsorb the NPGM layer, buffer solutions were added for 5 min to be stable on the surface of the sensor. The NPGM solutions were then added into the crystal for 40 min and the sensor was rinsed with buffer to remove unmodified NPGM.

The changes in f and D (5th overtone) of the adsorption of NPGM onto the sensor in buffers of pH 4 or 6.8 are shown in Fig. 2.6A. In both cases, NPGM solutions were rapidly adsorbed on the gold-coated sensor, as evidenced by the decrease in f (mass increase) and increase in D (viscoelasticity increase). As described in 2.4.1.2, this binding can be explained that the hydrophobic peptides residues of the non-glycosylated domains of mucin are exposed onto the gold surface by strong covalent bond (Sandberg *et al.*, 2008). When the signals of f and D of the mucin layer are stable, the buffer solution was added in order to remove unbounded NPGM by rinsing. This rinsing step confirms that the adsorption of NPGM is irreversible under the experiments, since rinsing induces no significant changes in f and D (Belegrinou *et al.*, 2008). These results support that the NPGM solutions at both pH were perfectly deposited on the QCM sensors. However, there were two differences observed. First, the changes in f and D were larger for pH 4 compared to those for pH 6.8, indicating higher adsorption for the NPGM layer at pH 4. These findings agree with the previous studies reported the binding of the probe to the diluted NPGM solutions varied with the pH of the medium, being highest at low pH and lowest at high pH (Gwozdnski *et al.*, 2014). In addition, at pH 6.8, the system of a NPGM-coated QCM-D sensor is not easily reproducible, resulting in the differences between 6 overtones for f and D that were not uniform (Fig. 2.7 and 2.8).
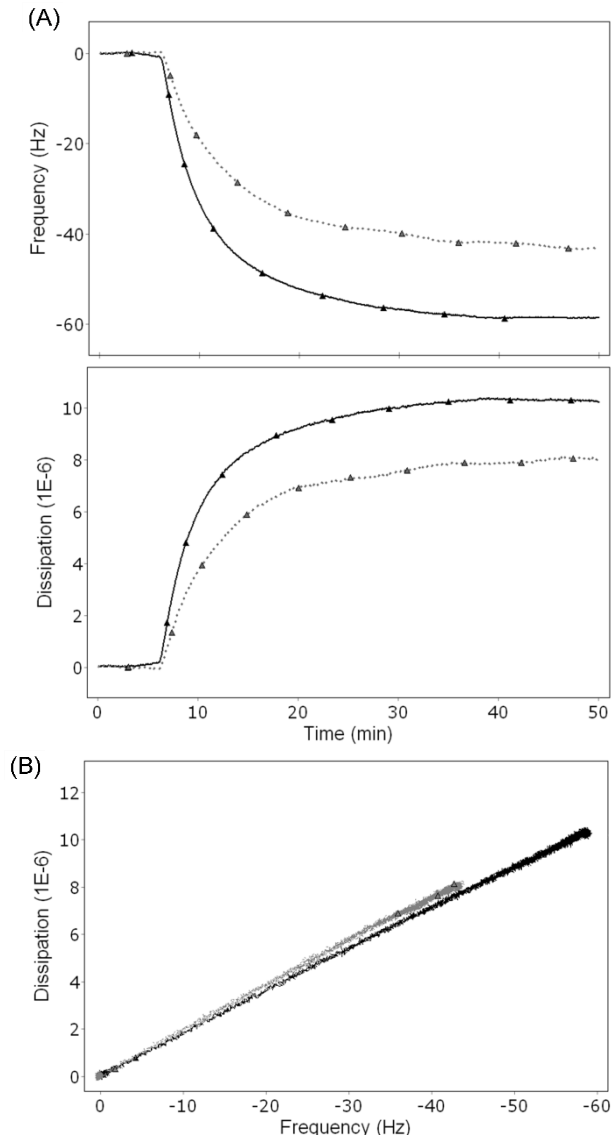
Fig. 2.6. (A) The changes in frequency and dissipation with time for the adsorption of NPGM at pH 4 (solid) and pH 6.8 (dot) onto the sensor. Arrow and star indicate the NPGM injection and the rinsing with buffer, respectively. (B) The change of dissipation vs. frequency obtained from these data: pH 4 (lower) and pH 6.8 (upper). Presented data were obtained at the 5th overtone.

The ratio between the changes in *D* vs. *f* ($\Delta D/\Delta f$) provides qualitative information regarding the viscoelasticity as described in 2.4.1.2. As shown in Fig. 2.6B, the $\Delta D/\Delta f$ plot for adsorption of the NPGM film at pH 4 onto the crystal was compared to that at pH 6.8. There were negligible differences in the slope of the $\Delta D/\Delta f$ plot observed for NPGM at pH 4 compared to pH 6.8, but lager changes in of *f* and *D* of NPGM, leading to the higher swelling capacity for pH 4.

The viscoelastic properties such as thickness, viscosity and shear modules of NPGM layer, which was shown to be not a rigid film ($D \geq 1$), were characterized by using Voigt model and the results were shown in Table 2.2. The thickness values of the NPGM layer at pH 4 and pH 6.8 are 15.9 and 12.6 nm, respectively, indicating that the mass of the adsorption of NPGM was higher at pH 4 buffers than at pH 6.8. The viscosity and shear modulus values for the NPGM layer at pH 4 are higher compared to those at pH 6.8. These results indicate that higher viscoelasticity of the NPGM film was obtained when prepared in buffers of pH 4.

Table 2.2. Mean values ± deviation for the thickness of the NPGM layers at pH 4 and 6.8 and its viscoelasticity properties, before rinsing obtained by using Voigt model. The results shown represent the mean values obtained from two independent measurements and the error values (±) are the deviation from the mean.

NPGM	Thickness (nm)	Viscosity (10^{-3}) (Pa)	Shear modulus (10^{3}) (Pa)
pH 4	15.9 ± 1.1	1.46 ± 0.05	113.1 ± 10.3
pH 6.8	12.6 ± 3.8	1.43 ± 0.12	67.8 ± 11.1

2.4.2.2. Interaction of thiolated chitosan polymers with NPGM

Previously, it was reported the interaction between several mucoadhseive polymers and a NPGM-coated gold sensor at pH 4. The results were described that the thiolated chitosan showed the highest adsorption, indicating the highest mucoadhesive properties, among the polymers tested. Regarding these findings, thiolated chitosans were chosen for further studies of thiolated chitosan-based complexes interaction with NPGM, and the experiments were carried out at two different pHs 4 and 6.8. In fact, it was reported that CPGM undergoes a pH dependent sol-gel transition, and CPGM at pH 4 is very nearly a critical gel (Celli *et al.*, 2007), thus it was chosen for previous study. In this section, we would like to evaluate the effect of pH factor on the behaviour of both NPGM and NPGM-particles

Here, the interaction of thiolated chitosans with the different content of thiol groups as a thiolated chitosan polymer, with low (TCL), medium (TCM), or high (TCH) contents of free thiol groups, was carried out at pH 4 and 6.8 using QCM-D and compared in order to study

the effect of the content of thiol groups on mucoadhesive character and swelling behaviour. All experiments with the thiolated chitosans were performed when the NPGM layer was completely established on the surface of the QCM-D sensor as shown in Fig. 2.7. A system of the NPGM layer formed on the gold-coated sensor in buffers for pH 4 is easier reproducible compared with that for pH 6.8 as described above. 5 overtones were recorded for TCL and TCM at pH 6.8 due to the difficult formed mucin-coated sensor, whereas the others were measured with 6 overtones.
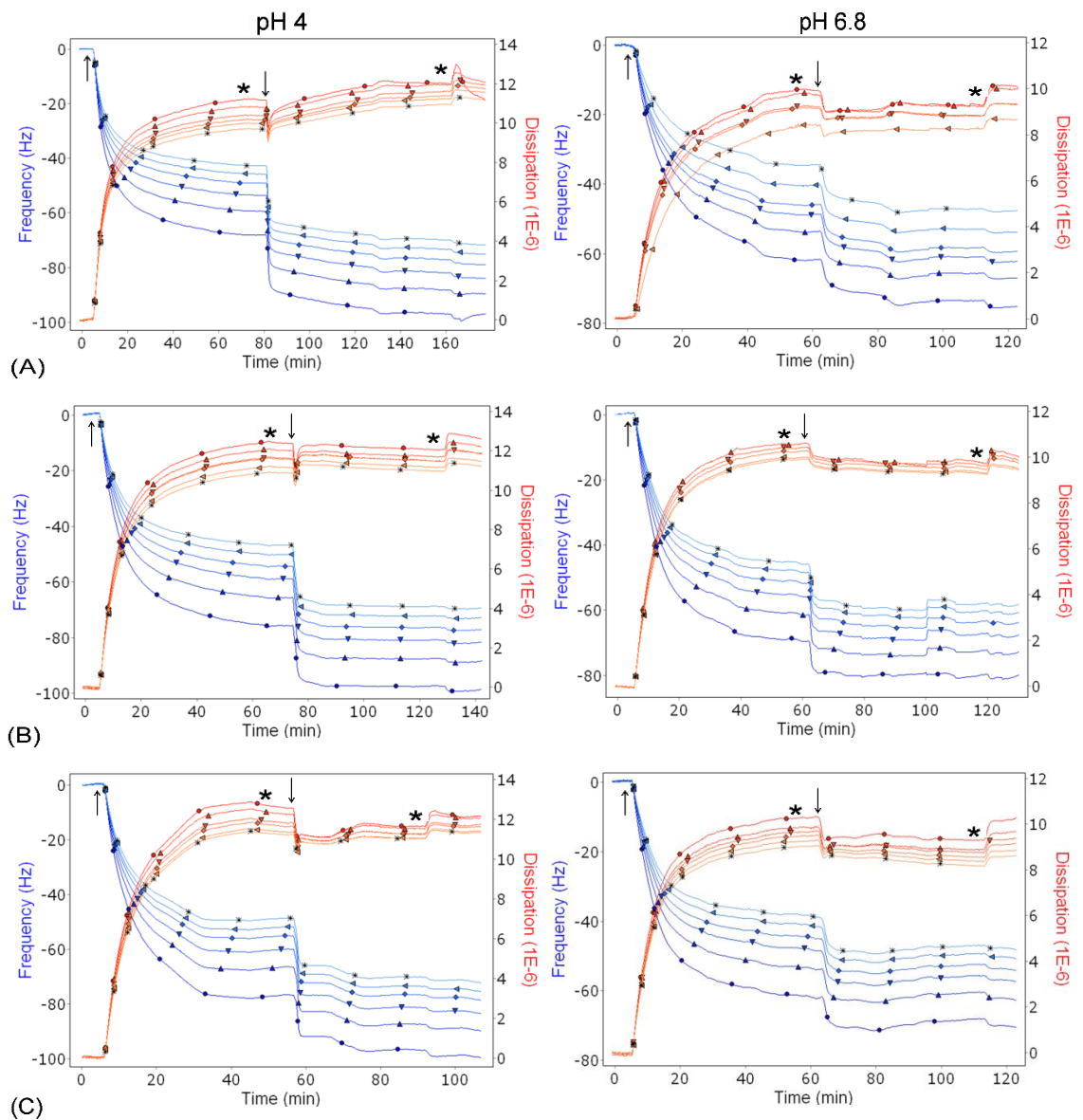
Fig. 2.7. Changes in frequency (Δf) and dissipation (ΔD) with time, blue line and red line, respectively, were recorded with QCM-D for interactions between NPGM with (A) TCL, (B) TCM and (C) TCH in buffers of pH 4 or 6.8. The 3rd (●), 5th (▲), 7th (▼), 9th (♦), 11th (◄), and 13th (✶) overtones are shown. First and second arrows indicate the addition of NPGM and polymers, respectively. Star indicates the rinsing with buffer.

At pH 4, the addition of 100 mg/L of thiolated chitosans resulted in a large decrease in *f*, indicating a mass increase. On adding these polymers, there were simultaneously observed a reduction of *D* within the first few minute and an increase in *D* accompanied without spreading of overtones, indicating a permeation or corruption of polymers into the mucin layer for a moment. After the first observation of the decline in *D*, Fig. 2.7A displays that the addition of TCL solution caused in a gradual increase in *D*. Unlike this result, the introduction of TCM induced that *D* rapidly increases for a moment and then remains constant (Fig. 2.7B). In the case of TCH as shown in Fig. 2.7C, the smallest increase in *D* was obtained in comparison with those of TCL and TCM, indicating relatively poor mucus permeating properties of TCH.

In this study, it is important to notice the changes in *D* of the polymer layers after shown the reduction. The increases in *D* of polymers were larger with decreasing the content of thiol groups, indicating higher viscoelastic properties of the polymer films. These findings are not in accordance with the results described in the literature (Kast and Bernkop-Schnürch 2001; Wang *et al.*, 2012). Regarding this concern, we focused on explaining and interpreting the combination of both mucus permeability and mucoadhesive properties of thiolated chitosan.

In the first step, all chitosan polymers with thiol bearing side changes exhibited an increase in permeability into the mucin layer. Afterwards, there was obtained stronger immobilization by forming covalent bonds with cysteine-rich subdomains between mucins and polymers via thiol-disulfide exchange reactions with higher amount of thiol groups (Bernkop-Schnürch 2005). In other words, TCL demonstrated an increase in viscoelasticity relatively higher than that of TCM and TCH, indicating that thiolated chitosan polymers with lower content of thiol groups still permeated into the mucin layers. However, we can hypothesize that the others may be only immobilized. Recently, Shahnaz et al. reported that there was observed an improved permeability of thiolated chitosan-based nanoparticles prepared by the oxidation process, resulting in a decrease in thiol groups (Shahnaz *et al.*, 2012). It is believed that the specific content of free thiol groups of polymers would play an important role in mucus permeability. Accordingly, TCL might be a promising candidate for the preparation of carriers capable of giving mucus permeability.

On the other hand, at pH 6.8, introduction of all thiolated chitosans induced decreased in *f*, indicating an increase in mass. At the same time, *D* immediately decreased in the first few minutes but then remained constant, indicating no mucus permeability. On the other hand, the polymer layers showed a higher immobilization with the NPGM layer. The higher the pH, the more thiolated anions are available, thus leading to strong immobilization into the mucin layer (Bernkop-Schnürch 2005). However, a slight increase in *D* was detected for TCL while there were negligible changes in *D* for the TCM and TCH layers observed. These results indicate that the viscoelastic changes for TCL are larger than the others.

According to the overall results obtained at both pHs, TCL polymer was chosen for further studies formulating nanoparticles as it showed higher both mucoadhesion and mucus permeability. In next study, it will be assessed the interaction between TCL-based particles and NPGM at pH 4 and 6.8 In all cases, there were detected small decreases in *f* and increases in *D* when rinsing with last buffer. These confirm the results obtained previously that the interaction of thiolated polymers with the NPGM layer clearly modifies the capability of the mucin to absorb water

2.4.2.3. Formation and characterization of complexes

Once we have established the QCM-D technique that can discriminate the mucoadhesive and mucus penetrating properties of polymers by characterizing the mechanism of interaction between polymers and mucins. We proposed that the developed QCM-D protocol can be used to study the behaviour of particles into the mucins. Recently, thiolated chitosan polymers have attractive considerable attention as potential mucosal delivery systems of macromolecular drugs such as DNA. However, a near neutral surface charge of drug delivery systems requires in order to avoid strong adhesion between particles and mucin fibers (EU-project FP7). To accomplish this, biodegradable poly(β-amino ester)s (PBAEs) were applied for the development of thiolated chitosan-based delivery systems with slightly positive zeta potential capable of both mucoadhesion and mucus permeability. Here PBAEs end-modified with two negative charged oligopeptide bearing aspartic or glutamic acid moieties were applies to formulate complexes. It is well known that PBAEs are a promising polymer for delivery systems of macromolecules. We will explain and discuss about PBAEs in detail in the next Chapter.

Polyelectrolyte complexes nanoparticles were prepared via electrostatic interaction between the positive charge (the amino groups) of thiolated chitosan and the negative charge (the carboxylic groups) of PBAEs in phosphate buffer at pH 6.2. The resulting complexes were diluted in simulated intestinal fluid without pancreatin (SIF) at pH 6.8 for complexes characterization. Table 2.3 shows the particle size, polydispersity index and zeta potential of TC/PBAE complexes with various weight ratios. TCL/D (TCD) complexes ranged from 130.3 to 259.4 nm in the particle size and from 2 to 7.1 mV in zeta potential depending on weight ratio. The physicochemical properties of TCL/E (TCE) complexes are similar to the values obtained for the TCD complexes. In both cases, the zeta potential decreased with increasing the amount of negative charged polymers. These results indicate that the physicochemical properties of thiolated chitosan-based nanoparticles can be adjusted by PBAEs bearing with negatively charged oligopeptides. The TCD and TCE complexes showed the smallest size when TCL:D=1.4:1 and TCL:E=1.2:1, respectively. Thus, these weight ratios were considered to be an optimal formulation for TCL/PBAE complexes due to their small size and slightly positive zeta potential.

Table 2.3. Particle size, polydispersity index (PI), and zeta potential of TCL/PBAE complexes. Results are mean ± SD (n ≥ 3).

| Formulation	Weight ratio (TC:PABE)	Particle size (nm)	PI	Zeta potential (mV)
TCD	3:1	156.8 ± 2.0	0.282 ± 0.040	8.9 ± 0.5
	2:1	146.8 ± 2.0	0.178 ± 0.025	7.1 ± 1.0
	1.4:1	130.3 ± 1.0	0.082 ± 0.020	3.9 ± 0.5
	1:1	164.2 ± 3.5	0.064 ± 0.020	3.4 ± 0.5
	1:2	227.7 ± 5.5	0.163 ± 0.015	2.2 ± 0.5
	1:3	259.4 ± 7.0	0.155 ± 0.025	2.0 ± 0.5
TCE	3:1	189.4 ± 3.5	0.392 ± 0.045	8.5 ± 1
	2:1	163.0 ± 0.5	0.164± 0.010	7.1 ± 0.5
	1.2:1	145.4 ± 2.0	0.117 ± 0.020	4.2 ± 0.5
	1:1	212.1 ± 2.5	0.141 ± 0.010	3.5 ± 0.5
	1:2	302.5 ± 12.0	0.173 ± 0.035	2.4 ± 0.5
	1:3	387.1 ± 17.5	0.200 ± 0.010	1.5 ± 0.5

After developing the TCL/PBAE nanoparticles, we attempted to prepare the novel formulation that can condense DNA into the nanoparticles. TCL/PBAE/DNA complexes nanoparticles were formulated by mixing polymer and DNA in a weight ratio of 100:1 or 150:1. There was optically observed some aggregation of nanoparticles when prepared with low amount of polymers (below 100:1 weight ratios) (data not shown). As shown in Table 2.4, smaller particle size formed with a 150:1 ratio of PBAE:DNA compared with a 100:1. The TCD/DNA complexes had a small particle size of 141.4 ± 1.1 nm and a slightly positive zeta potential of 2.4 ± 0.5 mV. The TCE/DNA complexes showed a little larger particle size of 175.2 ± 1.4 nm compared with TCD/DNA, but similar zeta potential. These results indicate that the formulation of these nanoparticles can condense DNA, and may tune their unique properties of mucoadhesion and mucus permeability due to changes in the zeta potential.

Table 2.4. Particle size, polydispersity index (PI), and zeta potential of TCL/PBAE/DNA complexes. Results are mean ± SD (n ≥ 3).

Formulation	Weight ratio (Polymer:DNA)	Particle size (nm)	PI	Zeta potential (mV)
TCD/DNA	100:1	212.6 ± 7.5	0.208 ± 0.220	1.9 ± 0.5
TCE/DNA	100:1	251.0 ± 9.5	0.195 ± 0.130	2.0 ± 0.5
TCD/DNA	150:1	141.4 ± 1.0	0.123 ± 0.010	2.4 ± 0.5
TCE/DNA	150:1	175.2 ± 1.5	0.191 ± 0.055	2.5 ± 0.5

2.4.2.4. Interaction of thiolated chitosan-based particles with NPGM

In order to study the interaction of TCD/DNA and TCE/DNA complexes with the NPGM layer, all experiments with complexes were conducted using QCM-D. Fig. 2.8 demonstrates the interaction between slightly positively charged TCL/PBAE/DNA complexes and negatively charged NPGM at pH 4 or 6.8, which followed the same procedure described above for thiolated chitosan polymers. Both nanoparticles were performed when the NPGM layer was completely established on the surface of the sensor. Fig. 2.8A shows that the introduction of TCD/DNA complexes in buffers of both pH 4 and 6.8 resulted in a large decrease in f, indicating a considerable increase in mass. In the case of the pH 4 buffers, there was detected simultaneously a noticeable decrease in D within in the first few minutes upon the addition of complexes and successively a large increase in D accompanied with spreading of overtones, indicating an increase in mucoadhesion as well as permeability into the NPGM layer. As described in 2.4.2, these findings had important implications in assessing the partial permeation of the mucoadhesive polymers through the NPGM film. These results support that complexes bearing with thiol groups led to transport into the mucin layer via thiol-disulfide exchange reaction (Dünnhaput *et al.*, 2015). Thus, these results might give insight on the mechanisms of the combination properties – mucoadhesion and mucus permeability - of thiolated chitosan-based nanoparticles. Unlike the results observed for pH 4, introduction of complexes at pH 6.8 produced a small reduction of D shift in the first few minutes, then D accompanied without spreading of overtones increased slightly for a moment and remained constant. These results indicate that there was firstly observed a little permeation of particles, then a large immobilization between particles and the NPGM layer. These confirmed previous results on the mucoadhesive properties of thiolated chitosan at pH 6.8 described above. These suggest that the viscoelastic properties of the thiolated chitosan-based nanoparticles at pH 4 were significantly altered compared to those at pH 6.8. Similar trends were observed for TCE/DNA complexes in buffers at pH 4 and 6.8 as shown in Fig. 2.8B. These indicate that the viscoelastic properties of the nanoparticles tested, which have shown the similar physicochemical properties, would be affected by thiolated chitosans. After rinsing with last buffer, in both pH, the changes in f and D follow the similar trends for thiolated chitosan polymers.
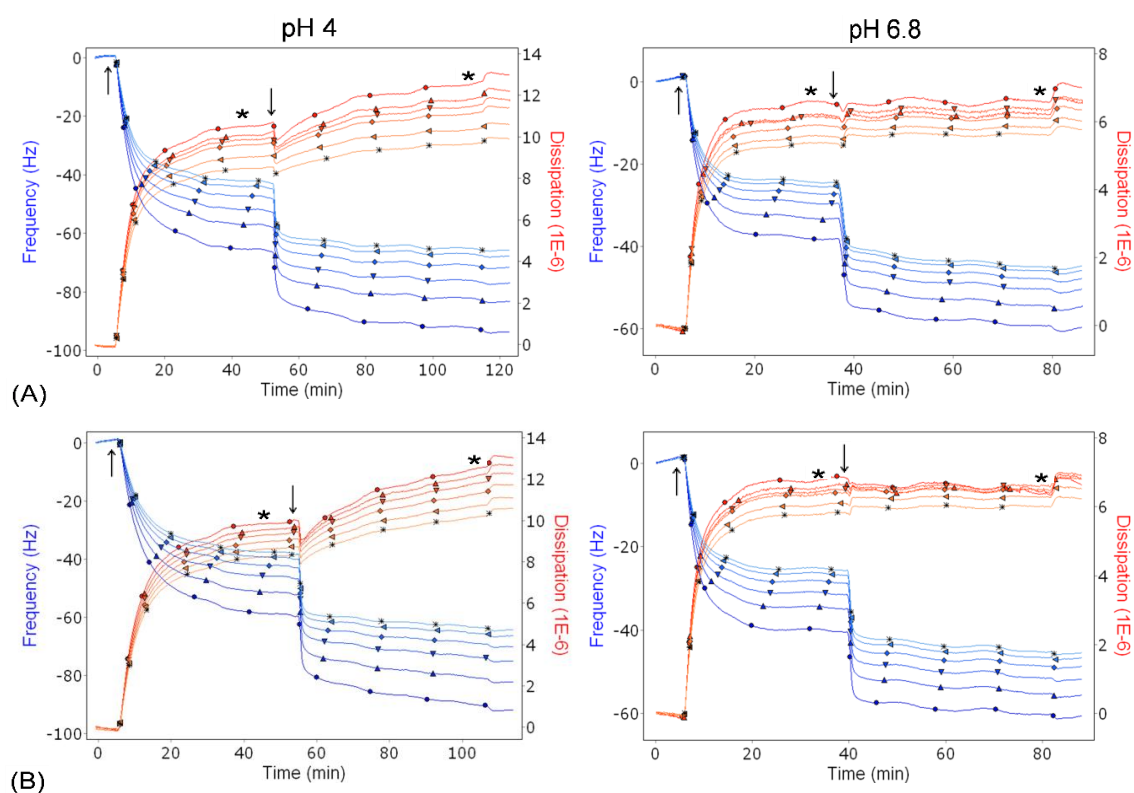
Fig. 2.8. Changes in frequency (Δf) and dissipation (ΔD) with time, blue line and red line, respectively, were recorded with QCM-D for interactions between NPGM with (A) TCD/DNA and (B) TCE/DNA in buffers of pH 4 or 6.8. The 3rd (●), 5th (▲), 7th (▼), 9th (♦), 11th (◄), and 13th (✶) overtones are shown. First and second arrows indicate the addition of NPGM and polymers, respectively. Star indicates the rinsing with buffer.

2.4.3. Study of interaction between particles and NPGM at pH 4

We have previously developed the efficient and simple QCM-D method to assess the interaction of thiolated chitosan polymers and their particles with NPGM at pH 4 and 6.8. The results obtained from previous section have shown that the QCM-D technique can allow to evaluate the mechanism of both mucoadhesion and mucus permeability. In addition, the experiments at pH 4 may provide more information regarding the viscoelastic properties. In this section, thus, we will evaluate the behaviours of several mucosal delivery systems into NPGM at pH 4.

2.4.3.1. Description of particles

We have analysed different particles coming from different EU- project FP7 Alexander Partners. To facilitate the reading of this part and the finding of a specific sample, we have

presented the results classified by mechanism of particle formation. These particles were prepared by 4 different strategies: (i) slippery surface; (ii) proteolytic enzyme; (iii) thiomer; (iv) SNEDDS. The description of particles analysed is shown in table 2.5.

2.4.3.2. Interaction of particles with NPGM

All particles were performed using QCM-D to study the interaction between particles and NPGM and the experiments were carried out in citric acid/phosphate buffer at pH 4. Briefly, particle solutions (100 mg/L) were conducted when the NPGM layer (25 mg/L) was perfectly coated on the surface of the QCM-D sensor. All results of the mucin layer are in accordance with previous reports. Recently, we studied the combined properties between mucoadhesion and mucus permeability of polymers or nanoparticles by means of QCM-D and the results were described by the changes in f and D, which were recorded with the several overtones.

Here 20 particles tested ranged from -54 to 20.2 mV in zeta potential and from 35 to 342 nm in the particle size. As shown in Fig. 1, the introduction of particles resulted in changes in f and D accompanied with 6 overtones. When particles had a highly negative zeta potential (≤-15 mV) except [F4], there were detected a slight change in f. Theoretically, the results used to be explained no interaction of samples with the negatively charged mucin layer due to the electrostatic repulsion However, there were simultaneously observed a change in D, indicating a change in viscoelastic properties. By studying how D changes with the sample film, it is possible to identify at which surface coverage particle-mucin interaction occurs (Olsson *et al.*, 2014). Conversely, the addition of particles with a highly positive zeta potential (≥ 15 mV) induced a large decrease in f and a large increase in D accompanied with spreading overtones for f and D. These results indicate a considerable increase in mass and viscoelasticity that is a significant interaction. Similar trends of changes in f and D for thiolated particles with a positive zeta potential from 1.1 to 6.2 mV were observed. In particular, there were observed the partial permeation, D rapidly decreases and then increases for the first few minutes upon the addition of particles. These confirm the results obtained previously. Interestingly, there were obtained this behaviour only for thiolated particles, which exhibit both mucoadhesive and mucus permeability properties. SNEDDSs, which had a small size from 35 to 45 nm with a neutral zeta potential except [S20], clearly interact with the NPGM layer, as seen by the decrease f. Moreover, there were obtained changes in D without spreading overtones. Since lower overtones, which senses the "entire film", is relatively to higher penetration/detection depth (Q-Sense reported data). Interestingly, all overtones of SNEDDSs were reversed after the addition of the samples. These resulted from that it is denser at the upper layer than at the down. Thus, it may be explained that the particles permeate through NPGM, but not all the way down to the bottom of the first layer. As described above, simultaneous measurements of multiple overtones is required to model viscoelastic

properties, and thus the different overtones may give information about the permeable behaviour.

To gain a deeper understanding of interaction of particles with the NPGM layer, not only the monitoring data were interpreted (changes in *f* and *D*) but also the calculated parameters such as thickness, viscous and shear modulus were reported. These values were calculated by using Voigt model. We hypothesize that the permeation of particles through the mucin layer is determined by the relationship between the dynamic thickness and the viscoelastic properties. When the adsorbed film is viscous and sufficiently soft like particles analysed here that it does not follow the sensor oscillation perfectly, this leads to internal friction (due to the deformation) in the adlayer (Dixon *et al.*, 2008). Thus, the calculated data of the layer is not the rest mass/thickness, but the hydrodynamic one (incorporating associated water). The calculated parameters and their relationship were presented in Table 2.5 and Fig 2, respectively. As shown in Fig 2, it was shown the relationship between interactions of particles (PI) with NPGM to viscoelastic properties. Positive and negative values of PI indicate adsorption and permeation of particles with the NPGM layer, respectively. If these values are close to zero or within 5% of the first layer, this indicates no interaction. When it is proposed to higher adsorbed or permeable particles to the NPGM layer, there were obtained higher changes in hydrodynamic both viscosity and shear modulus.

[E10] and [S19] had a relatively higher negative value of PI with larger differences in viscoelasticity before or after the addition of particles, indicating higher permeability of particles among the tested one. On the other hand, there were obtained a relatively higher positive value of PI with larger changes in viscosity for [E12], [T14] and [S17]. These indicate the adsorption of particles. In particular, the addition of [E12] induced a large difference in shear modulus, indicating the highest interaction among the particles shown PI > 0.

Table 2.5. The characteristics of particles and the changes in properties of the layers of particles with NPGM using QCM-D.

Strategy	Formulation	Code	Zeta potential (mV)	Particle size (nm)	Δ Interaction	Δ viscosity (10^{-3}) (Pa)	Δ shear modulus (10^3) (Pa)
Slippery surface	NPA-L	F1	-54	265	-0.068	0.006	0.61
	1-LMPEC-NPB-L	F2	-47	225	-0.853	0.049	5.26
	1-LMPEC-NPA-L	F3	-44	179	-7.799	0.264	43.28
	PLGA	F4	-30	161	3.699	0.331	26.23
	752peg5000	F5	-9.9	342	-0.713	0.022	0.52
	502peg2000	F6	0.1	291	2.307	0.089	1.64
	502peg5000	F7	6.1	286	-0.35	0.01	2.50
	R/DNA	F8	20.2	149	6.514	0.15	12.14
Proteolytic Eenzyme	PLGA-TRY	E9	-27.4	432	-2.121	0.103	5.63
	PLGA-BRO	E10	-22.4	352	-10.355	0.488	68.65
	PLGA-PAP	E11	-20.3	303	-3.274	0.114	7.41
	R/DNA/PB	E12	18.6	121	6.116	0.378	84.84
Thiomer	CSSH/DNA	T13	1.1	141	6.623	0.22	11.59
	CS-TGA/D/DNA	T14	2.8	167	6.352	0.343	36.21
	CS-MPA3/DNA	T15	4.8	140	5.711	0.051	11.85
	CS-NAC/D/DNA	T16	6.2	156	3.703	0.026	57.29
SNEDDS	SNEDDSa	S17	0.2	35	6.233	0.56	0.17
	SNEDDSb	S18	-0.1	45	2.610	0.464	30.03
	SNEDDSc	S19	0.1	40	-2.135	0.489	42.04
	SNEDDSb(UNA)	S20	-22	139	-0.702	0.047	3.78
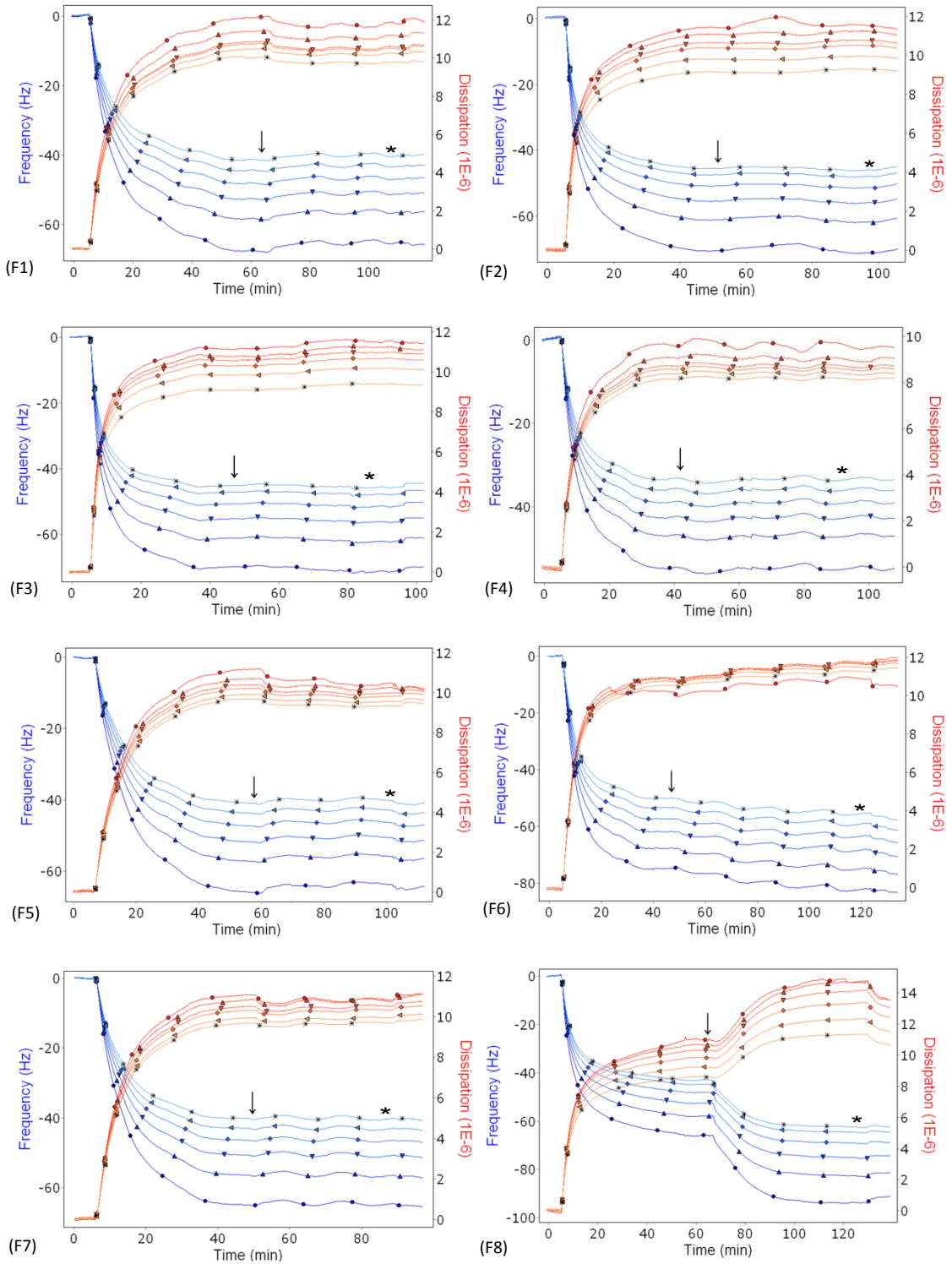
Fig. 2.9. Changes in frequency (Δf) and dissipation (ΔD) with time, blue line and red line, respectively, were recorded with QCM-D for interactions between NPGM with 8 particles, which were prepared by slippery surface strategy. The 3rd (●), 5th (▲), 7th (▼), 9th (♦), 11th (◄), and 13th (✳) overtones are shown. Arrow and star indicate the addition of particles and the rinsing with buffer, respectively.

(E9) (E10) (E11) (E12)
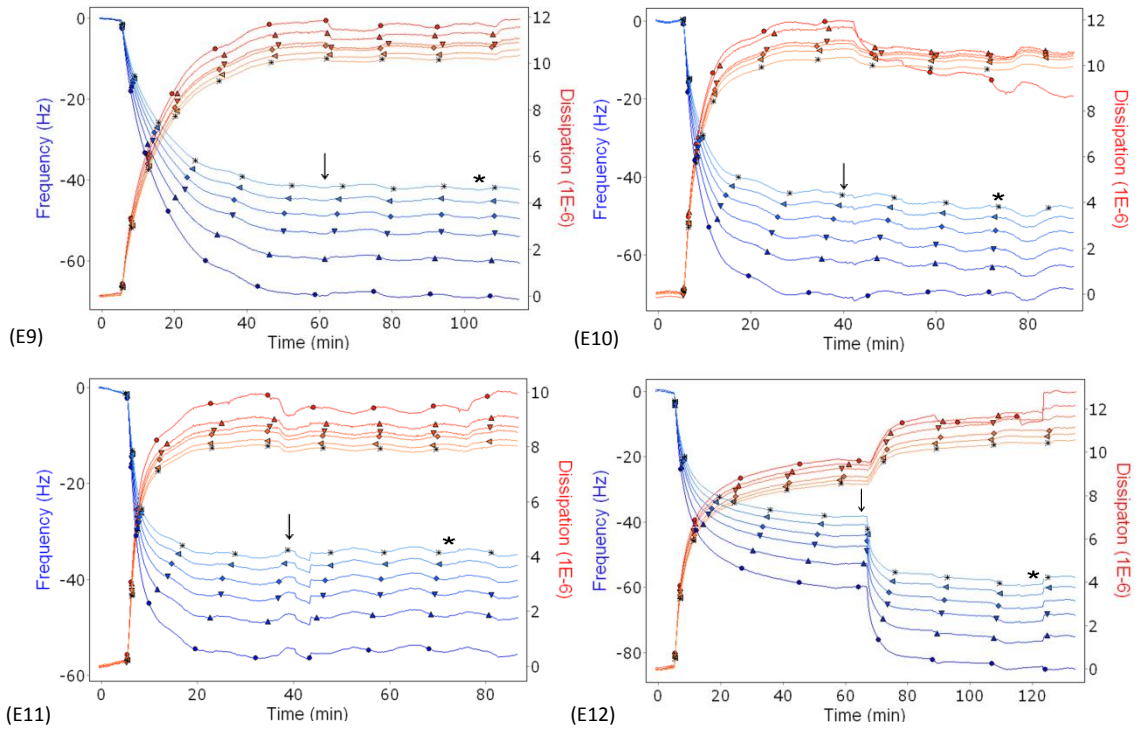
Fig. 2.10. Changes in frequency (Δ*f*) and dissipation (Δ*D*) with time, blue line and red line, respectively, were recorded with QCM-D for interactions between NPGM with 8 particles, which were prepared by proteolytic enzyme strategy.

(T13) (T14) (T15) (T16)

Fig. 2.11. Changes in frequency (Δ*f*) and dissipation (Δ*D*) with time, blue line and red line, respectively, were recorded with QCM-D for interactions between NPGM with 8 particles, which were prepared by thiomer strategy. .
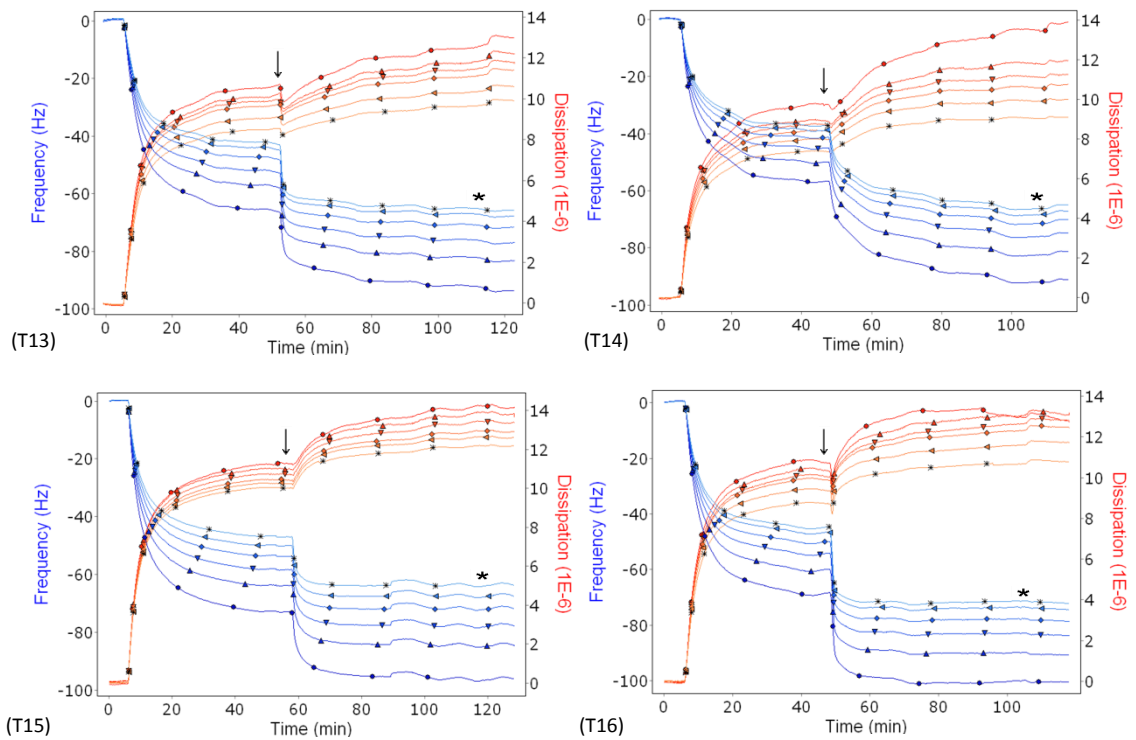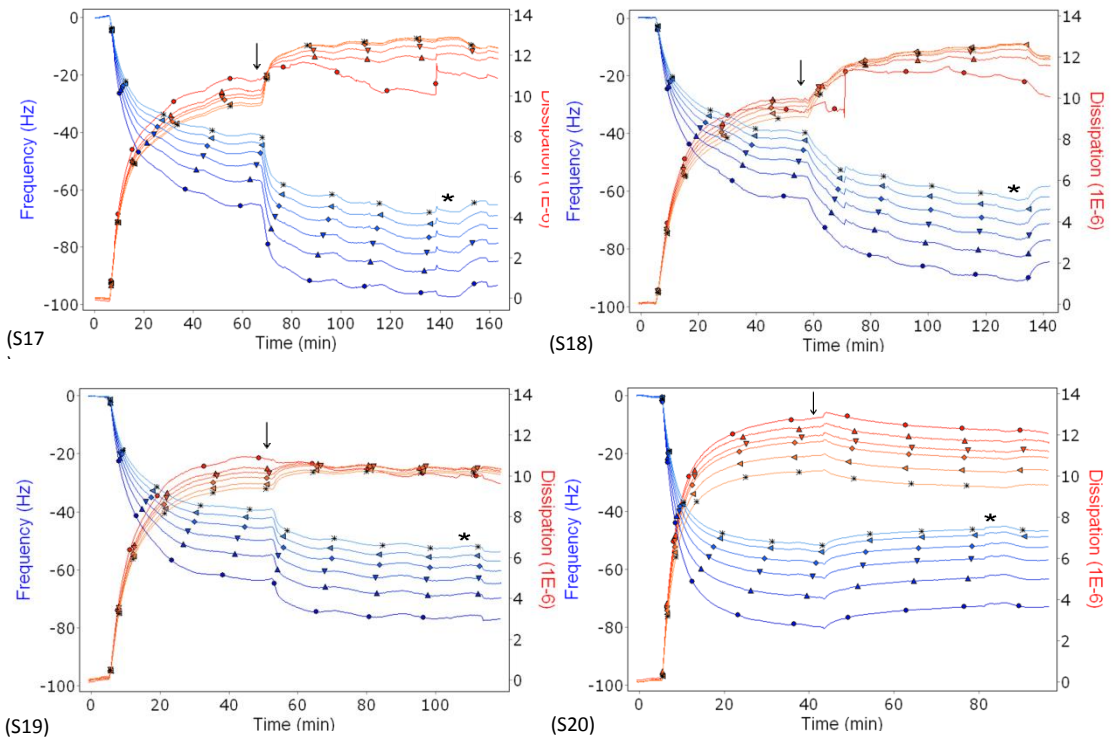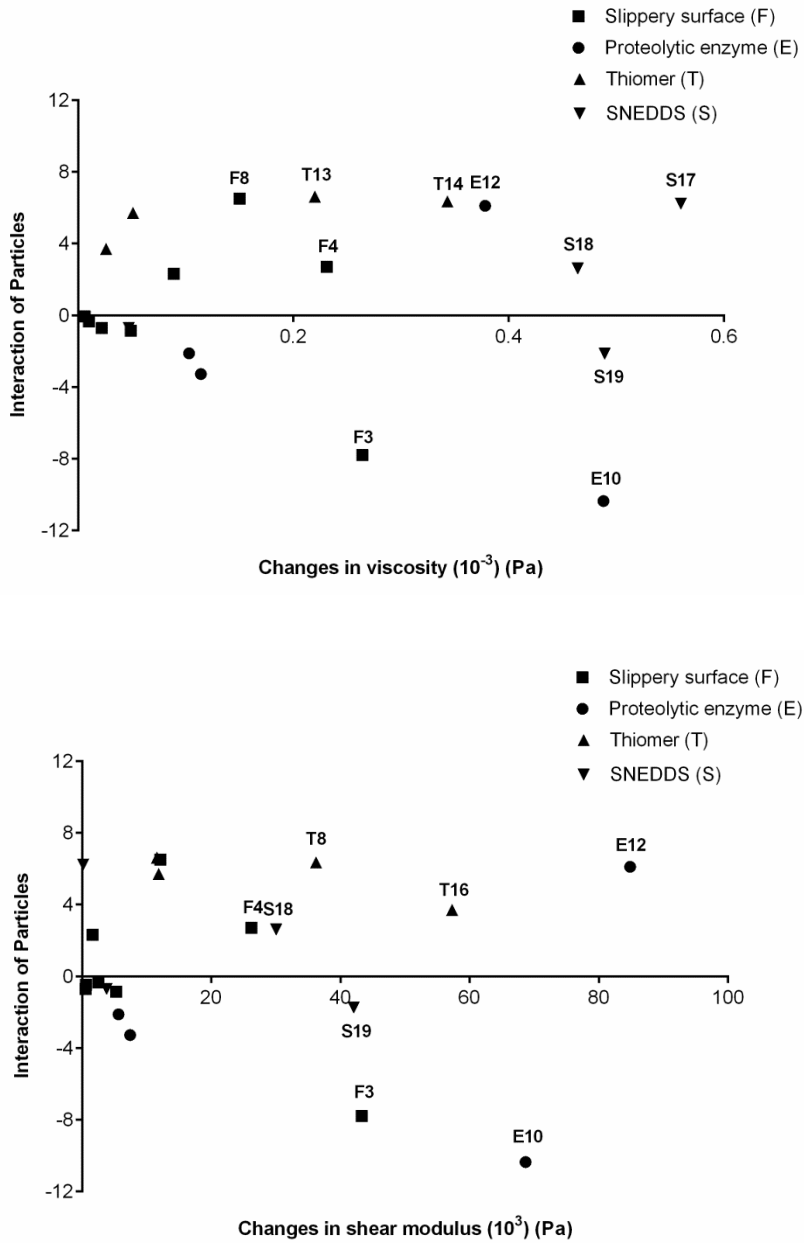
49

Fig. 2.12. Changes in frequency (Δf) and dissipation (ΔD) with time, blue line and red line, respectively, were recorded with QCM-D for interactions between NPGM with 8 particles, which were prepared bySNEDDS strategy.

Fig. 2.13. Relationship between interactions of particles with NPGM to their viscoelastic properties. (A) changes in viscosity; (B) changes in shear modulus.

2.5. Concluding remarks

For the first time, this study reports the interaction of mucoadhesive polymers with a NPGM layer, which was extracted from porcine stomach without enzymatic hydrolysis, using a developed QCM-D technique. As expected, due the net negative charge of the mucin layer, cationic polymers were significantly adsorbed onto the negative charged NPGM layer, but there was no interaction of anionic polymers to NPGM. In addition, the layer of cationic polymers-NPGM was dramatically increased in flexibility. In contrast, all polymers were unstably and successively adsorbed onto the precoated CPGM layer. The results presented in this study prove that the adsorption shape and viscoelastic behaviour of NPGM is clearly different to those of CPGM, thus it is recommended to use NPGM for interactions between mucin and either polymers or nanoparticles. More importantly, the developed QCM-D method is able to discriminate the partial permeation of the polymers into the mucin. It should be noted that when permeation is produced, D rapidly decreases and then increases, and then remains constant. The study of the change in the viscoelastic properties of the mucin using the D plot could give insight on the mechanisms of the interaction between polymers and mucin layers.

Thereafter, we investigated the combined properties between mucoadhesion and permeability of thiolated chitosans and their complexes with the NPGM layer using QCM-D technique. In parallel, the influence of pH buffer on the viscoelastic properties was examined. The higher the pH, the polymers and complexes bearing with thiol groups led to strong immobilization onto the NPGM layer. In all thiolated chitosan polymers, there were observed a small permeation and a significant adsorption with NPGM. Thiolated chitosan with low content of thiol groups showed the highest permeability among the polymers tested, and it was employed for further DNA carriers. These results support that these combined properties are strongly dependent on the content of the thiol groups. The changes in f and D of both TCD/DNA and TCE/DNA complexes showed the similar trend for those of thiolated chitosan, which was employed for the formulation of complexes. Unlike polymers, interestingly, there was obtained D accompanied with spreading overtones of complexes, resulting in that the movements of the transported particles was clearly observed into the NPGM layer.

Lastly, a set of different nanoparticles, coming from EU-project partners, was monitored using the QCM-D model. There were observed no interaction of highly negatively charged nanoparticles with NPGM while there were clearly shown the adsorption of highly positively charged nanoparticles. Similar trends of changes in f and D for polymers were shown previously. However, these results are not in accordance with those obtained by multiple particle tracking (MPT) technique. To better understand how nanoparticles may interact with the NPGM layer, the changes in thickness, viscosity and shear modulus of the layer of particles with NPGM were calculated, and these data were interpreted by comparison with the monitoring results described above.

This Chapter might provide that the QCM-D technique would be a promising method to monitor the interaction of polymers and particles with NPGM. Besides, this work may give that the novel formulation of TCL/PBAE/DNA complexes still required to improve the permeability through the mucin layer. More importantly, this formulation for mucosal delivery systems of macromolecular drugs must have high transfection efficiency. In fact, we evaluated and observed very low transfection efficiency of this formulation (data not shown). Therefore, in the next chapter, we will attempt to develop and optimize a novel formulation of DNA delivery systems.

2.6. References

Ahmed, A.; Yadav, H.K.; Lakshmi, S.V.; Namburi, B.V.; Shivakumar, H.G. *Curr. Drug. Ther.* **2012**, *7*, 42-55.

Allen, A. *Structure and function of gastrointestinal mucus*, in: L.R. Johnson (Ed.), Physiology of the Gastrointestinal Tract, vol. 1, Raven Press, New York, NY, USA, **1981**, pp. 617–639.

Anderson, D.G.; Akinc, A.; Hossain, N. Langer, R. *Mol. Ther.* **2005**, *11*, 426-434.

Andrews, G.P.; Laverty, T.P.; Jones, D.S. *Eur. J. Pharm. Biopharm.* **2009**, *71*, 505-518.

Bansil, R.; Turner, B.S. *Curr. Opin. Colloid. Interface Sci.* **2006**, *11*, 164-170.

Barrantes, A.; Arnebrant, T.; Lindh, L. *Colloids Surf A Physicochem Eng Asp.* **2014**, *442*, 56-62.

Belegrinou, S.; Mannelli, L.; Lisboa, P.; et al. *Langmuir* **2008**, *24*, 7251-7261.

Bernkop-Schnürch, A. *Drug Discovery Today: Technologies* **2005**, *2*, 83-87.

Bernkop-Schnürch, A. *Adv. Drug Deliv. Rev.* **2005**, *57*, 1569-1585.

Buschmann, M.D.; Merzouki, A.; Lavertu, M.; Thibault, M.; Jean, M.; Darras, V. *Adv. Drug Deliv. Rev.* **2013**, *66*, 1234-1270.

Celli, J.P.; Turner, B.S.; Afdhal, Z.H.; Ewoldt, R.H.; Mckinley, G.H.; Bansil, R.; Erramilli, S. *biomacromolecules* **2007**, *8*, 1580-1586.

Chayed, S.; Winnik, F.M. *Eur. J. Pharm. Biopharm.* **2007**, *65*, 363-370.

Choi, J.; Rubner, M.F. *Macromolecules* **2005**, *38*, 116-124.

Cone, R.A. Mucus. In Mucosal Immunology; 2nd edn; Orga PL, ed. Academic Press:San Diego, **1999**, 43–64.

Cone, R.A. *Adv. Drug Deliv. Rev.* **2009**, *61*, 75-85.

Dixon, M. *J. Biomol. Tech.* **2008**, *19*, 151-158.

Du, L.; Gao, Y.; Yang, H.; Li, Y.; Zhuang, Q.; Jia, H.; Nie, G.; Liu, Y. *RCS Advances* **2013**, *3*,

14791-14797.

Dünnhaput. S.; Kammona, O.; Waldner, C.; Kiparissides, C.; Bernkop-Schnürch, A. *Eur. J. Pharm. Biopharm*. **2015**, 96, 447-453.

Edelstein, M.L.; Abedi, M.R.; Wixon, J.; Edelstein, R.M. *J. Gene. Med*. **2004**, *6*, 597-602

Elfinger, M.; Pfeifer, C.; Uezguen, S.; Golas, M.M.; Sander, B.; Maucksch, C.; Stark, H.; Aneja, M.K.; Rudolph, C. *Biomacromolecules* **2009**, *10*, 2912-2920.

Feiler, A.A.; Sahlholm, A.; Sandberg, T.; Caldwell, K.D. *J. Coll. Int. Sci*. **2007**, *315*, 475-481.

Fogg, F.J.J.; Hutton, D.A.; Jumel, K.; Pearson, J.P.; Harding, S.E.; Allen, A. *Biochemical Journal* **1996**, *316*, 937-942.

Fredriksson, C.; Kihlman, S.; Rodahl, M.; Kasemo, B. *Langmuir* **1998**, *14*, 248-251.

Gao, Y.; Xu, Z.; Chen, S.; Gu, W.; Chen, L.; Li, Y. *Int. J. Pharm*. **2008**, *359*, 241-246.

Grabovac, V.; Guggi, D.; Bernkop-Schnurch, A. *Adv. Drug Deliv. Rev.* **2005**, *57*, 1713-1723.

Green, J.J.; Shi, J.; Chiu, E.; Leshchiner, E.S.; Langer, R.; Anderson, D.G. *Bioconjug. Chem.* **2006**, *17*, 1162-1169.

Green, J.J.; Zugates, G.T.; Tedford, N.C.; Huang, Y.H.; Griffith, L.G.; Lauffenburger, D.A.; Sawicki, J.A.; Langer, R.; Anderson, D.G. *Adv. Mater.* **2007**, 1*9,* 2836-2842.

Grießinger, J.; Dunnhaupt, S.; Cattoz, B.; Griffiths, P. et al. *Eur. J. Pharm. Biopharm.* **2015**, *96*, 464-476.

Halthur, T.J.; Arnebrant, T.; Macakova, L.; Feiler, A. *Langmuir* **2010**, *26*, 4901-4908.

Hanes, J. *Adv. Drug Deliv. Rev.* **2009**, *61*, 73-74.

Hook, F.; Rodahl, M.; Brzezinski, P.; Kasemo, B. *Langmuir* **1998**, *14*, 729-734.

Introduction and QCM-D Theory Q-Sense Basic Training **2006**, April 4-5,

Kast, C.E.; Bernkop-Schnürch, A. *Biomaterials* **2001**, *22*, 2345-2352.

Keeney, M.; Ong, S.G.; Padilla, A.; Yao, Z.; Goodman, S.; Wu, J.C.; Yang, F. *ACS Nano* **2013**, *7*, 7241-7250.

Kocevar-Nard, J.; Kristl, J.; Smid-Korbar, J. *Biomaterials* **1997**, *18*, 677-681.

Lai, S.K.; Wang, Y.Y.; Hanes, J. *Adv. Drug Deliv. Rev.* **2009**, *61*, 158-171.

Lee, M.K.; Chun, S.K.; Choi, W.J.; Kim, J.K.; Choi, S.H.; Kim, A.; Oungbho, K.; Park, J.S.; Ahn, W.S.; Kim, C.K. *Biomaterials* **2005**, *26*, 2147–2156.

Lens, P.; Moran, A.P.; Mahony, T.; Stoodley, P.; O'Flaherty, V. *Biofilms in Medicine*, Industry and Environmental Bitoechnolgy, IWA Publishing, London, UK, **2003**, pp. 450-460.

Lu, N.Y.; Yang, K.; Li, J.L.; Yuan, B.; Ma, Y.Q. *Biochim. Biophys. Acta.* **2013**, *1828*, 1918-1925.

Ludwig, A. *Adv. Drug Deliv. Rev.* **2005**, *57*, 1595-1639.

Mao, S.; Leong, K. *Adv. Drug Deliv. Rev*. **2010**, *62*, 12-27.

Marriott, C.; Gregory, N.P. *Mucus Physiology and Pathology*, Bioadhesive Drug Delivery Systems, in: V. Lenaerts, Gurny (Eds.), CRC, Boca Raton, **1990**, pp. 1–24.

Marx, K.A. *Biomacromolecules* **2003**, *4*, 1099-1120.

Mastorakos, P.; de Silva, A.L.; Chisholm, J.; Song, E.; Choi, W.K.; Boyle, M.P.; Morales, M.M.; Hanes, J.; Suk, J.S. *Proc. Nati. Acad. Sci. USA*. **2015**, *112*, 8720-8725.

Mazzarino, L.; Coche-Guerente, L.; Labbe, P.; Lemos-Senna, E.; Borail, R. *J. Biomed. Nanotechnol.* **2013**, *9*,1-8.

Mihai, M.; Stoica, G.I.; Popescu, I.; Fundueanu, G. Poly. *Letters* **2011**, *5,* 506-515.

Mikos, A.G.; Peppas, N.A. *STP Pharma*. **1986**, *2*, 705–716

Mintzer, M.A.; Simanek, E.E. *Chem. Rev*. **2009**, *109*, 259-302.

Molino, P.J.; Hodson, O.M.; Quinn, J.F.; Wetherbee, R. *Biomacromolecules* **2006**, *7*, 3276-3282.

Nagi, T. *J. Control. Release* **1985**, *2*, 121-134.

Nagi, T. Machida, Y. *Pharm. Int.* **1985**, *6,* 196-200.

Oh, S.; Borros, S. *Eur. J. Pharm. Biopharm*. **2015**, *96*, 477-483.

Olsson, A.L.J.; Quevedo, I.R.; He, D.; Basnet, M.; Tufenkji, N. *ACS Nano* **2013**, *7*, 7833-7843.

O´Sullivan, C.K.; Guilbault, G.G. *Biosensors and Bioelectronics* **1999**, *14*, 663-670.

Pearson, J.P.; Allen, A.; Hutton, D.A. *Rheology of Mucin*, In: Corfield, A.P, ed. Glycoprotein Methods and Protocols: The Mucins. Humana Press Inc, **2000**, pp. 99-109.

Rodahl, M.; Hook, F.; Krozer, A.; Brzezinski, P.; Kasemo, B. *Rev. Sci. Instrum*. **1995**, *66*, 3924–3929.

Rodahl, M.; Kasemo, B. *Rev. Sci. Instrum*. **1996**, *67*, 3238-3241.

Rodahl, M.; Hook, F.; Fredriksson, C.; Keller, C.A.; Krozer, A.; Brzezinski, P.; Voinova, M.; Kasemo, B. *Faraday Discuss* **1997**, *107*, 229–46.

Sandberg, T.; Carlsson, J.; Ott, M.K. *J. Mater. Sci. Mater. Med*. **2009**, *20*, 621-631.

Sato, T.; Ishii, T.; Okahata, Y. *Biomaterials* **2001**, *22*, 2075-2080.

Schuster, B.S.; Ensign, L.M.; Allan, D.B.; Suk, J.S.; Hanes, J. *Adv. Drug. Deliv. Rev*. **2015**, *91*, 70-91.

Segovia, N.; Dosta, P.; Cascante, A.; Ramos, V.; Borrós, S. *Acta Biomaterialia* **2014**, *10*, 2147-2158.

Serra, L.; Doménech, J.; Peppas, N.A. *Eur. J. Pharm. Biopharm.* **2009**, *71*, 519–528.

Shahnaz, G.; Vetter, A.; Barthelmes, J.; Rahmat, D.; Laffleur, F.; Iqbal, J.; Schlocker, W.;

Dünnhaput, S.; Augustijns, P.; Bernkop-Schnürch, A. *Int. J. Pharm.* **2012**, *428*, 164-170.

Shi, B.; Shen, Z.; Zhang, H.; Bi, J.; Dai, S. *Biomacromolecules* **2012**, *13*, 146-153.

Shu, X.Z.; Zhu, K.J. *Eur. J. Pharm. Biopharm.* **2002**, *54*, 235–243.

Sigurdsson, H.H.; Loftsson, T.; Lehr, C.M. *Int. J. Pharm.* **2006**, *325*, 75-81.

Stephenson, J. *J. Am. Med. Assoc.* **2001**, *285*, 2570.

Svensson, O.; Arnebrant, T. *Curr. Opin. Colloid Interface Sci.* **2010**, *15*, 396-405.

Taylor, C.; Allen, A.; Dettmar, P.W.; Pearson, J.P. *Biochim. Biophys. Acta.* **2004**, *1674*, 131-138.

Taylor, C.; Pearson, J.P.; Draget, K.I.; Dettmar, P.W.; Smidsrod, O. *Carbohydrate Polymers* **2005**, *59*, 189-195.

Thompson, C.J.; Tetley, L.; Uchegbu, I.F.; Cheng, W.P. *Int. J. Pharm.* **2009**, *376*, 45-55.

Thornton, D.J.; Sheehan, J.K. *Proc. Am. Thorac. Soc.* **2004**, *1*, 54–61.

Voinova, M.V.; Rodahl, M.; Jonson, M.; Kasemo, B. *Phys. Scr.* **1999**, *59*, 391–396.

Voinova, M.V.; Jonson, M.; Kasemo, B. *Biosens and Bioelectronics* **2002**, *17*, 835–41.

Wang, D.; Ye, J.; Hudson, S.D.; Scott, K.C.K.; Lin-Gibson, S. *J. Colloid Interf. Sci.* **2014**, *417*, 244-249.

Wang, X.; Iqbal, J.; Rahmat, D.; Bernkop-Schnürch, A. *Int. J. Pharm.* **2012**, *438*, 217-224.

Wiecinski, P.N.; Metz, K.M.; Mangham, A.N.; Jacobson, K.H.; Hamers, R.J.; Pedersen, J.A. *Nanotoxicology* **2009**, *3*, 202-214

Woetrz, C.; Preis, M.; Breitkreutz, J.; Kleinebudde, P. *Eur. J. Pharm. Biopharm.* **2013**, *85*, 843-853.

Xu, K.; Ouberia, M.M.; Welland, M.E. *Biomaterials* **2013**, *34*, 1461-1470.

Yin, H.; Kanasty, R.L.; Eltoukhy, A.; Vegas, A.J.; Dorkin, J.R.; Anderson, D.G. *Nat. Rev. Ganet.* **2014**, *15*, 541-55.

DEVELOPMENT OF NANOCARRIERS

WITH ENHANCED STABILTIY

AND TRANSFECTION EFFICIENCY

Patent derived from this work:

Oh, S. and Borrós. S. UKIPO Patent P065490GB (Patent application: 2015; Patent concession: 2016).

Publications derived from this work:

Oh, S. et al., 'Effect of biopolymers-modified poly(β-amino ester)/DNA complexes on stability and transfection efficiency. 1. Sugar and its derivatives' (Submitted to *Biomacromolecules* 2016).

Oh, S. et al., 'Effect of biopolymers-modified poly(β-amino ester)/DNA complexes on stability and transfection efficiency. 2. Chitosan of different molecular weights' (Submitted to *Biomacromolecules* 2016).

3.1.   Introduction

As described in Chapter 1, the main objective of this Thesis is to develop and optimize the innovative strategies for efficient delivery systems of macromolecules to mucosal tissue. The macromolecules such as peptides, proteins and nucleic acids (DNA and RNA) are very unstable that need to be protected from degradation in the biological environments. Moreover, their efficiency is highly limited by their ability to cross biological barriers and reach the target site (Janes *et al.*, 2001). Thus, the development of appropriate vehicles to deliver the macromolecules through those barriers has been attracting a great deal of interest in the pharmaceutical industry. As such, mucosal delivery of the macromolecular drugs is evidently dependent on design and development of nanoparticle-based drug delivery systems. In this Chapter, we focus on developing the novel drug delivery systems capable of both retaining stability in the physiological solution and high transfection efficiency.

Drug delivery system is defined as a formulation or device that enables the introduction of a therapeutic substance in the body and improves its efficacy and safety by controlling the rate, time, and place of release of drugs in the body (Jain 2008). The term therapeutic substance applies to an agent such as gene therapy that will induce in vivo production of the active therapeutic agent. Gene therapy can fit in the basic and abroad definition of the drug delivery system (Jain 2008). Over the past two decades, the clinical application of gene therapy for treating or preventing a wide range of both inherited and acquired disease has been investigated (Ginn *et al.*, 2013). However, as discussed above, the lack of safe and efficient vectors to deliver polynucleotides such as DNA and RNA remains the principal drawback for the success of gene therapy (Luo and Saltzman 2000; Kamimura *et al.*, 2011; Miele *et al.*, 2012; Mastorakos *et al.*, 2015). Given the large size and the negative charge of large molecules, their delivery is typically mediated by carriers or vectors (Yin *et al.*, 2014).

There are two approaches to gene delivery: viral and non-viral. Viral vectors are the more conventional approach because viruses have evolved to infect cells with high efficacy (Green *et al.*, 2008). In fact, ~70% of gene therapy clinical trials carried out so far have used modified viruses to delivery genes (Yin *et al.*, 2014). However, clinical trials have underscored the safety risks, such as immunogenicity and integration into the host genome which may lead to insertional mutagenesis (Robbins and Ghivizzani 1998; Walther and Stein 2000; Themis *et al.*, 2005; Basarkar and Singh 2007; Huang and Kamihira 2013). For this reasons, new attention has been focused on non-viral approaches for gene therapy as these have the potential to overcome many of the inherent challenges of viral vectors. Use of non-viral vectors in clinical trials increased from 2004-2014 while that of viral vector saw significant decrease (Ramamoorth and Narvekar 2015).

Non-viral vectors have been widely proposed for gene transfer because of safety and simplicity of the production procedure (Edelstein *et al.*, 2004; Green *et al.*, 2007 and 2008; Elfinger *et al.*, 2009). Numerous biomaterials have been studied as potential non-viral gene delivery vectors to enable improved DNA stability and uptake including lipids, polysaccharides, cationic polymers, and dendrimers (Merdan *et al.*, 2002; Putnam 2006). These non-viral vectors either bind to, complex with, or encapsulate DNA into systems that are comparatively easier to manufacture and scale-up than viral systems, although they are lower efficacy relative to viral vectors (Green *et al.*, 2008). For efficient gene delivery, several important steps must be overcome. Scheme 3.1 represents the mechanism of non-viral gene delivery, including: i) the non-viral vectors must be bind to and condense or encapsulate DNA, ii) facilitating cellular uptake of the DNA-containing particle, iii) the particles are inside the cell but is in the endosomal compartment instead of the cytoplasm, iv) the particle trafficks through the cell, v) vectors escape from endosome, vi) DNA dissociation from vector and nuclear translocation for gene expression to occur (Green *et al.*, 2008; Jin *et al.*, 2014; Yin *et al.*, 2014).
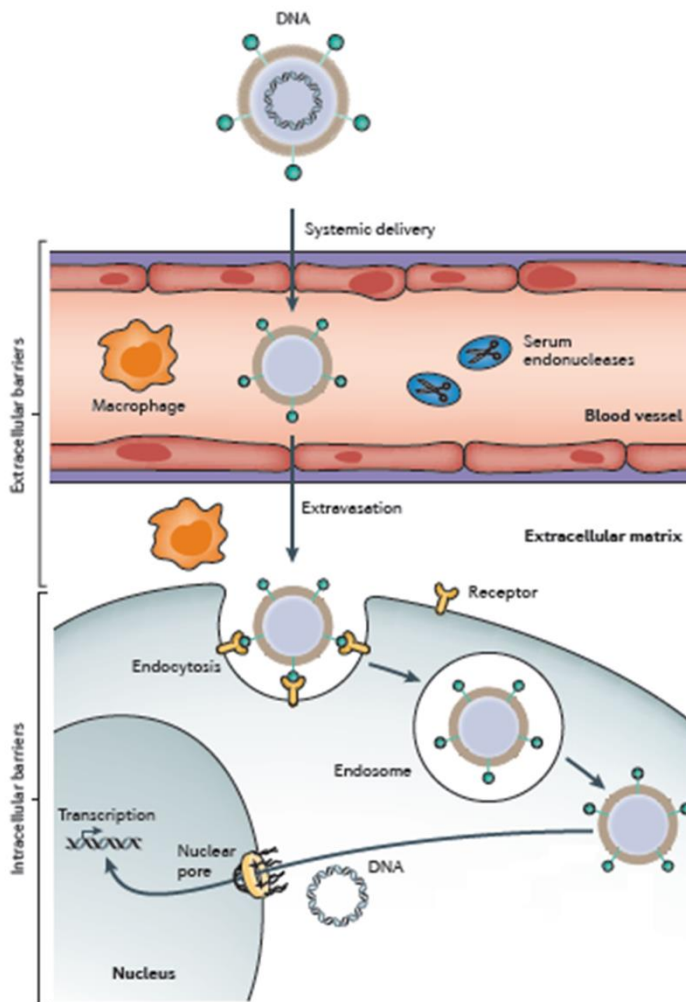

Scheme 3.1. Mechanism of non-viral gene delivery (Yin *et al.*, 2014).

Typical non-viral vectors include lipid, such as 2,3-dioleyloxy-N-(sperminecarboxamido)ethyl-N,Ndimethyl-1-propanaminium trifluoroacetate (DOSPA) and dioleyl phosphatidylethanolamine (DOPE) and (Simoes *et al.*, 2005), or cationic polymers, such as poly(L-lysine) (PLL) and polyethylenimine (PEI) (Scheme 3.2) (Eliyahu *et al.*, 2005). Recently, there have been extensively investigated non-viral gene vectors composed of plasmid DNA (pDNA) and cationic polymers are promising vector systems for gene delivery due to capability of condensing anionic DNA (Yin *et al.*, 2014).
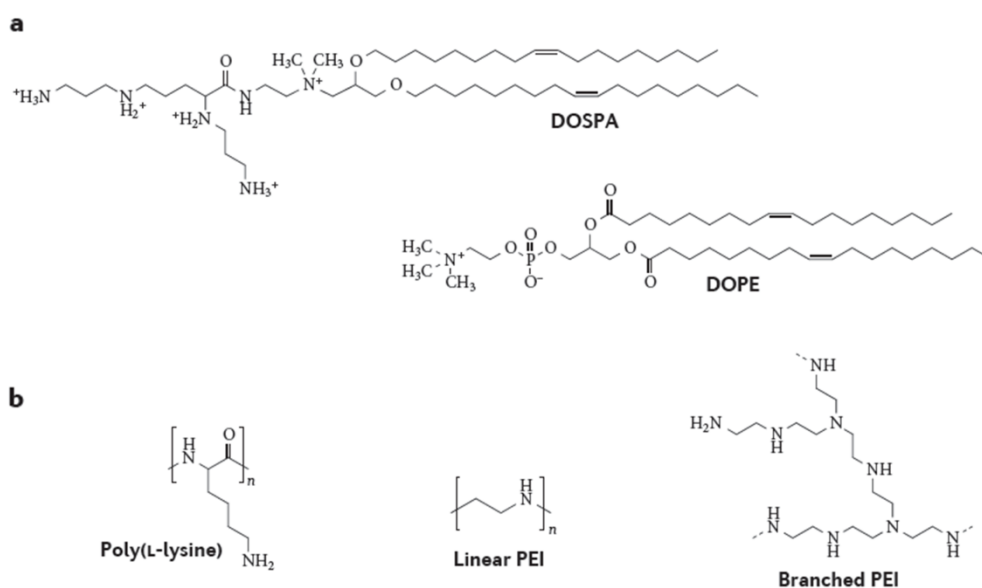
Scheme 3.2. Scheme of chemical structures of typical non-viral vectors. a) Cationic lipids of DOSPA and a neutral lipid of DOPE. b) Cationic polymers of PLL y PEI (Yin *et al.*, 2014).

Among cationic polymers, poly(β-amino ester)s (PBAEs) are a promising class of polymeric non-viral gene delivery vectors due to i) their ease of synthesis by Michael addition of amine monomers to diacrylates (Lynn *et al.*, 2000-2001; Akinc *et al.*, 2003; Anderson *et al.*, 2003-2004) (Scheme 3.3), ii) ability to condense DNA into small and stable nanoparticles (Luten *et al.*, 2008), iii) ability to buffer the endosome and facilitate endosomal escape (Anderson *et al.*, 2005; Green *et al.*, 2008), iv) biodegradability via hydrolytically degradable ester groups, v) low cytotoxicity compared with some other cationic polymers, and vi) relatively high efficacy in vitro and in vivo (Vuorimaa *et al.*, 2011; Sunshine *et al.*, 2012; Eltoukhy *et al.*, 2012; Sabzevari *et al.*, 2013; Mastorakos *et al.*, 2013). Chemical modification at the termini of PBAEs with primary amines has been shown to produce higher transfection efficacy with low toxicity than commercial transfection agents such as Lipofectamine 2000 (DOSPA:DOPE AT 3:1 molar ratio) (Green *et al.*, 2008) and PEI (Zugates *et al.*, 2007).
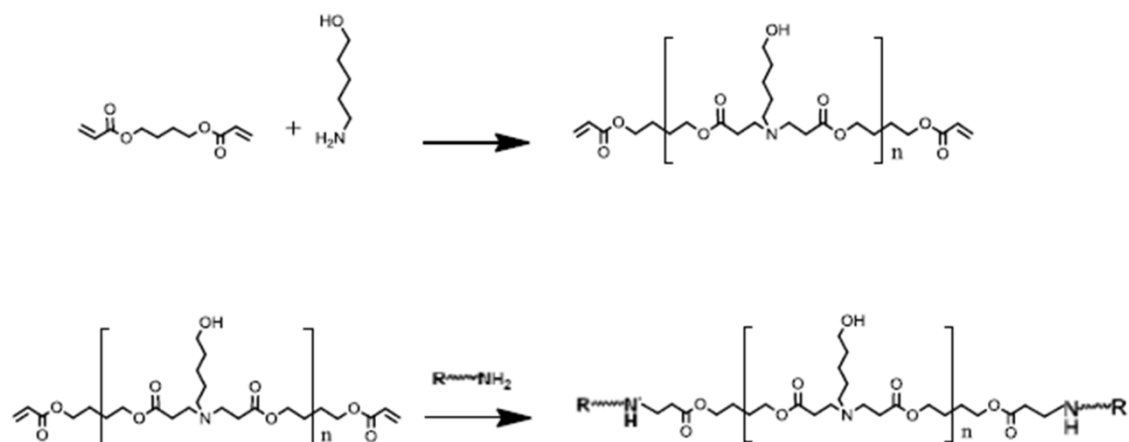
Scheme 3.3. Synthetic scheme of end-modified poly(β-amino ester)s (Green *et al.*, 2008).

In a previous study, our group reported the development of a novel PBAEs chemically modified at one or both termini with oligonucleotides which shown to be more biocompatible to cells than commercial transfection agents (Segovia *et al.*, 2014; Dosta *et al.*, 2015). Moreover, the new non-viral vectors resulted to present high gene expression levels and to be able to deliver polynucleotides directly into cells in vitro without the need for ligand-mediated mechanisms. However, there is a fundamental limitation of using these vectors in clinical trials. Most of these delivery systems are likely to be degraded or aggregated in endonucleases in physiological fluids and the extracellular space (Scheme 3.1). Thus, an emerging need still exists for improvement of stability of current nanoparticles, which could be used to transfect efficiently polynucleotides, to their biological functions (Pavlin and Bregar 2012, Xu *et al.*, 2015). If the drug is prematurely release, even if the nanoparticles reach its target, there will no longer be a therapeutic benefit (Patri *et al.*, 2005). In addition, the poor stability of polymeric gene delivery systems in an aqueous medium represents a major barrier to the development of these systems as marketable products (Anchordoquy *et al.*, 1999). Regarding these concerns, further an enhancement of stability in physiological condition is required for their practical use.

In this Chapter, we have developed the novel nanoparticles capable of being stable in the physiological solution for use in delivery of active agents comprising PBAEs and additives that are sugar and sugar alcohol, and chitosan.

Nature offers creative and sustainable alternatives to promote nanosystem stabilization, through the use of carbohydrate (Sizovs *et al.*, 2014). Thus, carbohydrate-modified delivery systems (such as sugar or chitosan-based modification) have become promising for clinical application (Ma *et al.*, 2015). Here we start by introducing the properties

and use of sugar and its derivatives for gene delivery systems, then address those of chitosan.

Sugar and its derivatives (the so-called sugars), which are common functional entities in biological systems, have been focused on developing new strategies to fabricate nanoconstructs for gene delivery systems (Abdelwahed *et al.*, 2006; Katti *et al.*, 2009; Noga *et al.*, 2014). Most of the materials under investigation were stabilized by surface coatings with sugars in order to enhance the stability of nanoparticles (Sameti *et al.*, 2003). Sugars are used as cryoprotectants and/or lyoprotectants and to increase stability on storage using freeze-drying, which is widely applied for stabilizing various pharmaceutical products (Tang and Pikal 2008). These systems are of current interest as a drug delivery system for gene materials including DNA and/or preventing aggregation (Tseng *et al.*, 2007; Wada *et al.*, 2011; Mancini *et al.*, 2012).
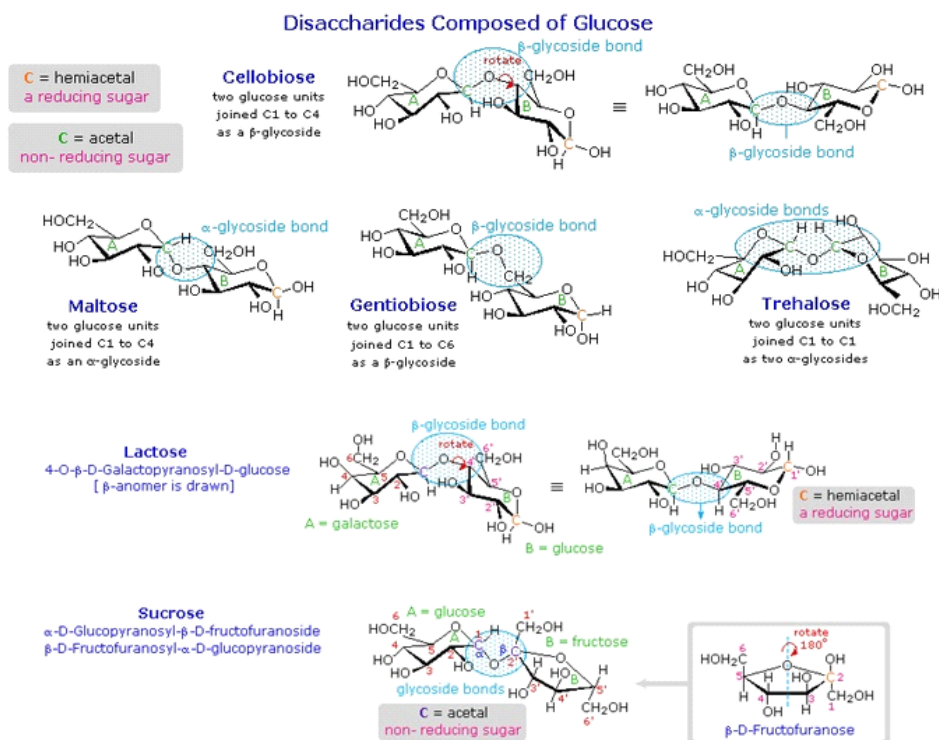
Scheme 3.4. Chemical structures of disaccharides composed of glucose. The individual glucopyranose rings are labeled A and B, and the glycoside bonding is circled in light blue. (Farmer and Emeritus. http://chemwiki.ucdavis.edu/Organic_Chemistry/Carbohydrates/Disaccharides).

Among the sugars reported in the literature, trehalose, sucrose and mannitol are the most popular, which are also called stabilizers (Kim *et al.*, 1998; Wang 2000; Zilles *et al.*, 2008; Agirre *et al.*, 2014). Trehalose and sucrose are disaccharides. Several disaccharides

composed of two glucose units are shown in Scheme 3.4. Both trehalose and sucrose: 1) protect proteins during both freezing and dehydration; 2) are non-reducing; 3) tend to remain amorphous during lyophilization; and 4) have been used in approved parenteral therapeutic products (Carpenter and Manning 2002; Jovanovic *et al.*, 2006). However, trehalose demonstrates unique stability, it is not easily hydrolyzed by acid, even at high temperature (Kumar and Roy 2008; Teramoto *et al.*, 2008; Ohtake and Wang 2011). This unusual property of trehalose has been attributed to its exceptionally large hydrated volume and the ability of this carbohydrate to modify the solvation layer around various biomolecules (Srinivasachari Li *et al.*, 2006). The use of reducing disaccharides, such as maltose or lactose, was restricted because they can degrade proteins between carbonyls of the sugar and free amino groups on the protein (Hageman 1992; Li *et al.*, 1996). (D-) Mannitol is a naturally occurring 6-carbon sugar alcohol or polyol. Mannitol is a unique cryoprotectant that crystallizes in frozen aqueous solutions (Al-Hussein and Gieseler 2012; Lindholm *et al.*, 2014). On the other hand, mannitol has the lowest aqueous solubility among the evaluated cryprotectants and this is due to ability to form intramolecular hydrogen bonding at the expense of solute-water hydrogen bonding (Alkilany *et al.*, 2014).

As described above, to date, sugars have been widely applied as nanoparticle stabilizers during the freeze-drying process. According to this conception, sugars are of current interest for their ability to enhance stability of nanoparticles in an aqueous medium before freeze-drying. Bae *et al.* have demonstrated that it is possible to utilize sugars, as dispersing and stabilizing agents for colloidal particles (Bae *et al.*, 2006). Srinivasachari et al. have shown that step-growth cationic polymers containing alternating units of ethyleneamine and sugars in their backbones yield high cellular delivery efficiency of pDNA (Srinivasachari *et al.*, 2006). Recently, Sizovs and coworkers have reported the synthesis of a methacrylamido trehalose monomer, its subsequent polymerization to poly(methacrylamidotrehalose) or ''poly(trehalose)'', followed by a synthetic procedure of reversible addition-fragmentation chain transfer (RAFT). The complexes comprising of these new polymers and siRNA were shown to promote stabilization and effective gene delivery (Sizovs *et al.*, 2014).

In parallel with sugars-modified delivery systems, there have been also investigated chitosan-modified formulations. Chitosan is typically obtained by the deacetylation of chitin, which is the second most abundant natural biopolymer found in the exoskeleton of crustacean (Du *et al.*, 2013). Chitosan is a linear polysaccharide, composed of glucosamine and N-acetyl-D-glucosamine units linked by β (1-4) glycosidic bonds (Scheme 3.5) (Rinki *et al.*, 2009). The content of glucosamine is called the degree of deacetylation. In fact, in a general way, it is considered that when the degree of deacetylation of chitin is higher than about 50% (depending on the origin of the polymer and on the distribution of acetyl groups along the chains), it becomes soluble in an aqueous acidic medium, and it is named chitosan (Alves and Mano 2008). Every deacetylated subunit of chitosan contains a primary amine group with a

pKa value of around 6.3-6.5 (Li *et al.*, 1996). Thus chitosan is generally soluble in acidic media, at pH below 6. The solution properties of chitosan depend on its molecular weight, degree of deacetylation and ionic strength of the solution.
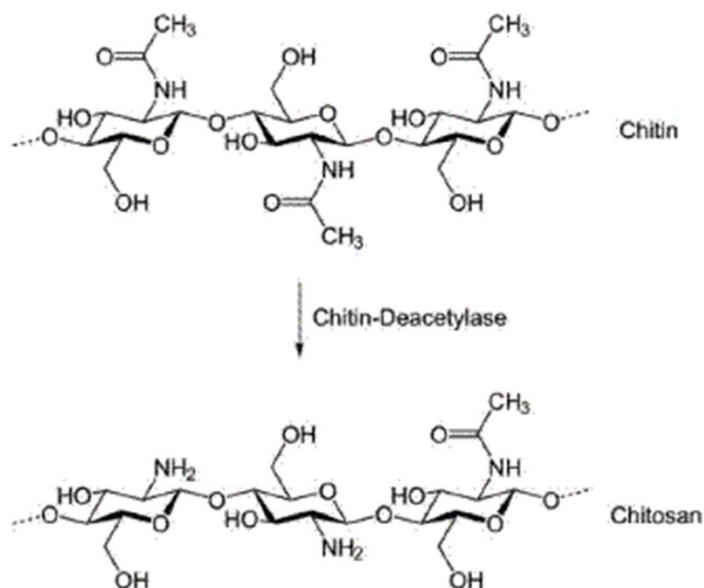
Scheme 3.5. The chemical structure and deacetylation process of chitin to chitosan (Rinki *et al.*, 2009).

Among non-viral vectors, chitosan has been considered to be a potential gene carrier candidate because it is known as a natural-derived, biocompatible, biodegradable, high stability, and low toxic material with high cationic charge potentials (Borchard *et al.*, 2001; Shu *et al.*, 2002; Agnihotri *et al.*, 2004; Alves *et al.*, 2008; de la Fuente *et al.*, 2010; Shi *et al.*, 2012; Bernkop-Schnürch and Dunnhaüpt 2012). At acidic pH, below the pKa, these primary amines in the chitosan backbone become positively charged (Kumar *et al.*, 2004). These protonated amines enable chitosan to bind to negatively charged nucleotides via an electrostatic interaction, which leads to the spontaneous formation of nano-size complexes (polyplexes) in the aqueous milieu. (Mao *et al.*, 2010).

However, as mentioned above, chitosan is only soluble in few dilute acid solutions, thus limits its applications (Sugimoto *et al.*, 1998). The acid solubility is explained by the protonation of the free amino group, characteristic in the chitosan, which change from NH_2 to NH_3^+, whereas in alkaline condition, the hydro solubility is due to the formation of carboxylate, from the introduced carboxylic group (Pillai *et al.*, 2009). Another drawback of chitosan is its strong condensation with DNA, resulting in the formation of highly stable particles. This condensation prevents DNA dissociation to the nucleus, which ultimately precludes the translation of DNA (Koping-Hoggard *et al.*, 2004; Toh *et al.*, 2010). It is well known that the

binding affinity of chitosan for DNA, the stability and the transfection efficiency of the chitosan/DNA is significantly influenced by formulation-related parameters, such as the molecular weight of chitosan, degree of deacetylation, stoichiometry of the chitosan/DNA complex (N/P ratio, charge ratio of amine (chitosan) to phosphate (DNA), plasmid concentration, serum concentration, pH of the transfection medium, cell type and so on (Sato *et al.*, 2001; Hoggard *et al.*, 2001; Romoren *et al.*, 2003; Kiang *et al.*, 2004; Strand *et al.*, 2005; Liu *et al.*, 2005; Lavertu *et al.*, 2006; Kumirska *et al.*, 2011). According to the investigation of the effect of these parameters, several groups have developed and optimized the chitosan/DNA complexes, resulting in improvement of transfection efficiency (Mao *et al.*, 2010; Buschmann *et al.*, 2013; Hu *et al.*, 2014). Nevertheless, enhancing transfection efficiency of chitosan-based complexes still remains a challenge for non-viral gene delivery. Therefore, in this Chapter, chitosan or sugar has been employed as a coating agent to shield on the surface of PBAE/DNA complexes, which already shown high gene transfection efficiency. We expect that a design and development of the the novel nanocarriers comprising PBAE/DNA and the additives may enhance the stability in physiological conditions while maintaining high transfection efficiency.

3.2. Aim and scope of this Chapter

The first aim of this Chapter is to enhance the stability of novel nanocomplexes comprising oligopeptide-modified PBAEs and sugars while maintaining high transfection efficiency. Trehalose, sucrose and mannitol have been chosen for this study as described above the most popular stabilizers. Two procedures of a simple formulation of the PBAE/DNA complexes based on the sugars were carried out and demonstrated the effect of these agents on the nanocomplexes stability and gene transfection efficiency. In a first approach, the sugar-coated PBAE/DNA complexes have been formulated in trehalose, sucrose or mannitol at various weight percentages, which was expressed relative to the total weight of the PBAEs. In a second approach, the sugar-modified complexes have been formulated by mixing DNA and a simple polymer mixture of the sugar or sugar alcohol and PBAEs. The PBAE/sugar polymer mixture was prepared by the same method for synthesis of PBAEs in the presence of trehalose, sucrose or mannitol at 10, 20 and 30% relative to the weight of the polymers. Prior to this study, we investigated the effect of experimental conditions such as ionic strength of medium, incubation time and temperature on the stability and transfection of unmodified PBAE/DNA complexes and the optimal method found here was used for further work described above. The results show a noticeable enhancement of stability and transfection efficiency of the sugar-modified PBAE/DNA complexes at optimum conditions, which are used for further studies.

The second aim of the Chapter is to develop a novel carrier based on a combination of PBAE and chitosan polymers. We propose that this system may integrate their advantages with minimizing their drawback, thus leading to enhanced transfection efficiency as well as stability. To approach this aim, chitosan has been employed as a coating agent to cover on the surface of PBAE/DNA complexes. We expect that the small amount of chitosan may improve the stability of complexes whilst maintaining their high transfection level. Here two different molecular weights of chitosan were chosen for this study as it showed higher gene expression in the literature: Chitosan with a 22 kDa (CS) and a 60-120 kDa (CSM) (Sato *et al.*, 2001; Mao *et al.*, 2010). All coating complexes tested exhibit a noticeable enhancement of stability. High transfection efficiency is sustained when prepared with CS while PBAE/DNA/CSM showed a significant decrease in transfection efficiency with increasing amount of CSM.

To achieve these aims the following steps will be developed:

- To synthesize arginine-terminated poly(β-amino ester)s (R).

- To investigate the influence of R/DNA formation factors such as ionic strength of medium, incubation time and temperature on the stability and transfection efficiency.

- To develop the sugar-coated R/DNA complexes, which were formulated in trehalose, sucrose and mannitol at 10, 20, 30 and 40 %, relative to the weight of the PBAEs.

- To synthesize PBAEs in the presence of trehalose, sucrose and mannitol (TreR, SucR and MntR) at 10, 20 and 30%, relative to the weight of the PBAEs, and to develop the sugar-modified R/DNA complexes.

- To develop the chitosan-coated R/DNA complexes, which were formulated with a coating of 0.17, 0.33, 0.67, 1.33 and 2.67 wt% of chitosans (CS and CSM).

- To evaluate stability, transfection efficiency and cell viability of the developed nanocomplexes described above.

3.3.   Experimental section

3.3.1. Materials

H-Cys-Arg-Arg-Arg-NH$_2$ (CR3) was obtained from GL Biochem Ltd. (Shanghai, China). Chitosan with a medium molecular weight (CSM, 60-120 kDa and deacetylation degree, DDA, 60%) and low molecular weight (CS, 22 kDa and DDA, 85%) were purchased from Sigma Aldrich and Fluka (Vienna, Austria), respectively. All chemicals were obtained from Sigma Aldrich and used as received, unless otherwise stated. All regents were analytical grade and used without further purification. Plasmid DNA encoding green fluorescent protein (pmaxGFP, 3486 bp) was purchased from Amaxa Inc. (Gaithersburg, MD, USA). COS-7 cells were obtained from ATCC (Manassas, VA) and cultured in DMEM (Gibco) supplemented with 10% fetal bovin serum (FBS), 1% Glutamine and 1% Streptomycin/Penicillin (complete DMEM).

3.3.2. Synthesis of polymers

3.3.2.1. Acrylate-terminated PBAEs

Acrylate-terminated PBAE was synthesized as the method described previously (Green *et al.*, 2007). In brief, acrylate-terminated C32 was obtained by the addition of 5-amino-1-pentanol (3.44 g, 33 mmol) to 1,4-butanediol diacrylate (8.81 g, 40 mmol) at a 1.2:1 molar ratio of amine monomer to diacrylate monomer under stirring at 90ºC for 24 h. Then it was cooled to room temperature to form a transparent yellow viscous solid, C32, dissolved in DMSO to 100 mg/ml, and stored at -20 ºC until further use.

3.3.2.2. Oligopeptide-terminated PBAEs

The procedure of synthesis has been previously described in detail in our research group (Segovia *et al.*, 2014). Oligopeptide-modified PBAEs were synthesized by end-modification of acrylate-terminated C32 with thiol-terminated oligopeptide at a 1:2.5 molar ratio. Briefly, C32 (150 mg, 0.07 mmol), CR3 (115 mg, 0.18 mmol) and DMSO (3 mL) were placed in Teflon-lined screw cap vials and stirred at room temperature for 24 h. Tri-arginine end-modified PBAE polymer (R) was purified by precipitation in diethyl ether/acetone (7:3 v/v) for twice and dried under vacuum. Dried polymers were finally dissolved at 100 mg/ml in DMSO and stored at -20 ºC until further use.

3.3.2.3. MntR, SucR and TreR

The R polymer was prepared in the presence of mannitol, sucrose or trehalose to form

MntR, TreR, or SucR, respectively. The procedure was as follows: C32 (75 mg, 0.035 mmol) and CR3 (55 mg, 0.09 mmol) were dissolved in DMSO (1.5 ml) and placed in Teflon-lined screw cap vials. Then, 10, 20, or 30% (w/w) of mannitol, sucrose or trehalose were added in each vial and stirred at room temperature for 24 h. The final products were purified and prepared by same procedure as described above for oligopeptide-modified PBAE polymers.

3.3.3. Characterization of polymers

The chemical structures of these functional polymers, C32, R, MntR, SucR and TreR were characterized by ^{1}H-NMR spectroscopy. ^{1}H-NMR spectra were acquired at 25 ºC on a Varian NMR instrument operating at 400 MHz with samples dissolved in deuterated dimethyl sulfoxide (d6-DMSO) or methanol-d4 and using tetramethylsilane (TMS) as internal reference. 8-10 mg of sample dissolved in 1 ml of solvent was used for ^{1}H-NMR. Gel permeating chromatogram was carried out at 35 ºC with a refraction-index detector. C32 was chromatographed with 0.05 M tetrahydrofuran (THF) using a GPC KF-603 column with a flow rate of 0.5 ml/min. Chromatograms were calibrated against polystyrene monodisperse standards.

3.3.4. Formulation of complexes

3.3.4.1. Conventional method for formation of PBAE/DNA complexes

Complexes were formulated by mixing polymer and pGFP (plasmid green fluorescent protein) in a weight ratio of 50:1. In the conventional method of PABE/DNA formulation (Nathay), DNA solution was diluted to 60 µg/ml in a final concentration of ~5 mM sodium acetate (NaAc) buffer at pH 5.2 and PBAE stock solution (100 mg/ml) in DMSO was diluted in the same buffer. 100 µl of diluted PBAE solution (3 mg/ml) was added to 100 µl of DNA, and mixed with vortex for a few seconds and incubated at 37 ºC for 30 min.

3.3.4.2. Further method for formulation of PBAE/DNA complexes

DNA stock solution was diluted to 60 µg/mL in a final concentration of 11-12 mM of NaAc buffer at pH 5.2. Polymer stock solutions (for example R, MntR, TreR or SucR; 100 mg/ml in DMSO) were diluted in the same buffer. 100 µl of diluted DNA was added into 100 µl of PBAE solutions (3 mg/ml), and mixed with vortex for a few seconds and incubated at room temperature for 10 min.

3.3.4.3. Formulation of sugar-coated PBAE/DNA complexes

Complexes of R and DNA prepared according to the method described above were coated with 10, 20 20, 30 and 40 weight percent of mannitol, sucrose or trehalose by incubation at room temperature for 10 min with a solution containing the relevant amount of mannitol, sucrose or trehalose.

3.3.4.4. Formulation of chitosan-coated PBAE/DNA complexes

Complexes were formulated by mixing polymer and pGFP (plasmid green fluorescent protein) in a weight ratio of 50:1, which is an optimal ratio as described in our previous research (Segovia *et al.*, 2014). The R polymer solution and pGFP solution were diluted to 25 mM sodium acetate (NaAc, pH 5.2) to a final concentration of 6 mg/ml and 0.06 mg/ml, respectively. To prepare CS solution, 16 mg of chitosan was suspended in 0.5% acetic acid (10 ml) and left overnight under stirring at room temperature. The CS stock solution (1.6 mg/ml) was adjusted at pH 5 with 0.1 M NaOH and filtered through 0.2 µm. The CS stock solution was diluted with 25 mM NaAc buffer in a proportion ranging from 0.17 to 2.67 weight percent relative to the weight of PBAE when mixed with the PBAE solution. 50 µl of diluted chitosan solution was then added to 50 µl of diluted PBAE solution, and mixed with vortex. 100 µl of GFP (60 µg/mL in the same buffer) was then added to the mixture solution, mixed slightly with vortex and incubated at room temperature for 10 min. As control, R/DNA complexes were formulated by same process as described for complexes coated with CT above. In this case, 0.06 mg/ml of pDNA was mixed into 3 mg/ml of R solutions.

3.3.5. Characterization of *complexes*

The particle size, zeta potential, and stability of complexes were determined, diluted in phosphate-buffered saline (PBS) at pH 7.4, by DLS using a Zetasizer Nano ZS (Malvern Instruments, Ltd., UK) at 25 ºC. Each experiment was carried out in triplicate and the means ± SD result was reported.

Complex formulation was evaluated by agarose gel electrophoresis. R/DNA complexes modified with or without chitosan were loaded onto a 0.8% agarose gel in Tris-Acetate-EDTA (TAE) buffer containing ethidium bromide (1µg/ml). The samples were run on the gel at 120 V for 80 min (Apelex PS305, France) and visualized using UV irradiation.

3.3.6. In vitro transfection and flow cytometry

Cellular transfection was carried out using pDNA plasmid in COS-7 cells. Cells were seeded at a density of 1×10^5 cells/well in 96-well plates and incubated overnight prior to performing the transfection experiments. PBAE/DNA complexes were prepared as described above (PABE:DNA =wt:wt, 50:1). Complexes were diluted in serum-free DMEM medium and added to cells at a final plasmid concentration of 0.3 μg pDNA/well. Briefly, 33 μl of PBAE/DNA complexes were diluted into 450 μl of serum-free DMEM medium and cells were washed once with PBS. Then, 150 μl of the resulting solutions were added to each well, achieving a final concentration of 0.3 μg DNA/well. Cells were incubated for 3 h at 37 ºC in 5% CO_2 atmosphere. Subsequently, cells were washed once with PBS, and complete DMEM medium was added. Cells were harvested after 48 h and analysed by flow cytometry (BD LSRFortessa cell analyzer) for GFP expression. GFP expression was compared against negative control (NC, untreated cells) and unmodified R/DNA as a positive control.

For effect of factors on transfection efficiency of R/DNA complexes, GeneJuice (Merck KGaA, Germany) was used as a positive control at a dose of 2.88 μl of GeneJuice and 0.3 μg DNA/well.

3.3.7. Cytotoxicity assay

MTS assay (CellTiter 96® AQueous One Solution Cell Proliferation Assay, Promega Corporation, USA) was used to evaluate the viability of COS-7 cells transfected with complexes at 48 h after post-transfection, as instructed by the manufacturer. At 48 h after transfection, the medium was removed, cells were washed with PBS and complete medium supplemented with 20% MTS reagent (v/v) was added. Cells were incubated at 37 °C and the absorbance was measured at 490 nm using a microplate reader (Elx808 Biotek Instruments Ltd, USA). Cell viability was expressed as a relative percentage compared with untreated cells.

3.4. Results and discussion

3.4.1. Synthesis and characterization of polymers

As discussed in 3.1, poly(β-amino ester)s (PBAEs), which is a specific class of cationic polymers, are promising for delivery systems of macromolecular drugs. In this section, we synthesized conventional acrylate and oligopeptide-terminated PBAEs and the novel polymer blending of PBAE/sugar.

3.4.1.1. C32 PBAEs

Firstly, we synthesized acrylate-terminated C32 PBAEs that was followed via two-steps procedure. Scheme 3.6A shows that Acrylate-terminated C32 intermediate polymer was obtained in the first step by conjugate addition of amines to acrylate groups. The chemical structure and the purity of C32 were assessed by ^{1}H-NMR spectroscopy (Fig. 3.1A). GPC analysis showed that the resulting C32 polymer was obtained with weight-average molecular weights of 2100 and number-average molecular weights of 1320, relative to polystyrene standard. C32 polymer was further modified with oligopeptide moieties to obtain a new family of oligopeptide-terminated PBAEs.

^{1}H NMR of C32 (400 MHz, d$_6$-DMSO, TMS), *δ* (ppm): 6.3–6.4 (m, C**H$_2$**CHCOOCH$_2$CH$_2$–), 6.1–6.2 (m, CH$_2$C**H** COOCH$_2$CH$_2$–), 5.9 (m, C**H$_2$**CHCOOCH$_2$CH$_2$–), 4.3 (bs, –N(CH$_2$)$_5$O**H**), 4.1 (m, CH$_2$CHCOOC**H$_2$**CH$_2$–), 4.0 (bs, -N(CH$_2$)$_2$COOC**H$_2$**CH$_2$–), 3.4 (bs, –N(CH$_2$)$_4$C**H$_2$**OH), 2.6-2.7 (m, -COOCH$_2$C**H$_2$**N–), 2.3–2.5 (m,–COOC**H$_2$**CH$_2$N– and –NC**H$_2$**(CH$_2$)$_4$OH), 1.6 (bs, -N(CH$_2$)$_2$COOCH$_2$C**H$_2$**–), 1.2–1.4 (m, –NCH$_2$(C**H$_2$**)$_3$CH$_2$OH),
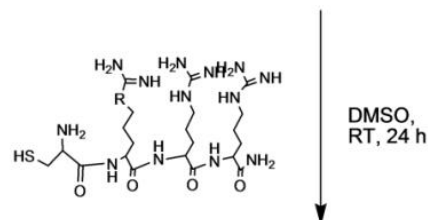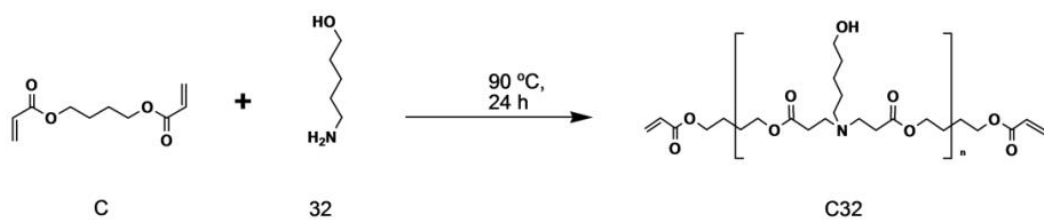
3.4.1.2. Tri-arginine end-modified PBAEs

As shown in Scheme 3.6B, oligopeptide-terminated PBAEs were obtained via addition of the thiol group of cysteine-terminate oligopeptides to the acrylate-terminated end-groups of C32 polymer. Oligopeptide-terminated PBAEs were characterized in terms of molecular structure by ^{1}H-NMR spectroscopy (Fig. 3.1B). The chemical structure of new oligopeptide-modified PBAEs was confirmed by the disappearance of acrylate signals and the presence of signals typically associated with amino acid moieties.
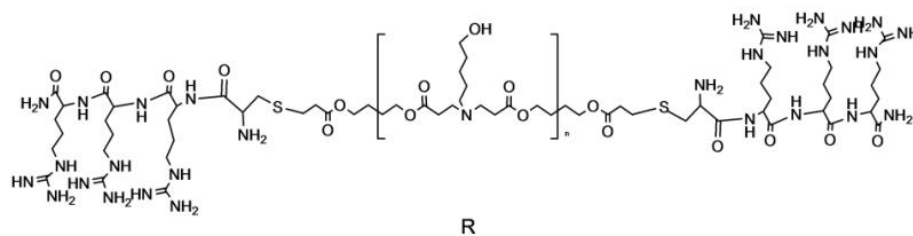
^{1}H-NMR of R (400 MHz, CD$_3$OD, TMS), δ (ppm): 4.45-4.35 (br, NH$_2$COC**H**NHCOC**H**NH- and COC**H**NHCOC**H**CH$_2$-), 4.15 (t, CH$_2$C**H$_2$**O), 3.56 (t, –N(CH$_2$)$_4$C**H$_2$**OH), 3.22 (br, NH$_2$C(NH)$_2$C**H$_2$**- and –N(CH$_2$)$_4$C**H$_2$**OH), 3.09 (br, CH$_2$C**H$_2$**N-), 2.85 (br, -C**H$_2$**SC**H$_2$**-), 2.78 (m, CH2C**H$_2$**N-), 2.67 (br, NH$_2$C(NH)$_2$C**H**-), 1.92 (m, NH$_2$C(NH)$_2$(CH$_2$)$_2$C**H$_2$**CH-), 1.75 (br, -OCH$_2$(C**H$_2$**)$_2$CH$_2$O), 1.57 (br, -N(CH$_2$)$_2$COOCH$_2$C**H$_2$**–), 1.3-1.4 (br, –NCH$_2$(C**H$_2$**)$_3$CH$_2$OH).
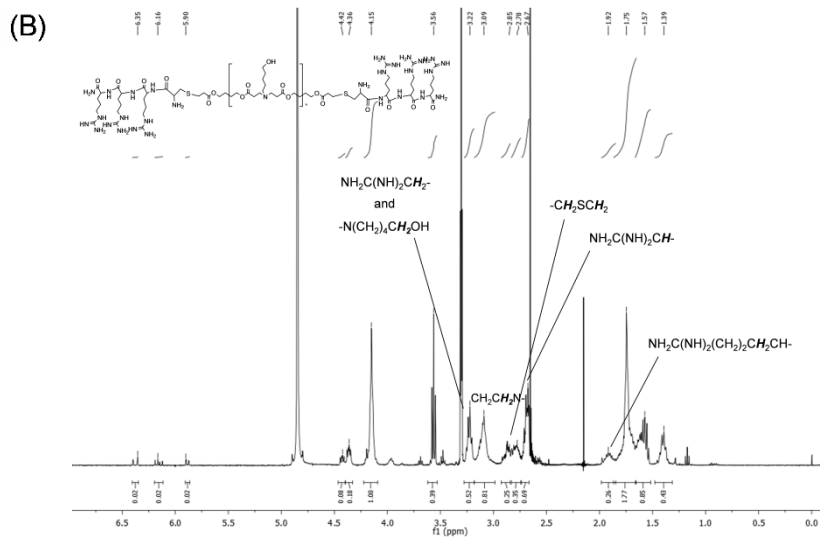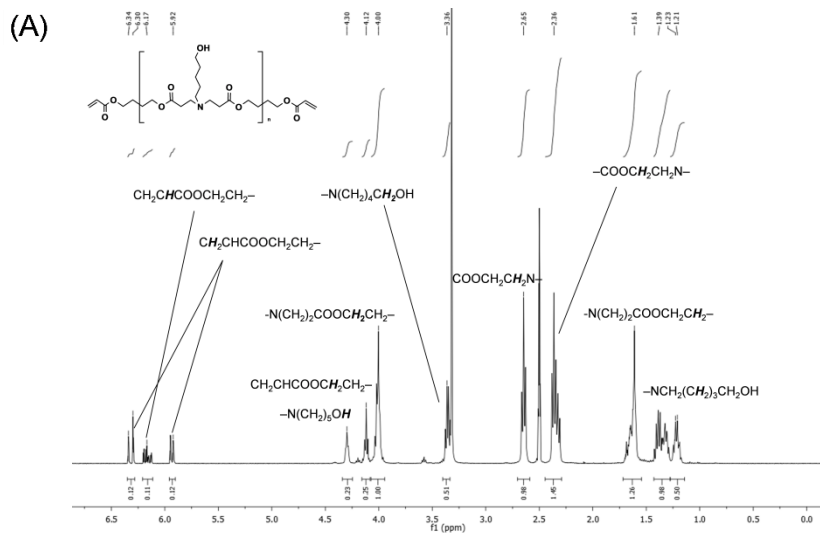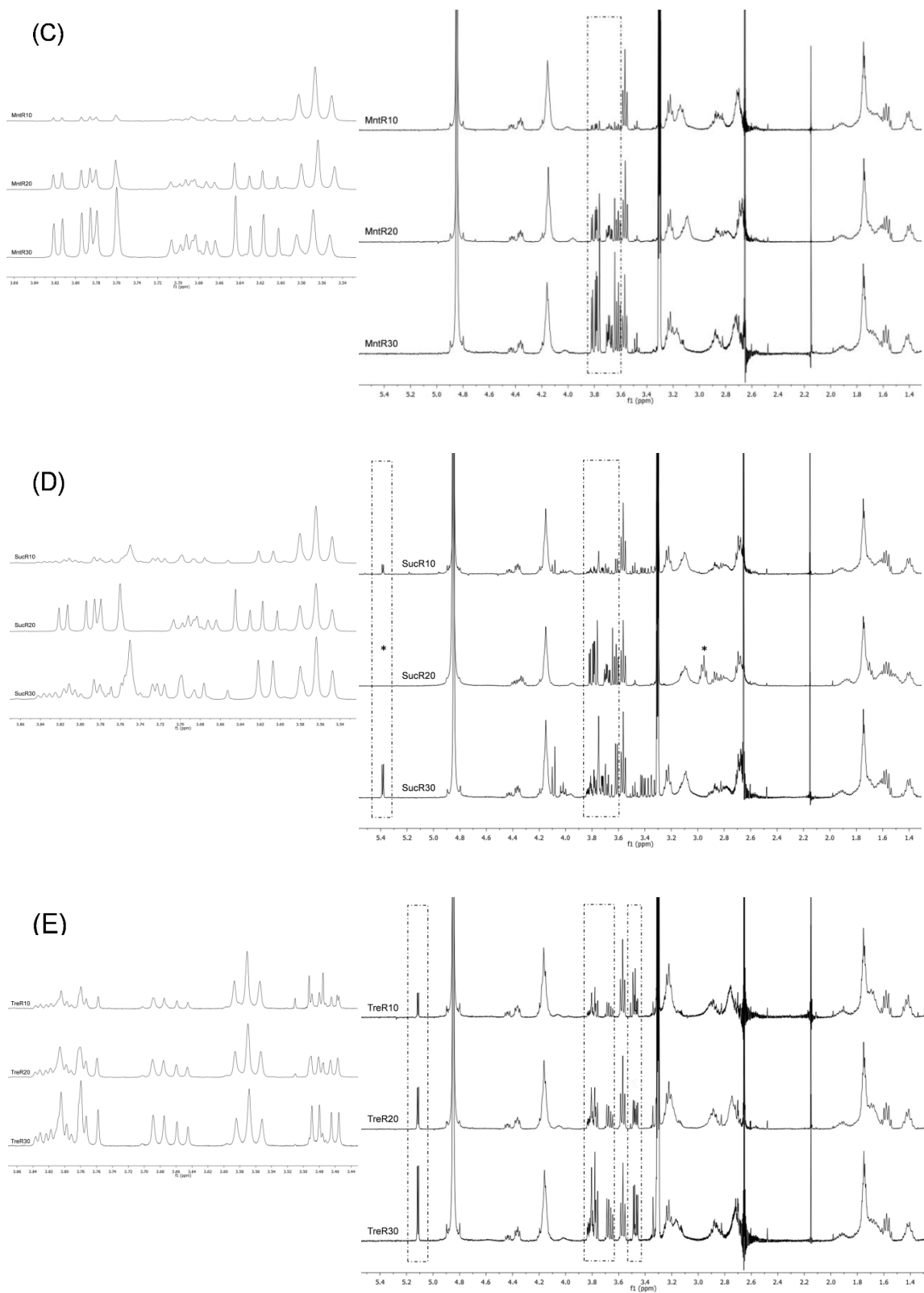
(A)

(B)

Scheme 3.6. Synthesis of end-modified poly(β-amino ester)s. (A) acrylated-terminated C32 polymer by 1.2:1, diacrylate:amine polymerization. (B) arginine end-modified PBAE polymers by 1:2.5, C32:oligopeptide polymerization.

(A)

(B)

Fig. 3.1. ^{1}H NMR spectrum of (A) acrylate-terminated PBAE and (B) oligopeptide-terminated PBAE; The ^{1}H NMR spectrum of the polymer mixture of (C) MntR, (D) SucR and (E) TreR.

3.4.1.3. Sugar/PBAEs blending

To develop the novel sugar-modified formulations, as described in 3.2, two procedures such as blending and coating strategies were conducted. For the blending approach, the sugar/PBAE mixture polymers were prepared before formulating nanoparticles. The polymer mixture (MntR, SucR or TreR) was obtained by simple mixing oligopeptide-modified PBAEs and sugar or sugar alcohol (Scheme 3.7). 10, 20, or 30% of mannitol, sucrose or trehalose was added prior to the polymerization step of oligopeptide-modified PBAE polymers. The chemical structure of all polymer mixtures was assessed by ^{1}H-NMR spectroscopy and confirmed by the presence of signals of both tri-arginine end-modified PBAEs and the agents (Fig. 3.1C-E). Interestingly, SucR20 showed the chemical shift of 2.9 ppm and the disappearance of glycosidic linkage signal of 5.4 ppm. It may be explained that 20% of sugar would be somewhat polymerized with the PBAEs.

i) MntR

ii) SucR

iii) TreR

i) mannitol   ii) sucrose   iii) trehalose
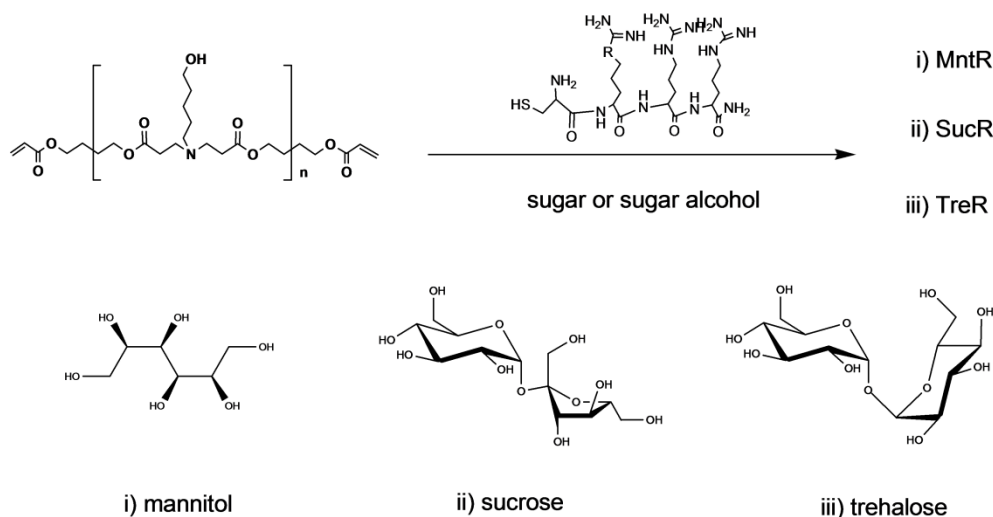
Scheme 3.7. Preparation of the polymer mixture: i) MntR; ii) SucR; iii) TreR

### 3.4.2. Factors affecting stability and in vitro transfection

The main challenge in this Chapter was to study and develop the novel nanoparticles capable of stability and transfection efficiency. Prior to approach this objective, we firstly focused on studying the experimental conditions to improve the conventional complexes nanoparticles. It is well known that cationic polymer/DNA complexes are vulnerable to external ionic strength, thus required for the formation of stable complexes (Kim *et al.*, 2004; Jeong *et al.*, 2011; Jonassen *et al.*, 2012). Consequently, the effect of the factors such as ionic strength and incubation conditions on the stability of complexes was investigated. (i) Preparation according to method described above (i.e. incubation at 37 °C for 30 min) with a final concentration of ~5mM sodium acetate; (ii) Preparation according to the same method but with a final concentration of 11-12mM sodium acetate and (iii) The complexes were prepared by different procedures (i.e. incubation at 37 ºC for 10 or 30 min, room temperature (RT) for 10 or 30 min) with a final concentration of 11-12mM sodium acetate. The stability of the complexes, diluted in PBS, was determined by DLS.

It should be noted that DNA stock solutions can be obtained at various concentrations while PBAE stock solutions can be obtained at a constant concentration of 100 mg/ml. However, an initial concentration of 25 mM NaAc buffer has been always applied for conventional formulation comprising of PBAE and DNA, inducing that there have obtained various size and zeta potential of these complexes. In other words, it is difficult to obtain reproducible formulations. As such, we expected that the factor of ionic strength between polymers and DNA may influence the various size and zeta potential of complexes. To explore the relationship between the final concentration of buffer solution and the stability of complexes, PBAE and DNA stock solutions were diluted in an initial concentration of buffers range up to 30 mM. The effects of ionic strength on the size of PABE/DNA complexes were studied and the results are shown in Fig. 3.2. The complexes at a final concentration of 11-12 mM of NaAc buffer were slightly smaller and much more stable than those in ~5 mM of NaAc. These results suggest that the final concentration of NaAc buffer affects the ionic strength of the complexes, and preparation of complexes in the presence of buffers at 11-12 mM significantly increases stability. On the other hand, the complexes at a final concentration of above 12 mM buffer showed slightly lower stability relative to those of 11-12 mM (data not shown). These indicate that the particle size may be dependent on the ionic strength of the medium concentration, resulting in that the physicochemical properties of complexes can be adjusted to a preferred value by changing the medium concentration. Thus, the final concentration of 11-12 mM of buffer was chosen and used for all further studies due to the highest stability of complexes.
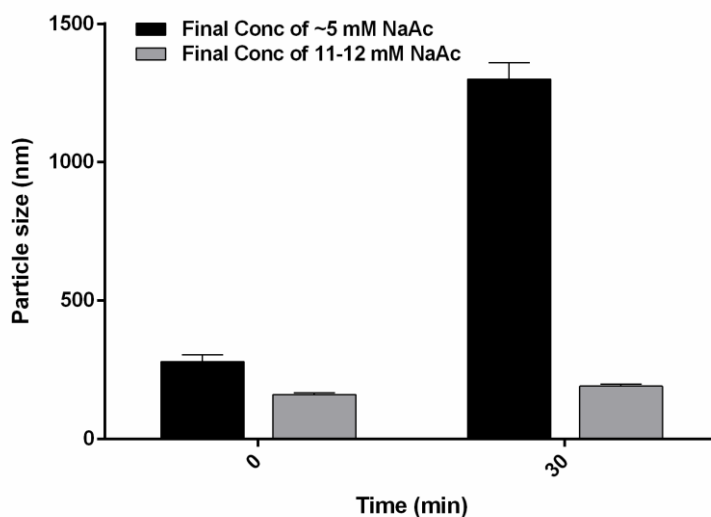
Fig. 3.2. The particle size of complexes in the presence of buffers of different ionic strength.

Thereafter, the influence of the incubation conditions was studied for the stability of complexes. The PBAE/DNA complexes were prepared by various procedures (i.e. incubation time and temperature) in the literature. In order to achieve the optimum formulation of complexes, indicating of the stable complexes in PBS, we studied the effects of the procedures on the stability of complexes. As shown in Fig. 3.3, the particle size and zeta potential of PBAE/DNA complexes formulated by 4 different conditions of incubation; i) at 37 ⁰C for 30 min, ii) at 37 ⁰C for 10 min. iii) at RT for 30 min, and iv) at RT for 10 min. There were obtained slight changes in the particle size and zeta potential of all complexes. However, the complexes incubated at RT for 10 min considerably enhanced the stability in PBS for 60 min. On the other hand, zeta potential of all complexes gradually decreased in PBS for 60 min. These results indicate the duration of incubation for preparing the formulations did not have a significant effect on the stability of the complexes over the 30 min measurement time frame, whereas the temperature of incubation noticeably affected. Accordingly, it is noted that the stability of complexes are not influenced by the incubation time, but by the concentration of sodium acetate buffer (ionic strength) as well as the incubation conditions.
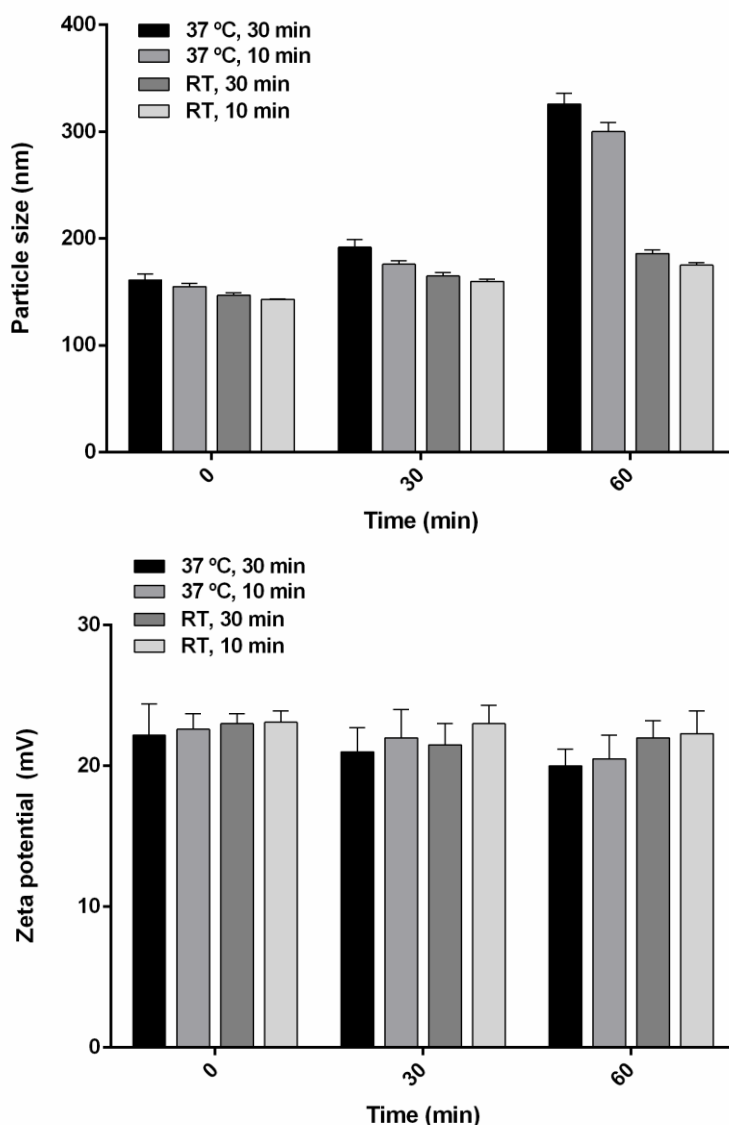
Fig. 3.3. The particle size and zeta potential of complexes prepared by different procedures.

It has been previously reported the transfection results for various oligopeptide-terminated PBAE polymers at 50:1 ratio (w/w) without modification and they were shown higher transfection efficacy than other end-modified PBAE and commercial transfection agents, i.e. GeneJuice (Segovia *et. al.*, 2014). As stated above, the particle size and the stability were dependent on the incubation procedures. Thus, the influence of incubation conditions on transfection efficiency was also investigated. The transfection efficiency of R/DNA obtained under different incubation conditions as shown in Fig. 3.4. The transfection efficiency complexes considerably increased when prepared at RT. However, there were

negligible changes in expression efficiency between those made at different time. Similar trends were obtained from MntR20/DNA (data not shown). These results indicate that transfection efficiency was also influenced by the complexes made by different incubation temperature. PBAE/DNA formulated at RT was considered to be an optimal formulation procedure, thus it was selected for further study.
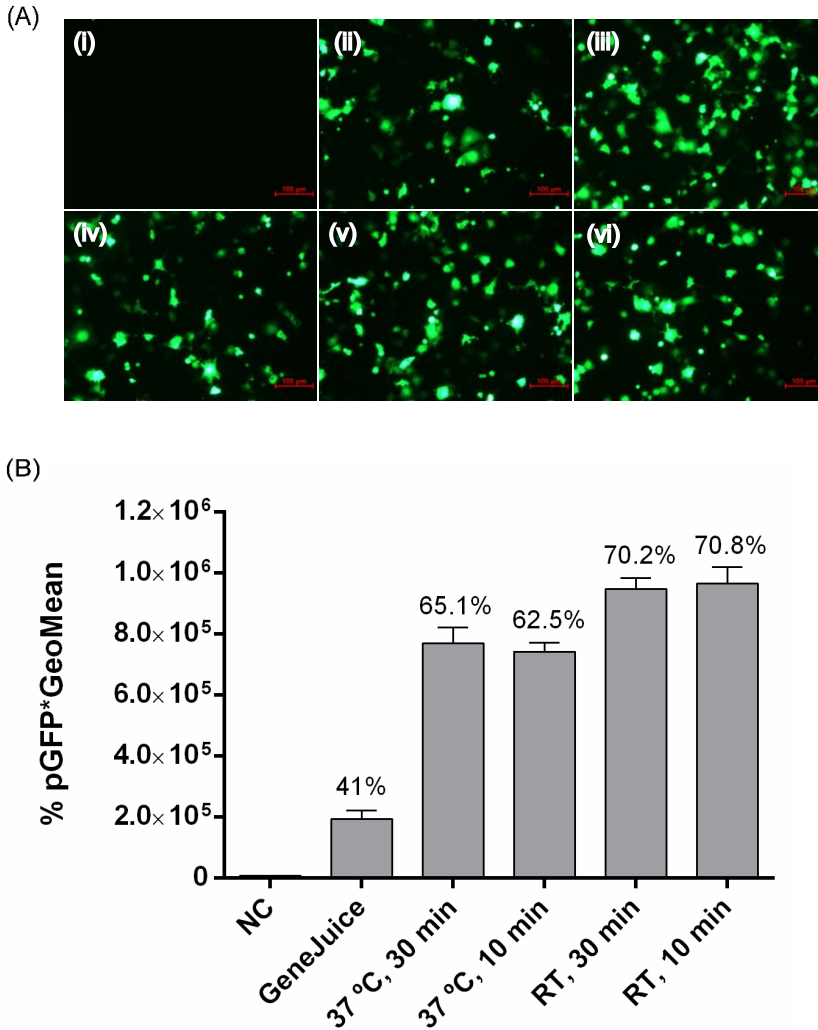
(A)

(B)

Fig. 3.4. Transfection efficiency of complexes formulated by different procedures in COS-7 cells was determined by flow cytometry. (A) Fluorescent images of GFP expression in COS-7 cells: (i) NC; (ii) GeneJuice; (iii) 37 ℃, 30 min; (iv) 37 ℃, 10 min; (v) RT, 30 min; (vi) RT, 10 min. (B) Bars represent a percentage of GFP-positive cells multiplied by the GeoMean fluorescence of the positive population. Percentage numbers above each bar represent percentage of transfected cell (%). Each bar presents the mean ± SD of three experiments. NC: negative control (the group without any treatment).

3.4.3. Sugar-modified PBAE/DNA complexes

3.4.3.1. Stability of R/DNA complexes coated with mannitol, sucrose or trehalose

We have previously described experimental preparing conditions for enhancing stability of R/DNA complexes, which had a particle size of 143.2 ± 0.3 nm with a positive zeta potential of 22.1 mV, and the size of complexes increased slightly within 1 h (Fig. 3.3). After 2 h in PBS, however, the size of complexes increased readily (n ≥ 1000 nm). Thus, further work is needed to have an enough stable formulation for in vivo applications. In order to overcome this issue, mannitol, sucrose or trehalose was employed as coating agents for complexes. The particle size and zeta potential of R/DNA complexes with a coating of 10, 20, 30 and 40 wt% of mannitol, sucrose or trehalose in PBS were analysed by DLS and the results are shown in Fig. 3.5. The R/DNA complexes coated with different amount of coating agents ranged from 130.2 to 154.3 nm in diameter and from 19.2 to 23.2 mV in zeta potential, indicating that there were observed the small differences in size and zeta potential of complexes when prepared with sugar or sugar alcohol compared to non-coated complexes. In the case of mannitol coating, the particle size of complexes increased from 130.2 to 149.7 nm with increasing the amount of mannitol, whereas there were no significant changes in zeta potential observed. These results indicate that the size of R/DNA complexes depended on the amount of mannitol. On the contrary, the particle size and zeta potential of complexes coated with sucrose or trehalose were not dependent on the amount of coating agents. As a result, no significant changes in the size and zeta potential were observed for the complexes coated with and/or without all the additives, indicating that they are unlikely to affect the ionic strength between polymers and DNA. Surprisingly, however, there were observed a notable change in the size of some coating complexes for 4 h in PBS, which were described below.
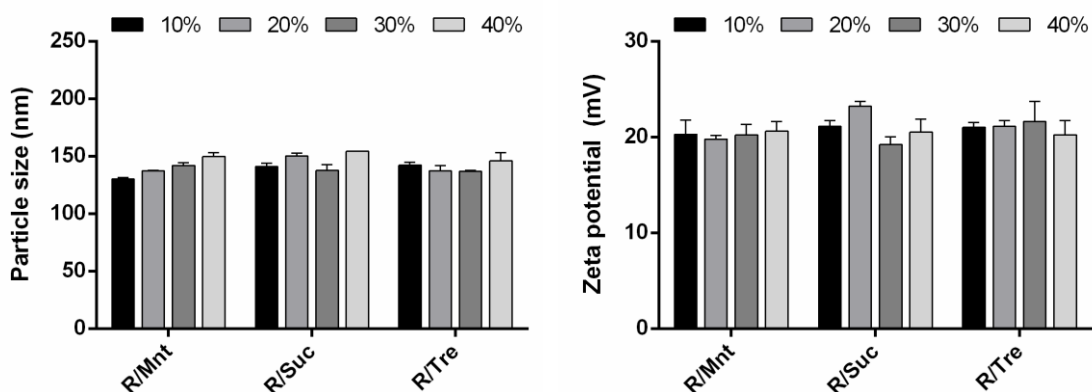

Fig. 3.5. The particle size and zeta potential of complexes coated with mannitol, sucrose and trehalose at various weight percent. Each bar represents the mean ± SD (n ≥ 3).

Complexes having from 10 to 40% of coating agents were incubated for 4 h in PBS and analysed by DLS every hour in order to observe changes in the size of complexes and the results are shown in Fig. 3.6. There were obtained the highest stability of R/DNA coated with 10% of mannitol (R/Mnt10%), 30 % of both sucrose (R/Suc30%) and trehalose (R/Tre30%), which were shown the highest stability among each family. It should be noted that we proposed that high stability can be considered maintained if the particle size is ≤1000 nm (nanomeric particle) for 4 hours, which is turnover time in gastricintestinal (GI) track as described in Chapter 1. These results indicate that the stability of complexes was independent on the amount of coating agents. Surprisingly, the mean size of R/Mnt10% and R/Tre30% was less than 1000 nm within 4h. These results indicate that these complexes improved the stability with the specific amount of mannitol and trehalose. In the case of R/Suc complexes, on the other hand, the size of R/Suc30% (1502 nm) increased larger than that of the other coating complexes within 4 h. Nevertheless, the coating with sucrose also considerably enhanced the stability of non-coated complexes. This observation supports that the sugar additives affect the formulation of the non-coated one. Moreover, 10 weight percent of mannitol or 30 weight percent of both sucrose and trehalose are the optimal contents for improving the stability of R/DNA complexes. We expect that the additives may cover the surface of the R/DNA complexes via hydrogen bonding interaction. The functional groups such as hydroxyl and/or carbonyl groups of sugars can offer sugar-coated formation of complexes due to a unique H-bonding capability in constructing supramolecular architecture (Katti *et al.*, 2009). In general, sugar-polymer conjugates have been applied for enhancing the stability of nanoparticles in either physiological condition, such as PBS, or freeze-drying process. This general concept motivated us to attempt to develop nanoparticles capable of being stable in PBS by a simple coating formulation with crude sugar before or after polymerization of PBAE polymers. In a first approach, sugars were added into PBAE/DNA complexes, related to after polymerization of PBAEs. The results obtained here clearly support our hypothesis of coating particles that may improve the stability.
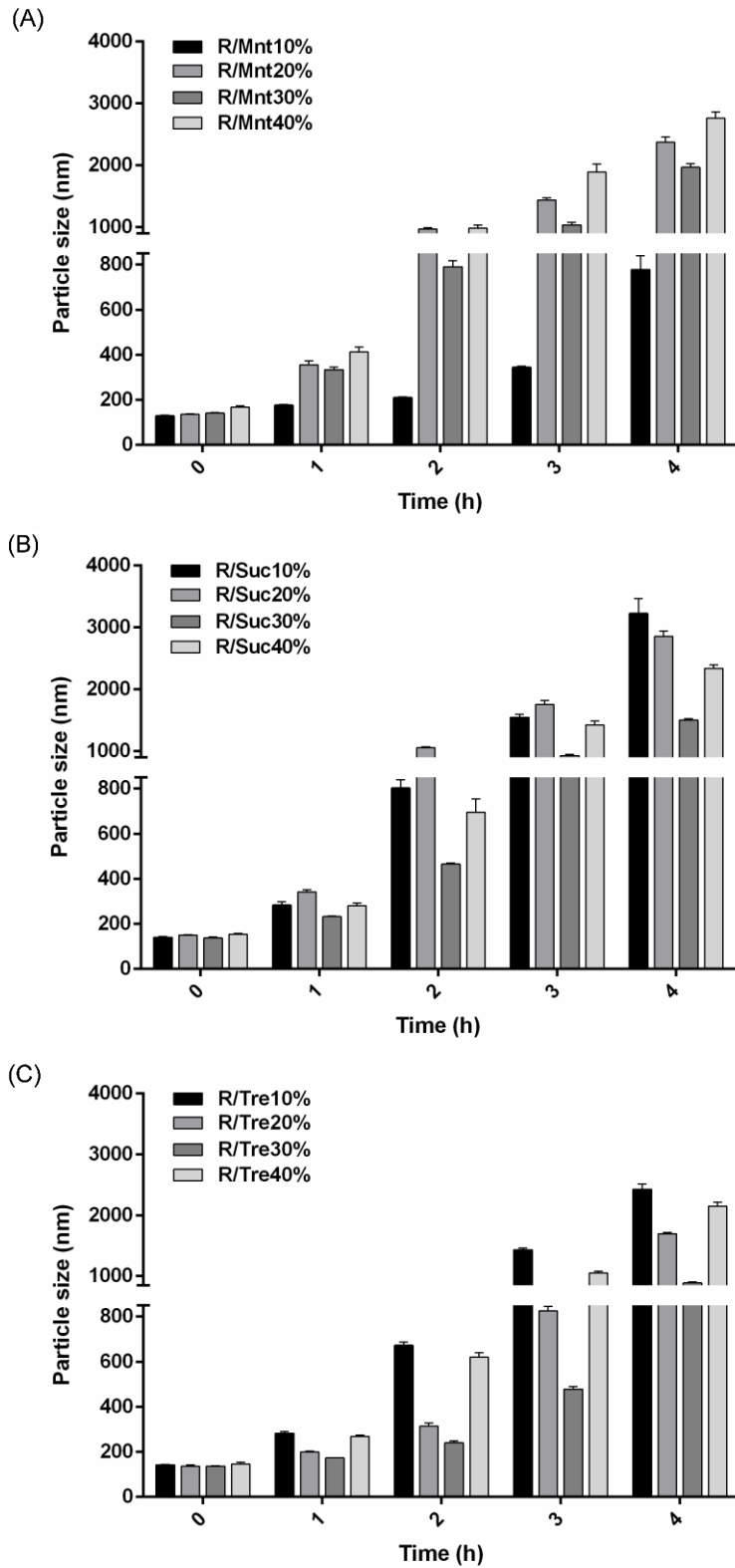
.

Fig. 3.6. Time-dependent changes in the size of complexes coated with 10, 20, 30 and 40 wt% of (A) mannitol; (B) sucrose; (C) trehalose. Complexes were incubated for 4 h in phosphate buffer saline at pH 7.4 and were analyzed by DLS every hour. Each bar represents the mean ± SD (n ≥ 3).

3.4.3.2. Stability of DNA-based complexes formed from MntR, SucR and TreR

In a second approach, we introduced a novel polymer blending of PBAEs and the additives, which were added prior to polymerization step of PBAEs (R). The preparation of mannitol, sucrose or trehalose containing R polymers, the so called MntR, SucR and TreR, was described above. The particle size and zeta potential of complexes of DNA and polymer formed in the presence of 10, 20 or 30% of mannitol, sucrose or trehalose are shown in Fig. 3.7. MntR and SucR polymers were formulated with DNA at a weight ratio of 50:1, which was general ratio of formulation for PBAE/DNA, and the complexes were prepared according to the same protocol as PBAE/DNA complexes. MntR/DNA and SucR/DNA formed with a 20% of mannitol (MntR20) and sucrose (SucR20) showed smaller size of 120.7 ± 1.1 and 133.9 ± 2.7 nm, respectively, compared to those with 10 or 30%. Moreover, MntR20/DNA showed the smallest particle size with the highest zeta potential among all tested complexes via two approaches, indicating of more compact particles. These results indicate that the particle size and zeta potential of complexes were independent on the amount of mannitol or sucrose of blending PBAEs. As described previously, the changes in size and zeta potential of complexes suggest the role of the hydrogen bonding interactions in their stabilization. This is supported the high stabilization obtained using mannitol and sucrose, which would present stronger hydrogen bonding interactions, due to their small size.
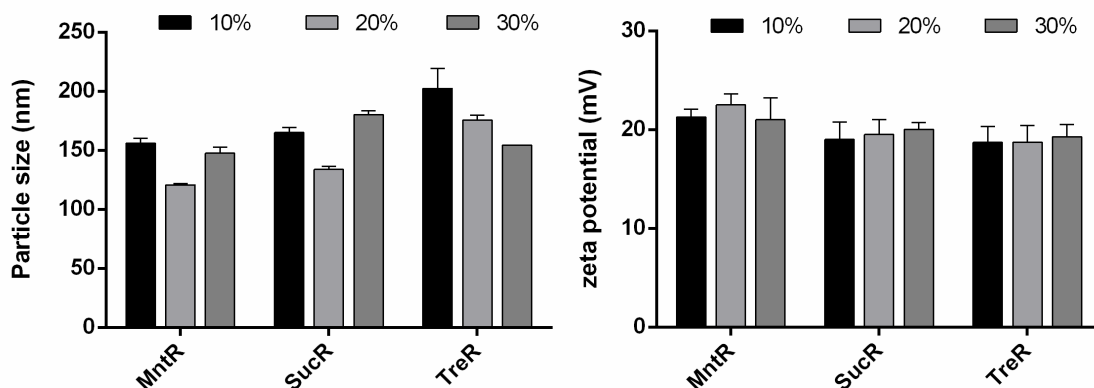

Fig. 3.7. The particle size and zeta potential of complexes formulated with mannitol, sucrose and trehalose at 10, 20 or 30%. Each bar represents the mean ± SD (n ≥ 3).

In the case of TreR, increasing the amount of trehalose from 10 to 30 decreased the mean size of TreR/DNA complexes from 202.4 to 154.3 nm and negligible changed their zeta potential. Interestingly, unlike the blending with PBAEs and mannitol or sucrose, a blending of PBAE and trehalose required use of TreR/DNA with weight ratios up to 100:1 to reach an optimal formulation. These indicate that the trehalose motif in PBAEs may obstacle PBAEs to

condense DNA. It is important to notice that the using at a 50:1 PBAE polymer to DNA weight ratio as the optimum ratio caused higher transfection efficiency with low toxicity. As a result, using of TreR/DNA complexes would be limited for further biological evaluation study. For this reason, the stability of TreR/DNA complexes was not evaluated.

Fig. 3.8 shows the stability over 10 h of complexes formed with 20% of mannitol and sucrose, which displayed the highest stability among the complexes having sugar or sugar alcohol added prior to the polymerization step of oligopeptide-modified PBAEs. Very surprisingly, there was shown no significant increase in the particle size of MntR20 and SucR20 within 4 h in PBS, indicating that a polymer blend with 20% of mannitol or sucrose noticeably enhanced the stability of complexes (n ≤ 160 nm). These results exhibited much higher stability compared to the R/DNA complexes coated with sugar by first approach. These findings suggest two hypotheses. In the first hypothesis, it may be possible to obtain unexpected sugar-PBAE conjugates during polymerization step. In the second one, sugars might stay between the functional groups of PBAEs and play as conjugates. It could be expected that a lot of hydroxyl and carboxyl groups of sugars may interact with PBAE polymers somehow, via H-bonding or entanglement interaction, thus demonstrated the significant improvement of stability. The detailed mechanism of these complexes is not yet well understood.
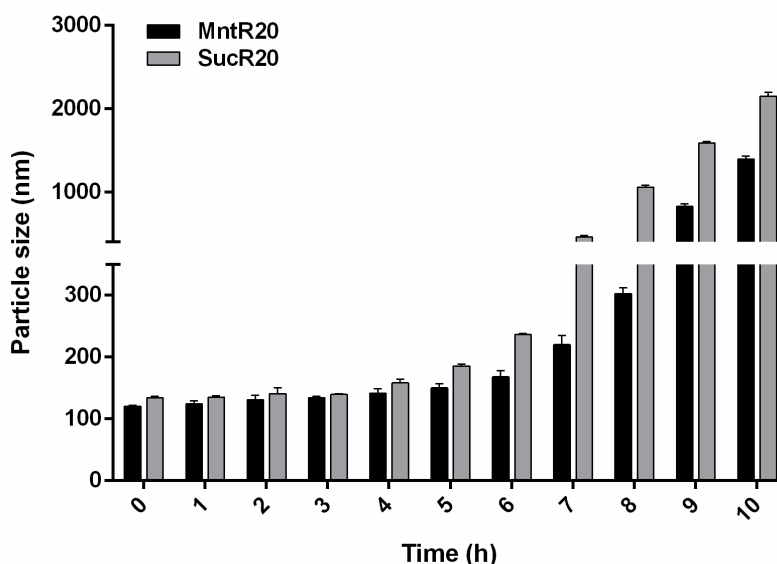

Fig. 3.8. Time-dependent changes in the size of representative complexes of MntR20/DNA and SucR20/DNA. Complexes were incubated for 4 h in phosphate buffer saline at pH 7.4 and were analyzed by DLS every hour. Each bar represents the mean ± SD (n ≥ 3).

The stability of these particles overtime was also measured. The particle size of MntR20/DNA was 827.3 ± 26.7 nm within 9 h, while SucR/DNA has a size of 1053 ± 25.4 nm within 8 h. These indicate that DNA complexes formed with MntR20 or SucR20 significantly increased the stability of the complexes. The particle size of complexes increased with decreasing zeta potential, indicating the weak binding between DNA and polymers (data not shown). All results support that the mixture of PABE and mannitol or sucrose may promote the stability of complexes with DNA.

3.4.3.3. Effect of sugar or sugar alcohol on in vitro transfection efficiency

To accomplish the main objective of this Chapter, firstly, we developed the sugar-modified formulation that can considerably enhance the stability of R/DNA complexes. As important as stability, the novel DNA-based complexes must play a fundamental role in the efficiency of transfection. In order to study the influence of sugar or sugar alcohol on gene transfection efficiency in vitro, all the experiments were performed in COS-7 cells, using pGFP plasmid DNA. Cells were incubated with complexes for 3 h and the results were analysed for GFP expression by flow cytometry at 48 h post-transfection as illustrated in Fig. 3.9. Non-modified R/DNA (RD) complexes was used here as a positive control to compare the effect of mannitol, sucrose or trehalose on transfection efficiency. Based on optimized R/DNA complexes (the final concentration of 11-12 mM of buffer, RT, 10 min), sugar or sugar alcohol-modified PBAE/DNA complexes were prepared. In the group of the coated complexes, a coating of 10 wt% of mannitol or 30 wt% of sucrose depicted higher transfection efficiency compared with non-coated complexes while the lowest expression efficiencies were seen using 20 wt% of mannitol and 10 wt% of trehalose. These results indicate the transfection efficiency of complexes is dependent on either amount or type of sugar or sugar alcohol, and mannitol and sucrose can enhance higher both stability and transfection of complexes than those of trehalsoe. In the group of complexes based on the polymer blending, overall high transfection efficiency was obtained from MntR/DNA and SucR/DNA. In particular, an appreciable increase of transfection efficiency with both 10 and 30 wt% of sucrose was observed for SucR10/DNA and SucR30/DNA complexes, respectively, being a 1.5- and 1.7-fold, respectively, more effective than non-coated complexes. On the other hand, complexes having 20 wt% of sucrose (SucR20/DNA) demonstrated the lowest transfection efficiency among the mixture of sucrose. Interestingly, the polymer blending of mannitol resulted in similar trends for that of sucrose. MntR10/DNA and MntR30/DNA showed a 1.2-fold increase in transfection efficiency compared to RD complexes, while MntR20/DNA significantly decreased the transfection efficiency. These results confirm that the transfection efficiency of complexes is dependent on either weight percent or type of sugar, and sucrose and mannitol can promote higher both stability and transfection of particles than those of trehalose. Most of the mixture polymers with mannitol and sucrose showed much higher transfection efficiency

than the coated complexes. Moreover, SucR showed the highest expression efficiency among all complexes tested. Interestingly, there was observed a significant decrease in transfection efficiency for MntR20. This corresponds to the results obtained from the complexes coated with 20 wt% of mannitol (R/Mnt20%). The lowest transfection efficiency was detected for MntR20 and SucR20, which showed the best formulation and the highest stability, among their series. Similar trends were detected in the results of percentage of positive cells. Overall, the transfection efficiency was above 70%. It is well known that polymer/DNA binding helps determine particle stability, which is important to ensure that the DNA stays protected from degradation and has high cell uptake efficiency (Green *et al.,* 2007-2008, Mintzer *et al.,* 2009). However, it is also important to consider that the particle should not bind or encapsulate the DNA so tightly as to prevent the timely release of the DNA once in the cytoplasm (Green *et al.,* 2008; Vuorimaa *et al.,* 2011). According to this, the transfection efficiency is strongly correlated with the stability of complexes, indicating that the lower GFP expression after transfection with 20% of both mannitol and sucrose seems to be a result of the increased stability of these particles, which leads to decreased release of GFP within transfected cells.

On the other hand, very low transfection efficiency was observed with the TreR-based complexes, which may be a result of the lower plasmid dosage of 0.075 µg/well. This dosage was used to avoid cytotoxicity resulting from the high TreR:DNA ratio of 100:1 that was needed for formulated complexes. In fact, we attempted to study the toxicity of TreR/DNA as same dosage as the other complexes (0.3 µg/well) and there was obtained very low viability of TreR/DNA complexes (data not shown), inducing the reduced plasmid dosage. As described in 3.1, PBAEs have lower cytotoxicity compared to other cationic polymers. However, increasing PBAE content, whether through increasing wt/wt content of PBAE within the particles, or via increasing NP dose, resulted in increasing toxicity of the particles (Fields *et al.*, 2012). It is important to notice that the using at a 50:1 PBAEs to DNA weight ratio as the optimum ratio caused higher transfection efficiency with low toxicity as described previously. Thus, the use of the polymer blending of R and trehalose would be limited due to the lower transfection efficiency.
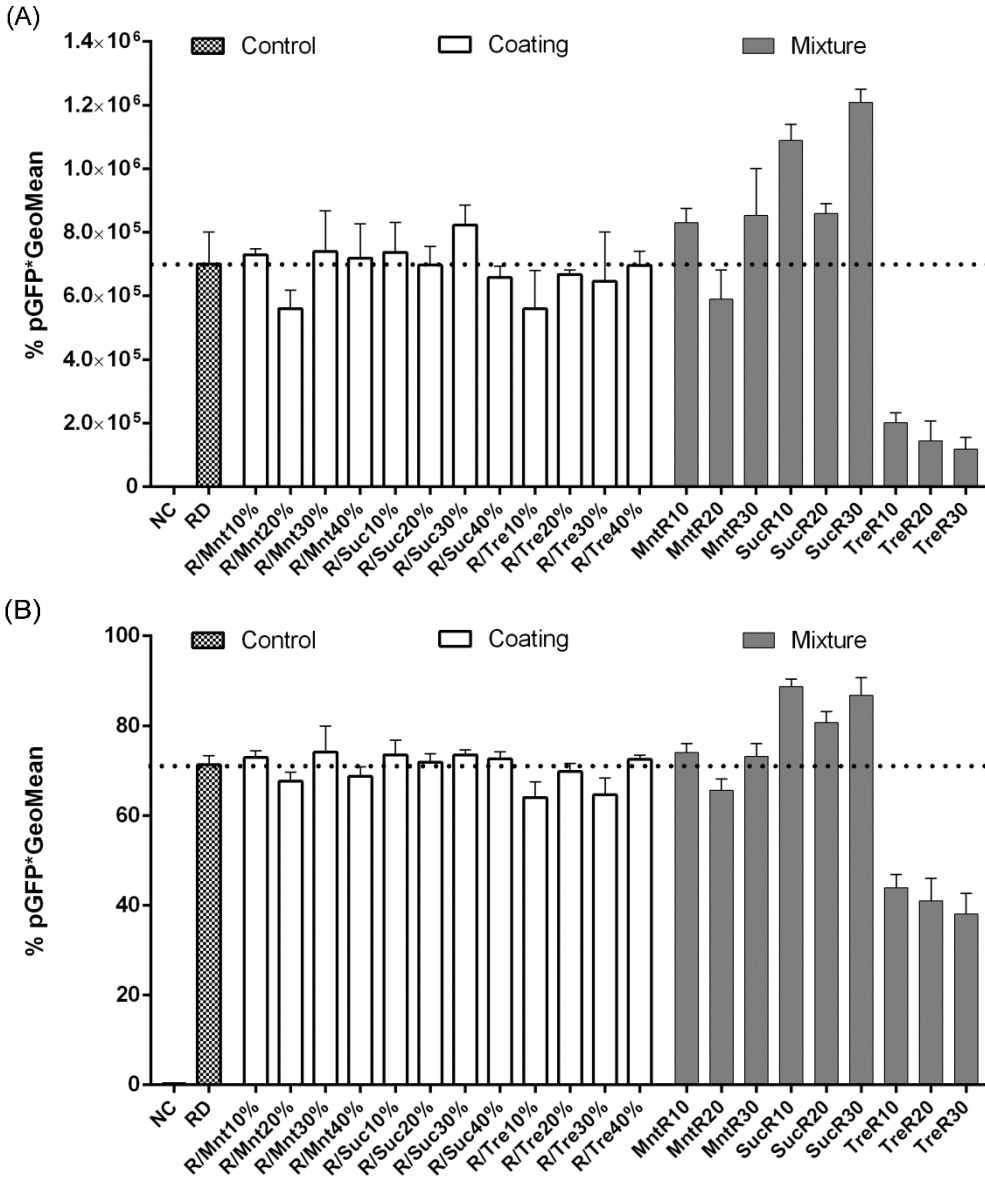
Fig. 3.9. Transfection efficiency of sugar or sugar alcohol-modified PBAE/DNA complexes in COS-7 cells was determined by flow cytometry. (A) Bars represent a percentage of GFP positive cells multiplied by the GeoMean fluorescence of the positive population. (B) GFP expression was determined after 48 h by flow cytometry and bars represent percentage of cells positively transfected and the normalized total gene expression. Each bar presents the mean ± SD (n ≥ 3). NC: negative control (the group without any treatment).

3.4.3.4. Cell viability

All modified complexes were tested for their effect on cell viability of transfected cells. Most of complexes formulated at a 50:1 polymer:DNA weight ratio was tested using a plasmid dosage of 0.3 μg/well, while TreR/DNA complexes formulated at a 100:1 weight ratio of polymer to DNA was tested using a 0.075 μg DNA /well. As shown in Fig. 3.10, no significant decrease in cell viability was observed for all complexes tested in this study compared with the unmodified RD complexes, which presented cell viability ~81%. These results indicate that the sugar or sugar alcohol would be safer additives for modified-PBAE/DNA complexes. TreR/DNA complexes showed relatively lower viability among the complexes based on the polymer mixture although lower plasmid and polymer dosage per well was used.
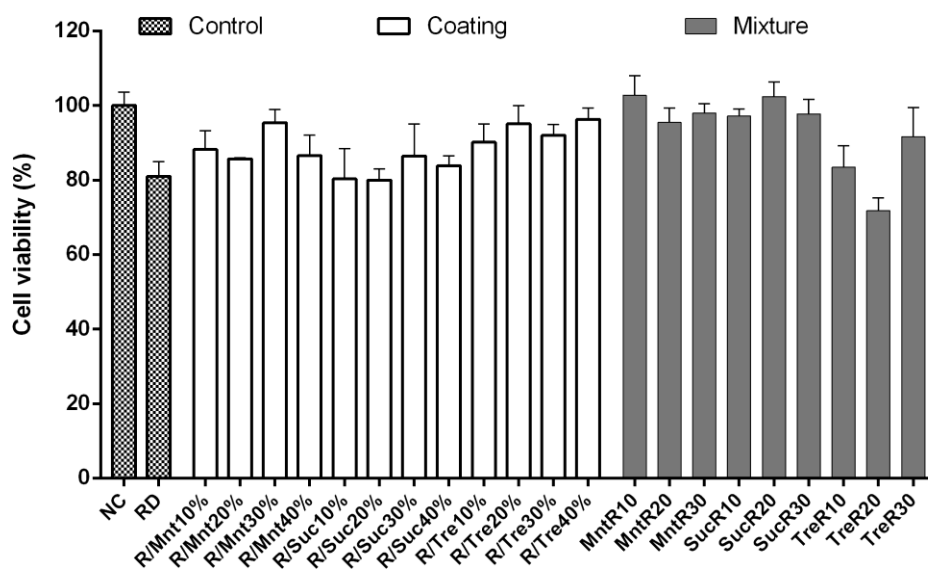

Fig. 3.10. Cell viability of cells after transfection, measured using the MTS assay. Viability was determined at 48 h post-transfection. Bars represent a percentage of viable cells relative to a control of untreated cells (NC). Each bar represents the mean ± SD (n ≥ 3).

3.4.4. Chitosan-modified PBAE/DNA complexes

In parallel with the development of sugar-modified formulations, we have designed and developed a chitosan-coated formulation of PBAE/DNA complexes nanoparticles. As described in 3.1, in general, chitosan as a non-viral vehicle for transferring DNA molecules into the cells has recently attracted much attention because of its unique properties such as high stability, but lack the efficacy in transfection compared to commercial agents. It is known that numerous factors affect the stability and transfection efficiency of chitosan-based nanoparticles. Among them, the molecular weight of chitosan is one of the most important factors to enhance the transfection efficiency. Here we have studied the effect of chitosan as a coating agent on stability, transfection efficiency and viability. Moreover, two different molecular weights were applied to evaluate the effect of this factor.

3.4.4.1. Formulation and characterization of chitosan-coated R/DNA complexes

The formation of PBAEs with DNA coated with CS (22 kDa) or CSM (60-120 kDa) added in a proportion ranging from 0.17 to 2.67 wt% of the PBAE polymers was confirmed by agarose gel electrophoresis. In comparison with the mobility of the naked pDNA, the movement of DNA was completely retarded in all test complexes. As shown in Fig. 3.11, DNA was retained completely at all differing weight ratios. These indicate that the addition of CS or CSM did not affect the PBAE/DNA complex formation ability.
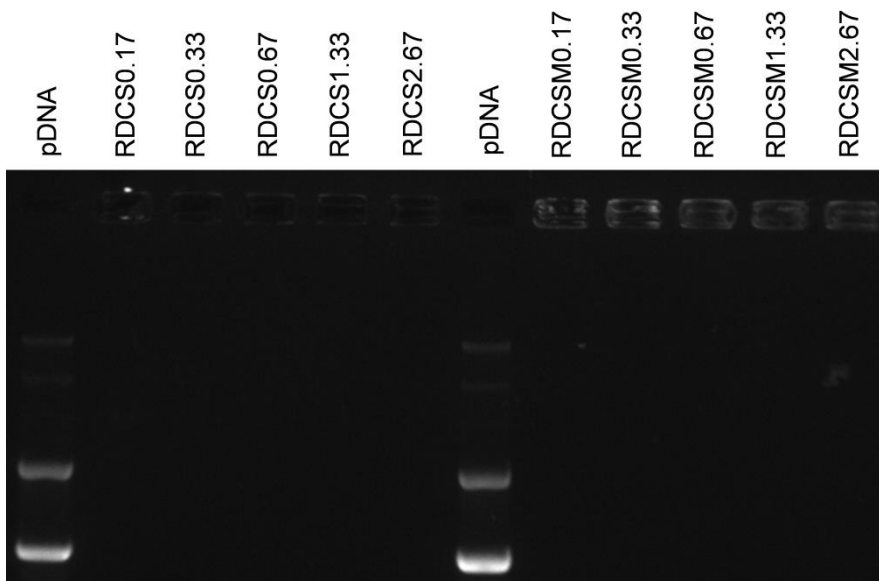

Fig. 3.11. Gel retardation assay of R/DNA coated with CS or CSM. Complexes were formulated by mixing polymers and GFP in a weight ratio of 50:1 and loaded onto an agarose gel containing ethidium bromide to assess DNA mobility by electrophoresis.

The particle size and zeta potential of R/DNA complexes without or with a coating of 0.17, 0.33, 0.67, 1.33, and 2.67 weight percent of CS or CSM was measured and the results are shown in Fig. 3.12. The particle size and zeta potential of R/DNA (RD) used as control was 149 nm and 19.5 mV, respectively. The RD complexes coated with CS (RDCS) ranged from 134 to 165 nm in the mean diameter and from 12 to 14 mV in zeta potential (Fig. 3.12A). There were obtained small differences in size between CS-coated complexes and non-coated complexes. However, zeta potential values show a notable decrease when prepared with CS. Interestingly, the smallest size was obtained when prepared with 0.67 wt% of CS, indicating that the size of complexes was not dependent on the amount of CS. In the case of a coating of CSM, the particle size of CSM-coated RD (RDCSM) complexes was found in a range of 165-232 nm with a zeta potential of 10-3 mV (Fig. 3.12B). With an increased in the amount of CSM among coating complexes, the size of complexes increased considerably while zeta potential value decreased significantly, resulting in less compact complexes. These results suggest that the size and zeta potential of complexes were dependent on the amount of CSM. The complexes with 0.67 wt% of CS and 0.33 wt% of CSM was considered to be an optimal formulation among their series due to their small size, and high stability as described below.
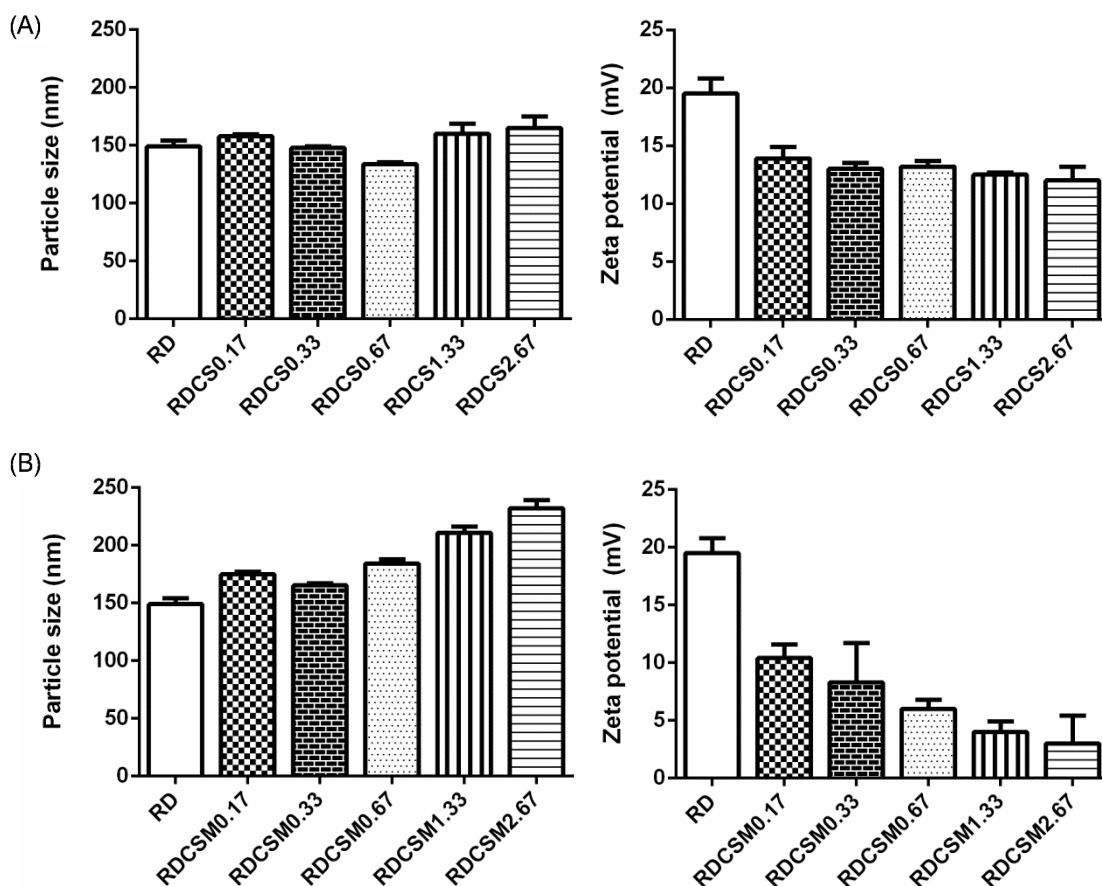

Fig. 3.12. The particle size and zeta potential of complexes coated with CS (A) and CSM (B) at various weight percent. Each bar represents the mean ± SD (n ≥ 3).

3.4.4.2. Effect of chitosan of different molecular weights on stability

We have previously found that the sugar-modified formulations via both coating and blending significantly improved the stability of non-modified R/DNA complexes. In order to compare with the results obtained with the novel sugar-modified formulations, there has been studied the effect of chitosan on stability. The stability of R/DNA complexes prepared with a coating of 0.17, 0.33, 0.67, 1.33 and 2.67 wt% of CS or CSM was measured. All the testing complexes were incubated for 4 h in PBS and analysed every hour and monitored changes in the particle size. The results of complexes comprising PBAE/DNA in combination with different amount of CS or CSM are shown in Fig. 3.13. Surprisingly, we saw an appreciable enhancement of the overall stability compared with both sugar-coated complexes and non-coated one. In the case of a CS coating (Fig. 3.13A), all complexes coated with CS improved the stability over time and the size of them were less than 750 nm within 4 h. Notably, the particle size of RD coated with 0.67 wt% of CS was still less than 400 nm, indicating that 0.67 wt% of CS may be an optimal content to sustain the formulation of RDCS complexes. On the other hand, there was shown a gradually increase in size of complexes with increasing the amount of CSM (Fig. 3.13B). The size of all CSM-coated complexes were still less than 450 nm within 4 h, indicating that the coating of CSM were more stable than that of CS. These results confirm that the stability of complexes was strongly dependent on a coating agent of chitosan and its molecular mass is considered to influence the stability of PBAE/DNA complexes. In particular, the complexes coated with 0.33 wt% of CSM showed the smallest size and the highest stability among all testing complexes, indicating that this amount could be an optimal content for enhancing the stability of RDCSM complexes.
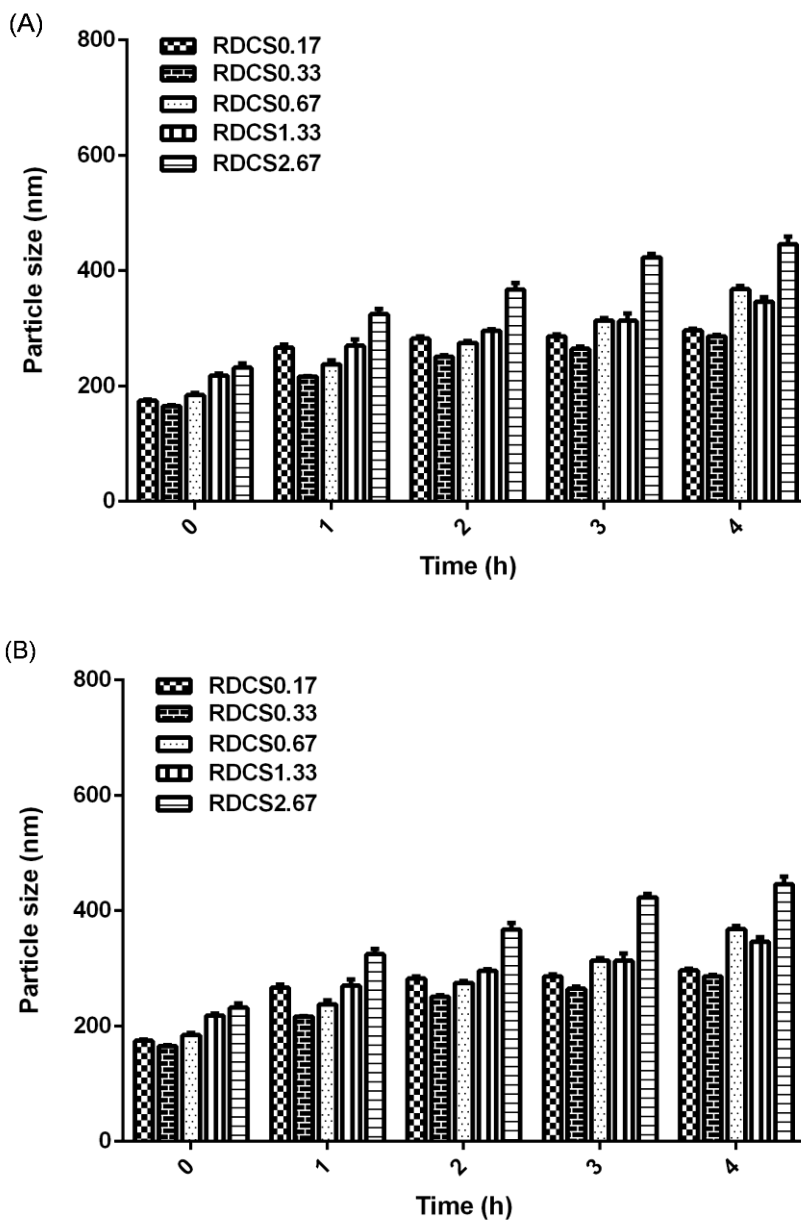
Fig. 3.13. Time-dependent changes in the size of R/DNA coated without or with 0.17, 0.33, 0.67, 1.33 and 2.67 wt% of CS (A) and CSM (B). Complexes were incubated for 4 h in phosphate buffer saline at pH 7.4 and were analyzed by DLS every hour. Each bar represents the mean ± SD (n ≥ 3).

3.4.4.3. Effect of chitosan of different molecular weights on transfection in vitro

After studying the effect of a coating of chitosan and its different molecular weights on stability, the effect of those on transfection efficiency was studied. To accomplish this, all the experiments were performed in COS-7 cells, using pGFP plasmid DNA. The pGFP expression was determined by flow cytometry analysis at 48 h post-transfection. Results of flow cytometry and fluorescence microscopy are illustrated in Fig. 3.14. R/DNA complexes were reported higher gene expression in cell-type-specific manner and better cellular viability compared to other end-modified PBAE and commercial transfection agents (Segovia *et al.*, 2014). Thus, non-coated RD was used here as a positive control to compare the influence of CS or CSM on the transfection efficiency. The objective of this study was to sustain high transfection efficiency of PBAE/DNA complexes when bearing chitosan as enhancing the stability.

In the case of a coating of chitosan 60-120 kDa, the transfection efficiency of R/DNA coated with chitosan 60-120 kDa decreased noticeably with increasing the amount of CSM, indicating that CSM caused a significant decrease in transfection efficiency. The lower GFP expression after transfection with complexes comprising CSM seems to be a result of the increased size and the decreased zeta potential of these complexes, which leads to reduced release of GFP within transfected cells. In addition, it is also because the transfection efficiency of complexes formulated with chitosan is largely dependent on the pH of the medium due to its pKa, and efficiency is dramatically decreased at a transfection medium pH of 7.4 (Mao *et al.*, 2010). On the other hand, with a coating of chitosan 20-40 kDa, GFP expression levels slightly decreased with increasing the amount of CS. However, all RDCS complexes except RDCS2.67 showed high transfection efficiency, which can be considered if it is ≥ 75% (Fig. 3.14C). These indicate that transfection efficiency mediated by chitosan of medium molecular mass was much less than that by chitosan of low molecular mass. Interestingly, higher gene expression was maintained at a coated with 0.67 wt% of CS, which showed the smallest size and the highest stability among the RDCS complexes. These confirmed that 0.67 wt% of CS may be an optimal weight for chitosan coating the PBAE/DNA complexes due to their relative small size, higher stability and transfection efficiency. As a result, there were observed the reduction in transfection efficiency of the overall chitosan-coated complexes. Thus, this formulation still requires improving its transfection efficiency,

(A)

(B)

(C)
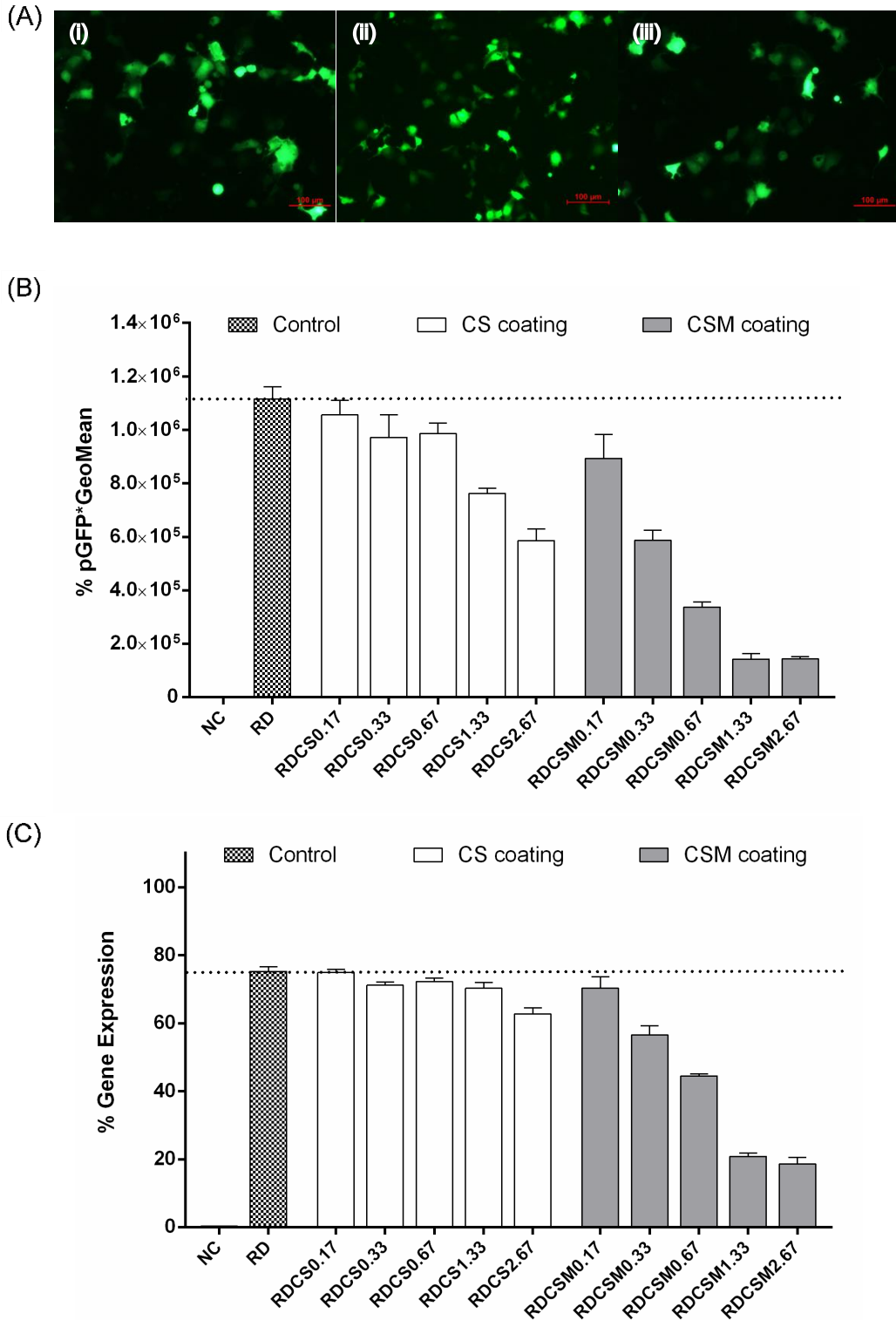
Fig. 3.14. Transfection efficiency of complexes with or without coating agents in COS-7 cells was determined by flow cytometry. (A) Fluorescent images of GFP expression in COS-7 cells: (i) RD; (ii) RDCS0.17; (iii) RDCSM0.17. (B) Bars represent a percentage of GFP positive cells multiplied by the GeoMean fluorescence of the positive population. (C) GFP expression was determined after 48 h by flow cytometry and bars represent percentage of cells positively transfected and the normalized total gene expression. Each bar presents the mean ± SD (n ≥ 3). NC: negative control (the group without any treatment).

3.4.4.4. Cell viability

All modified complexes were tested for their effect on cell viability of transfected cells. Fig. 3.15 showed the viability of COS-7 cells in media treated with PABE/DNA/chitosan complexes. The viability of RDCS and RDCSM complexes increased with an increase in the amount of the coating agents. All chitosan coated complexes showed relatively high cell viability when compared to non-coated complexes. These results indicate that coating PBAE/DNA/chitosan complexes should be safer carriers.
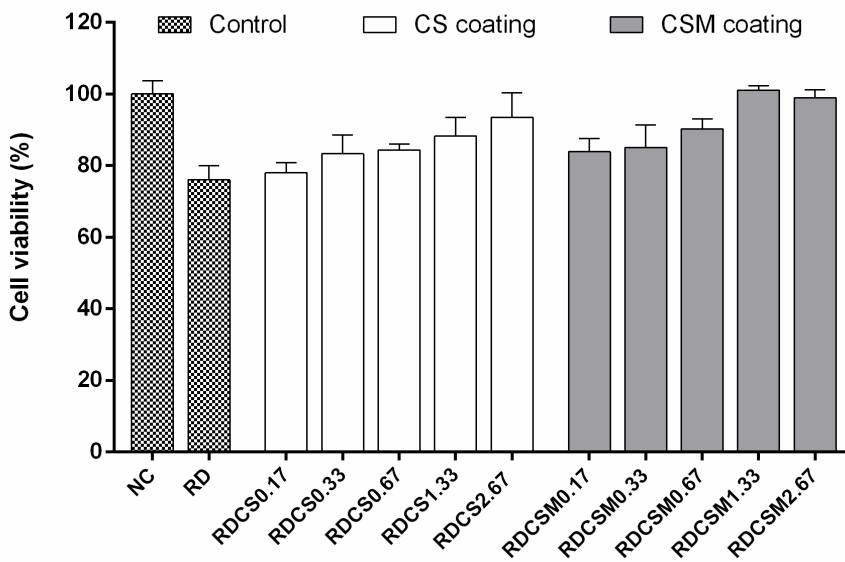
Fig. 3.15. Cell viability of cells after transfection, measured using the MTS assay. Viability was determined at 48 h post-transfection. Bars represent a percentage of viable cells relative to a control of untreated cells (NC). Each bar represents the mean ± SD (n ≥ 3).

3.5.   Concluding remarks

We investigated the stability and cell transfection efficiency of PBAE/DNA complexes modified with mannitol, sucrose or trehalose as a non-viral gene delivery system. Our first approach was to develop a sugar coating formulation, which further improved the stability of complexes and maintained high transfection efficiency compared to non-coating complexes. Our second approach was to prepare DNA complexes based on a novel polymer mixture of PBAEs and mannitol, sucrose or trehalose (MntR, SucR or TreR). As compared with unmodified complexes, MntR and SucR enhanced considerably stability and transfection efficiency. We reported here that the novel surface-modified formulation with mannitol or sucrose provide an attractive biocompatible profile with high stability and transfection efficiency, high biodegradability and reduced toxicity, thus would be applied as a promising gene delivery vehicle.

In parallel, we investigated the effect of chitosan and its molecular weight on the stability and transfection efficiency of the resulting PBAE/DNA/chitosan complexes. Therefore, we have developed promising PBAE/DNA/chitosan complexes via electrostatically coatings as non-delivery gene carriers to integrate the advantages of PBAE and chitosan. We found that the addition of chitosan with a 22 kDa (CS) led to enhanced stability of PBAE/DNA/CS compared to non-coated PBAE/DNA complexes while sustaining high transfection efficiency at the specific weight ratio. Chitosan with a 60-120 kDa (CSM) is superior to those with CS in enhancing the stability of complexes, but inhibit the release of DNA from its complex when using COS-7 cells, indicating of low transfection efficiency. On the other hand, CS exhibited enhanced stability compared to the RD complexes while transfection efficiency is slightly decreased with increasing the amount of CS. Consequently, CS for surface-modified formulations may be more efficient coating agent compared with CSM. However, chitosan-coated formulation still remains to improve transfection efficiency. As discussed in the previous Chapter, the thiolated chitosan has been a promising polymer for gene delivery applications due to its efficacy for gene transfer. Thus, in the next Chapter, we will develop an engineer formulation modified with thiolated chitosan that can enhance the stability, transfection efficiency as well as mucus permeability. Moreover, polymer-bromelain conjugates will be applied as a coating agent for the PBAE/DNA formulations since it showed highest mucus permeability in Chapter 2.

3.6.   References

Abdelwashed, W.; Degobert, G.; Stainmesse, S.; Fessi, H. *Adv. Drug Deliv. Rev.* **2006**, *58*, 1688-1713.

Agirre, M.; Zarate, J.; Ojeda, E.; Puras, G.; Desbrieres, J.; Pedraz, J.L. *Polymer* **2014**, *6*, 1727-1755.

Agnihotri, S.A.; Mallikarjuna, N.N.; Aminabhavi, T.M. *J. Control. Release* **2004**, *100*, 5-28.

Ai-Hussein, A.; Gieseler, H. *J. Pharm. Sci.* **2012**, *101*, 2534-2544.

Akinc, A.; Lynn, D.M.; Anderson, D.G.; Langer, R. *J. Am. Chem. Soc.* **2003**, *125*, 5316-5323.

Alves, N.M.; Mano, J.F. Int. *J. Biol. Macromol.* **2008**, *43*, 401-414.

Anchordoquy, T.; Koe, G.S. *J. Pharm. Sci.* **1999**, *89*, 289-296.

Anderson, D.G.; Lynn, D.M.; Langer, R. *Angew. Chem. Int. Ed.* **2003**, *42*, 3153–3158.

Anderson, D.; Peng, W.; Akinc, A.; Hossain, N.; Kohn, A.; Padera, R.; et al. *Proc. Natl. Acad. Sci. USA* **2004**, *101*, 16028e33.

Anderson, D.G.; Akinc, A.; Hossain, N. Langer, R. *Mol. Ther.* **2005**, *11*, 426-434.

Basarkar, A.; Singh, J. *Int. J. Nanomedicine* **2007**, *2*, 353-360

Bernkop-Schnürch, A.; Dunnhaüpt, S. *Eur. J. Pharm. Biopharm.* **2012**, *81*, 463-469.

Borchard, G. *Adv. Drug Deliv. Rev.* **2001**, *52*, 145-150.

Buschmann, M.D.; Merzouki, A.; Lavertu, M.; Thibault, M.; Jean, M.; Darras, V. *Adv. Drug Deliv. Rev.* **2013**, *66*, 1234-1270.

Carpenter, J.F.; Manning, M.C. *Rational design of stable protein formulations. Theroy and practice.* Vol. 3, Plenum Press, New York, USA, **2002**, pp.120-121.

Dang, J.M.; Leong, K.W. *Adv. Drug. Deliv. Rev.* **2006**. *58*, 467–486.

de la Fuente, M.; Ravina, M.; Paolicelli, P.; Sanchez, A.; Seijo, B.; Alonso, M.J. *Adv. Drug Deliv. Rev.* **2010**, *62*, 100-117.

Dosta, P.; Segovia, N.; Cascante, A.; Ramos, V.; Borrós, S. *Acta Biomater.* **2015**. *20*, 82-93.

Du, L.; Gao, Y.; Yang, H.; Li, Y.; Zhuang, Q.; Jia, H.; Nie, G.; Liu, Y. *RCS Advances* **2013**, *3*, 14791-14797.

Edelstein, M.L.; Abedi, M.R.; Wixon, J.; Edelstein, R.M. *J. Gene. Med.* **2004**, *6*, 597-602

Elfinger, M.; Pfeifer, C.; Uezguen, S.; Golas, M.M.; Sander, B.; Maucksch, C.; Stark, H.; Aneja, M.K.; Rudolph, C. *Biomacromolecules* **2009**, *10*, 2912-2920.

Eliyahu, H.; Barenholz, Y. Domb, A.J. *Molecules* **2005**, 1*0*, 34–64.

Eltoukhy, A.A.; Siegwart, D.J. Alabi, C.A.; Rajan, J.S.; Langer, R.; Anderson, D.G. *Biomaterials*

2012, *33*, 3594-3603.

Farmer, S.; Emeritus, W. Virtual textbook of organic chemistry,
http://chemwiki.ucdavis.edu/Organic_Chemistry/Carbohydrates/Disaccharides.

Gao, S.; Chen, J.; Dong, L.; Ding, Z.; Yang, Y.h.; Zhang, J. *Eur. J. Pharm. Biopharm*. **2005**, *60*,
327–334.

Gao, Y.; Xu, Z.; Chen, S.; Gu, W.; Chen, L.; Li, Y. *Int. J. Pharm*. **2008**, *359*, 241-246.

Ginn, S.L., Alexander, I.E., Edelstein, M.L., Abedi, M.R., Wixon, J. *J. Gene. Med*. **2013**, *15*, 65-
77.

Green, J.J.; Shi, J.; Chiu, E.; Leshchiner, E.S.; Langer, R.; Anderson, D.G. *Bioconjug. Chem*.
2006, *17*, 1162-1169.

Green, J.J.; Zugates, G.T.; Tedford, N.C.; Huang, Y.H.; Griffith, L.G.; Lauffenburger, D.A.;
Sawicki, J.A.; Langer, R.; Anderson, D.G. *Adv. Mater*. **2007**, *19*, 2836-2842.

Green, J.J.; Langer, R.; Anderson, D.G. *Acc. Chem. Res*. **2008**, *41*, 749-759.

Green, J.J.; Zhou, B.Y.; Mitalipova, M.M.; Beard, C.; Langer, R.; Jaenisch, R.; Anderson, D.G.
Nano. Lett. **2008**, *8*, 3126-3130.

Hoggard, M.K.; Tubulekas, I.; Guan, H.; Edwards, K.; Nilsson, M.; Varum, K.M.; Rtursson, A.P.
Gene Ther. **2001**, *8*, 1108–1121.

Hu, W.W.; Chen, Y.J.; Ruaan, R.C.; Chen, W.Y.; Cheng, Y.C.; Chien, C.C. *Carbohydr. Polym*.
2014, *99*, 394-402.

Hung, S.; Kamihira, M. *Biotech. Adv*. **2013**, *31*, 208-223.

Jin , L.; Zeng, X.; Liu, M.; Deng, Y.; He, N. *Theranostics* **2014**, *4*, 240-255.

Jonassen, H.; Kjoniksen, A.L.; Hiorth, M. *Colloid. Polym. Sci*. **2012**, *290*, 919-929.

Jovanovic, N.; Bouchard, A.; Hofland, G.W.; Witkamp, G.J.; Crommelin, D.J.; Jisroot, W. *Eur. J.
Pharm. Sci*. **2006**, *27*, 336-345.

Kamimura, K.; Suda, T.; Zhang, G.; Liu, D. *Pharm. Med*. **2011**, *25*, 293-306.

Katti, K.; Kattumuri, V.; Bhaskaran, S.; Kannan, R. *Int. J. Green Nanotechnol. Biomed*. **2009**, *1*,
B53-59.

Keeney, M.; Ong, S.G.; Padilla, A.; Yao, Z.; Goodman, S.; Wu, J.C.; Yang, F. *ACS Nano* **2013**,
7, 7241-7250.

Kiang, T.; Wen, J.; Lim, H.W.; Leong, K.W. *Biomaterials* **2004**, *25*, 5293–5301.

Kim, A.I.; Akers, M.J.; Nail, S.L. *J. Pharm. Sci*. **1998**, *87*, 931-935.

Kim, T.; Seo, H.J.; Choi, J.S.; Jang, H.S.; Beak, J.; Kim, K.; Park, J.-S. *Biomacromolecules*
2004, *5*, 2487–2492.

Koping-Hoggard, M.; Varum, K.M.; Issa, M.; Danielsen, S.; Christensen, B.E.; Stokke, B.T.
Gene. Ther. **2004**, *11*, 1441-1452.

Kumar, M.; Muzzarelli, R.A.; Muzzarelli, C.; Sashiwa, H.; Domb, A.J. *Chem. Rev.* **2004**, *104*, 6017–6084.

Kumirska, J.; Weinhold, M.X.; Thoming, J.; Stepnowski, P. *Polymers* **2011**, *3*, 1875-1901.

Janes, K.A.; Calvo, P.; Alonso, M.J. *Adv. Drug Deliv. Rev.* **2001**, *47*, 83-97.

Jain, N.K.; Roy, I. *Protein Sci.* **2008**, *18,* 24-36.

Jeong, Y.; Jin, G.W.; Choi, E.; Jung, J.H.; Park, J.S. *Int. J. Pharm.* **2011**, *420*, 366-370.

Lavertu, M.; Methot, S.; Tran-Khanh, N.; Buschmann, M.D. *Biomaterials* **2006**, *27*, 4815–4824.

Lee, M.K.; Chun, S.K.; Choi, W.J.; Kim, J.K.; Choi, S.H.; Kim, A.; Oungbho, K.; Park, J.S.; Ahn, W.S.; Kim, C.K. *Biomaterials* **2005**, *26*, 2147–2156.

Li, J.; Revol, J.F.; Marchessault, R.H. *J. Colloid. Interface Sci.* **1996**, *183*, 365-373.

Lindholm, H.M.; Trnka, H.; Grohganz, H. *Int. J. Pharm.* **2014**, *460*, 45-52.

Liu, W.G.; Sun, S.J.; Cao, Z.Q.; Zhang, X.; Yao, K.D.; Lu, W.W.; Luk, K.D. *Biomaterials* **2005,** *26*, 2705–2711.

Luo, D.; Saltzman, W.M. *Nat. Biotechnol.* **2000**, *18*, 893-895.

Lynn, D.M.; Langer, R. *J. Am. Chem. Soc.* **2000**, *122*,10761-10768.

Lynn, D.M.; Anderson, D.G.; Putnam, D.; Langer, R. *J. Am. Chem. Soc.* **2001**, *123*, 8155-8160.

Luten, J.; van Nostrum, C.F.; de Smedt, S.C.;, Hennink, W.E. *J. Control. Release* **2008**, *126*, 97e110.

Ma, Y.; Yang, Q. *Nanotoxicology aspects of carbohydrate nanostructures*. in; Stine, K.J. *Carbohydrate nanotechnology*. John Wiley & Sons. New Jersey, Press,1st edn. **2015**, pp. 423-439.

Mao, S.; Leong, K. *Adv. Drug Deliv. Rev.* **2010**, *62*, 12-27.

Mastorakos, P.; de Silva, A.L.; Chisholm, J.; Song, E.; Choi, W.K.; Boyle, M.P.; Morales, M.M.; Hanes, J.; Suk, J.S. *Proc. Nati. Acad. Sci. USA.* **2015**, *112*, 8720-8725.

Merdan, T.; Kopecek, J.; Kissel, T. *Adv. Drug Deliv. Rev.* **2002**, *54*, 715–758.

Miele, E.; Spinelli, G.P.; Miele, E.; Fabrizio, E.D.; Ferretti, E.; Tomao, S.; Gulino, A. Int. J. *Nanomedicine* **2012**, *7*, 3637-3657.

Mintzer, M.A.; Simanek, E.E. *Chem. Rev.* **2009**, *109*, 259-302.

Noga, M.; Edinger, D.; Wagner, E.; Winter, G.; Besheer, A. *Int. J. Pharm.* **2014**, *469*, 50-58.

Ohtake, S.; Wang, Y.J. *J. Pham. Sci.* **2011**, *100*, 2020-53.

Patri, A.K.; Kukowska-Latallo, J.F.; Baker, J.R. *Adv. Drug Deliv. Rev.* **2005**, *57*, 2203-2214.

Pavlin, M.; Bregar, V.B. *Dig. J. Nanomater. Bios*. **2012**, *7*, 1389-1400.

Putnam, D. *Nat. Mater.* **2006**, *5*, 439–451.

Ramammorth, M.; Narvekar, *J. Clin. Diagn. Res.* **2015**, *9*, GE01-06.

Rinki, K.; Tripathi, S.; Dutta, P.K.; Hunt, A.J.; Macquarrie, D.J.; Clark, J.H. *J. Mater. Chem.* **2009**, *19*, 8651-8655.

Robbins, P.D.; Ghivizzani, S.C. *Pharmacol. Ther*. **1998**, *80*, 35-47.

Rochelle, C.; Lee, G. *J. Pharm. Sci.* **2007**, *96*, 2296-2309.

Romoren, K.; Pedersen, S.; Smistad, G.; Evensen, O. Thu, B.J. *Int. J. Pharm*. **2003**, *261*, 115–127.

Sameti, M.; Bohr, G.; Kumar, M.; Kneuer, C.; Bakowsky, U.; Nacken, M.; Schmidt, H.; Lehr, C. *Int. J. Pharm*. **2003**, *266*, 51-60.

Sanjoh, M.; Miyata, K.; Christie, R.J.; Ishii, T.; Maeda, Y.; Pittella, F.; Hiki, S.; Nishiyama, N.; Kataoka, K. *Biomacromolecules* **2012**, *13*, 3641-3649.

Sato, T.; Ishii, T.; Okahata, Y. *Biomaterials* **2001**, *22*, 2075-2080.

Sabzevari, A.; Adibkia, K.; Hashemi, H.; de Geest, B.G.; et al. *Invest. Ophthalmol. Vis. Sci.* **2013,** *54*, 5520-5526.

Segovia, N.; Dosta, P.; Cascante, A.; Ramos, V.; Borrós, S. *Acta Biomaterialia* **2014**, *10*, 2147-2158.

Shi, B.; Shen, Z.; Zhang, H.; Bi, J.; Dai, S. *Biomacromolecules* **2012**, *13*, 146-153.

Shu, X.Z.; Zhu, K.J. *Eur. J. Pharm. Biopharm*. **2002**, *54*, 235–243.

Simoes, S.; Filipe, A.; Faneca, H.; Mano, M.; Penacho, N.; Düzgünes, N.; et al. *Expert Opin. Drug. Deliv*. **2005**, *2*, 237–54.

Sizovs, A.; Xue, L.; Tolstyka, Z.P.; Ingle, N.P.; Wu, Y.; Cortez, M.; Reineke, T.M. *J. AM. Chem. Soc*. **2013**, *135*, 15417-15424.

Srinivasachari, S.; Liu, Y.; Zhang, G.; Prevette, L.; Reineke, T.M. *J. Am. Chem. Soc.* **2006**, *128,* 8176−8184.

Stephenson, J. *J. Am. Med. Assoc*. **2001**, *285*, 2570.

Strand, S.P.; Danielsen, S.; Christensen, B.E.; Varum, K.M. *Biomacromolecules* **2005**, *6*, 3357–3366.

Sugimoto, M.; Morimoto, M.; Sachiwa, H. *Carbohydro. Polym*. **1998**, *36*, 45-59.

Sunshine, J.C.; Sunshine, S.B.; Bhutto, I.; Handa, J.T.; Green, J.J. PLoS One 2012, 7, e37543

Tang, X.; Pikal, M.J. *Pharm. Res.* **2004**, *21*, 191–200.

Themis, M.; Waddington, S. N.; Schmidt, M.; von Kalle, C.; Wang, Y.; et al. *Mol. Ther.* **2005**, *12,*

763–771.

Toh E.K.W.; Chen, H.Y.; Lo, Y.L.; Huang, S.J.; Wang, L.F. *Nanomed. Nanotechnol. Biol. Med.* **2011**, *7*, 174-183.

Walther, W.; Stein, U. *Drugs* **2000**, *60,* 249-271.

Wang, W. *Int. J. Pharm*. **2000**, *203*, 1–60.

Xu, D.; Dustin, D.; Jiang, L.; Samways, D.S.; Dong, H. *Chem. Commun*. **2015,** *51*, 11757-11760.

Yin, H.; Kanasty, R. L.; Eltoukhy, A.; Vegas, A.J.; Dorkin, J.R.; Anderson, D.G. *Nat. Rev. Ganet.* **2014**, *15*, 541-555.

Zillies, J.C.; Zwiorek, K.; Hoffmann, F.; Vollmar, A.; Anchordoquy, T.J.; Winter, G.; Coester, C. *Eur. J. Pharm. Biopharm*. **2008**, *70*, 514-521.

Zugates, G.T.; Tedford, N.C. Zumbuehl, A.; Jhunjhunwala, S.; Kang, C.S.; Griffith, L.G.; Lauffenburger, D.A.; Langer, R.; Anderson, D.G. *Bioconjugate Chem.* **2007**, *18*, 1887-1896.

ENGINEERING MUCUS PERMEATING NANOPARTICLES

Patent derived from this work:

Oh, S. and Borrós. S. (Patent pending: 2016).

Publications derived from this work:

Oh, S. et al., 'Enhanced mucus permeability and transfection efficiency of coating poly(β-amino ester)s/DNA complexes with poly(acrylic acid)-bromelain conjugates'. (In preparation).

## 4.1.   Introduction

As described in Chapter 3, we developed the novel formulation consisting of the poly(β-amino ester)s/DNA the coating agents stabilized by surface-modification strategies, and investigated the effect of the additives such as chitosan polymers on their stability and transfection efficiency. The results obtained in the previous Chapter demonstrated that chitosan-coated formulation of PBAE/DNA complexes significantly enhanced their stability with increasing the amount of chitosan, but presented lower transfection efficiency compared with non-coated formulations. According to this result, we hypothesize that the coating agents may play an important role in developing the delivery systems of macromolecular drugs. In this Chapter, therefore, our interest has been focused on the development the suitable coating agents, and further design and development of engineer PBAE/DNA formulations with the advanced coating agents in order to enhance stability and transfection level, and facilitate efficient mucus transport, which is the main objective of this Thesis.

In the previous Chapter, we have chosen chitosan as coating agents for the PBAE/DNA formulations due to its favorable properties, such as biodegradability, biocompatibility, non-toxic, and high stability (Felt *et al.*, 1998; Lee *et al.*, 1998; Shu *et al.*, 2002; Lee *et al.*, 2007; Mao *et al.*, 2010). However, we found that its low transfection efficiency still limits its application as a gene delivery system. To overcome this problem, various modifications have been carried out on chitosan as an alternative for gene vectors. The abundant amine and hydroxyl groups on the chitosan backbone allow easy chemical modification which further enhanced its efficacy for gene transfer (Zhao *et al.*, 2010). Thiolated chitosan is a class of chitosan derivatives showing desired features in the field of mucosal gene delivery (Guang 2002; Lee *et al.*, 2007; Martien *et al.*, 2007). As introduced in Chapter 1, since the concept of thiolated polymers-or so-called thiomers- had been pioneered in the late 1990s, thiolated chitosan polymers have gained considerable attention due to their valuable properties, especially mucoadhesive and permeation enhancing properties (Kast and Bernkop-Schnürch 2001; Bernkop-Schnürch *et al.*, 1999, 2003, 2004, 2007; Bravo-Osuna *et al.*, 2007; Lichen *et al.*, 2009; Anitha *et al.*, 2010). These unique properties have been also investigated and described in detail in Chapter 2.

Bernkop-Schnürch et al. firstly synthesized the thiolated chitosan polymers such as chitosan-cysteine (CS-Cys) (Bernkop-Schnürch *et al.*, 1999). Thereafter, as shown in scheme 4.1, various thiolated chitosans including, chitosan-thioglycolic acid (CS-TGA) (Kast and Bernkop-Schnürch 2001; Hornof *et al.*, 2003), chitosan-tributylamidine (CS-TBA) (Bernkop-Schnürch *et al.*, 2003), chitosan-glutathione (CS-GSH) (Kafedjiiski *et al.*, 2005), chitosan-glutatione (CS-GSH), chitosan-6-mercaptonicotinic acid (CS-6MNA) and chitosan-N-acytel cysteine (CS-NAC) (Schmiz *et al.*, 2008) have been synthesized and evaluated. Thiolated chitosans, which display thiol bearing side chains, were shown to improve the mucoadhesion

properties by forming covalent bonds with cysteine-rich subdomains of mucins via thiol-disulfide exchange reactions. The bridging structure most commonly encountered in biological systems-the disulfide bond-has thereby been discovered for the covalent adhesion of polymers to the mucus gel layer of the mucosa (Bernkop-Schnürch *et al.*, 2005). Moreover, thiolated chitosan exhibited significant enhancement of both transfection efficiency and mucosal permeation properties. For this reason, these thiolated chitosans have been recently used for the development of efficient mucosal delivery systems of macromolecules.
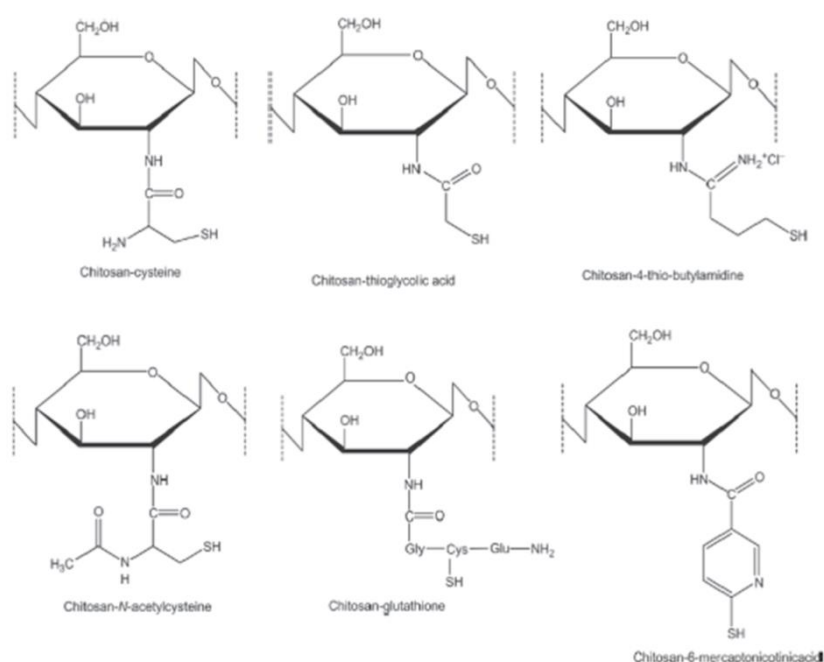
Scheme 4.1. Chemical structures of thiolated chitosan (Sakloetasakun *et al.*, 2011).

As explained in the previous paragraph, the free sulphydryl groups (-SH) can form disulfide bonds with cysteine-rich subdomains of mucus glycoproteins on cell membranes, thereby promoting cellular uptake of the thiolated chitosan/DNA complexes. This mechanism may result in high transfection efficiency (Loretz *et al.*, 2007; Lee *et al.*, 2007; Martien *et al.*, 2007; Schmitz *et al.*, 2007; Zaho *et al.*, 2010). However, it should be noteworthy that transfection of thiolated chitosan-based vectors is highly pH-dependent. Martien and coworkers reported that nanocarriers based on chitosan-thioglycolic acid conjugates (CS-TGA) improved gene transfer efficiency with low toxicity (Martien *et al.*, 2007). This study was carried out at pH 4 compared to pH 5, and the results showed that the transfection of nanoparticles was higher at pH 4 than those of pH 5. Lee et al. demonstrated that nanocomplexes composing CS-TGA and DNA exhibit a significantly higher gene transfer potential and sustained gene expression, indicating their great potential for gene therapy. Both unmodified and thiolated chitosans

showed considerably higher transfection efficient at pH 7 than at pH 7.5 (Lee *et al.*, 2007). Recently, Li et al. developed the novel gene vector based on poly[poly(ethylene glycol) methacrylate]-CS-GSH (CS-PMPEG-GSH) conjugates that improved the binding ability to cell membrane efficiency, resulting in high transfection efficiency compared to unmodified chitosan or CS-PMPEG. However, they showed still lower transfection efficiency at pH 7.2 compared to commercial transfection agents such as polyethylenimine (PEI) (Li *et al.*, 20011). To our knowledge, applications of thoilated chitosans in gene delivery systems are still limited due to low transfection efficiency under physiological pH conditions. Thus, thiolated chitosan have been employed here as coating agents in order to formulate the novel mucosal drug delivery systems consisting of PBAE/DNA and thiolated chitosan. We propose that these formulations can integrate the benefits of both PBAEs and coating agents with minimizing their disadvantages.

With the same hypothesis mentioned above, proteolytic enzymes have been also applied as the coating agents in order to achieve the main objective of this Thesis, which is to develop the delivery systems based on PBAE/DNA that can enhance stability and transfection efficiency, and cross the mucus gel layer. Proteases such as trypsin, papain or bromelain are well established to cleave protein structures within the mucus, resulting in reducing rheological properties of mucus (Majjima *et al.*, 1988; Lai *et al.*, 2009). Thereby, they can play as mucolytic agents.

In this sense, nanoparticles based on biopolymers in combination with proteolytic enzymes have been recently considered as promising nanocarriers for facilitated deep mucus penetration (Müller *et al.*, 2014; Samaridou *et al.*, 2014). Müller and coworkers studied the efficiency of proteolytic enzymes such as trypsin, chymotrypsin, papain, bromelain, pepsin, and proteinase. Among all enzyme tested, papain and proteinase exhibited a considerable decrease in the viscous and elastic properties of mucus through the enzymatic breakdown of complex protein substances (Müller *et al.*, 2013). In addition, they firstly synthesized poly(acrylic acid)-papain conjugates by covalent attachment of papain to poly(acrylic acid), and prepared nanoparticles by ionic gelation. The results exhibited that these conjugates facilitated their transport through the mucus layer (Müller *et al.*, 2014). Recently, Köllner et al. supported that the nanocarriers composed of poly(acrylic acid) and mucolytic enzyme such as papain, cysteine or papain-cysteine, considerably improved the particle transport rates and decreased the viscoelastic properties of the mucus compared to unmodified (Köllner *et al.*, 2015). Afterward, it was compared that other mucolytic enzyme bromelain, which is a cysteine protease (thiol protease) derived from the stem of the pineapple plant (Borrelli *et al.*, 2012), exhibited more significant effect in altering the mucus structure and higher performance in permeating the mucus layer comparison with poly(acrylic acid)-papain (Pereira de Sousa *et al.*, 2015). For this reason, poly(acrylic acid)-bromelain conjugates have been chosen for this study as coating agents for PBAE/DNA complexes. In fact, in Chapter 2, we have evaluated and

studied the interaction between mucin and the several mucosal delivery systems using the quartz crystal microbalance with dissipation (QCM-D) technique. Among all nanocarriers tested using QCM-D, nanoparticles bearing with bromelain have shown the highest permeation through the mucin layer. For investigating the interaction of particles with mucus, in this Chapter, the novel mucosal nanocarriers have been assessed for the mucus permeation behaviour by rotating silicone tube technique and/or multiple particle tracking (MPT).

After preparing two different coating agents; chitosan-thioglycolic acid (CS-TGA or CT) and poly(acrylic acid)-bromelain (PAA-BRO or PB) conjugates, we have designed and developed the surface-modified formulation of PBAE/DNA with coating agents via electrostatic interaction. We propose that this coating formulation can show the synergistic effect of PBAE/DNA, related to high transfection efficiency, and the coating agents, related to high stability and facilitating particle transport through the mucus layer.

4.2.   Aim and scope of this Chapter

As presented above, the first aim of this Chapter is to develop a simple surface-modified formulation of PBAE/DNA complexes with different amounts of CS-TGA via electrostatic interaction. PBAEs bearing with arginine (R), which showed higher gene expression among non-mixtures of PBAEs, have been chosen as control. Here PBAEs bearing with other oligopeptides such as histidine (H) and lysine (K) have been applied. The polymer mixture of K/H and R/H-based complexes has been chosen for this study since it showed highest transfection efficiencies for COS-7 cells in comparison with other PBAEs bearing oligopeptide moieties, but with inferior viability (Segovia *et al.* 2014). The results show that the coating PBAE/DNA/CS-TGA complexes improved significantly the stability with increasing the amounts of CS-TGA. In addition, there are observed the sustained high transfection efficiency with low toxicity and the improved particle diffusion through the mucus layer.

The second aim of this Chapter is to develop a coating formulation of the cationic PBAE/DNA complexes with anionic PAA-BRO via electrostatic interaction. The formation of complexes having different amount of coating agents is determined using agarose gel electrophoresis. The effect of the variety of PAA-BRO on physicochemical properties and particle diffusion studies using two different techniques are investigated. Furthermore, transfection efficiency and cytotoxicity are evaluated in COS-7 cells. The non-coating PBAE/DNA complexes without PAA-BRO are used as a control. The results show the coating PBAE/DNA/PAA-BRO complexes could improve particle penetration through the mucus layer, stability and transfection efficiency with low cytotoxicity.

To achieve these aims the following steps will be developed:

- To synthesize and characterize poly(β-amino ester)s bearing with arginine, histidine and lysine (R, H and K).

- To prepare the polymer mixtures (K/H and R/H)

- To synthesize and characterize chitosan-thioglycolic acid (CS-TGA) and poly(acrylic acid)-bromelain (PAA-BRO) conjugates.

- To develop the thiolated chitosan-coated PBAE/DNA formulations, which were formulated with a coating of 0.17, 0.33, 0.67, 1.33 and 2.67 wt% of CS-TGA, and these formulations incorporating fluorescence dye Lumogen.

- To evaluate stability, transfection efficiency, cell viability and particle diffusion study of the developed PBAE/DNA/CS-TGA.

- To develop the proteolytic enzyme-coated PBAE/DNA formulations, which were formulated with a coating of 0.17, 0.33, 0.67, 1.33 and 2.67 wt% of PAA-BRO, and these formulations incorporating fluorescence dye Lumogen.

- To evaluate stability, transfection efficiency, cell viability and particle diffusion study of the developed R/DNA/PAA-BRO.

4.3. Experimental section

4.3.1. Materials

Reagents and solvent were obtained from Sigma Aldrich and used as received, unless otherwise stated. Chitosan (22 kDa) with a degree of deacetylation of 85% was purchased from Fluka (Vienna, Austria). HS-Cys-Arg-Arg-Arg-NH$_2$ (CR3), H-Cys-Lys-Lys-Lys-NH$_2$ (CK3), H-Cys-His-His-His-NH$_2$ (CH3), H-Cys-Asp-Asp-Asp-NH2 (CD3) and H-Cys-Glu-Glu-Glu-NH2 (CE3) were obtained from GL Biochem Ltd. (Shanghai, China). Lumogen red was purchased from Kremerpigmente GmbH & Co.KG (Aichstetten, Germany). Bicinchoninic acid kit (BCA) was purchased from Thermo Scientific (Vienna, Austria). Native porcine intestinal mucus (PImucus) was purified and kindly provided by Prof. Jeffrey Pearson of Newcastle University (UK). Plasmid DNA encoding green fluorescent protein (pmaxGFP, 3486 bp) was purchased

from Amaxa Inc. (Gaithersburg, MD, USA). COS-7 cells were obtained from ATCC (Manassas, VA) and cultured in DMEM (Gibco) supplemented with 10% fetal bovin serum (FBS), 1% Glutamine and 1% Streptomycin/Penicillin (complete DMEM). All regents were analytical grade and used without further purification.

4.3.2. Synthesis and characterization of polymers

4.3.2.1. Oligopeptide-terminated PBAEs

The procedure of synthesis of acrylate or oligopeptide-terminated poly(β-amino ester)s (PBAEs) has been described in detail in 3.3.2. In brief, oligopeptide-modified PBAEs were synthesized by end-modification of acrylate-terminated C32 with thiol-terminated oligopeptide at 1:2.5 molar ratio in dimethyl sulfoxide (DMSO). The mixture was stirred at room temperature for 24 h and the resulting polymer was purified by precipitation in diethyl ether and acetone for twice and dried under vacuum. The polymers were then dissolved at 100 mg/ml in DMSO and stored at -20 ºC until further use. The chemical structure of the oligopeptide-modified PBAEs was confirmed by ^{1}H-NMR spectroscopy. The chemical structure of the acrylate-terminated and the oligopeptide-terminated PBAE polymers were confirmed by ^{1}H-NMR, which was conducted on a Varian NMR instrument operating at 400 MHz.

^{1}H-NMR of R (400 MHz, CD_3OD, TMS), δ (ppm): 4.45-4.35 (br, NH_2COCHNHCOCHNH- and COCHNHCOCHCH$_2$-), 4.15 (t, CH_2CH_2O), 3.56 (t, $-N(CH_2)_4CH_2OH$), 3.22 (br, $NH_2C(NH)_2CH_2$- and $-N(CH_2)_4CH_2OH$), 3.09 (br, CH_2CH_2N-), 2.85 (br, $-CH_2SCH_2$-), 2.78 (m, CH2CH_2N-), 2.67 (br, $NH_2C(NH)_2CH$-), 1.92 (m, $NH_2C(NH)_2(CH_2)_2CH_2$CH-), 1.75 (br, $-OCH_2(CH_2)_2CH_2O$), 1.57 (br, $-N(CH_2)_2COOCH_2CH_2$–), 1.3-1.4 (br, $-NCH_2(CH_2)_3CH_2OH$).

^{1}H-NMR of K (Tri-lysine end-modified PBAE polymer, K3C-C32-CK3) (400 MHz, CD_3OD, TMS), δ (ppm): 4.38-4.29 (br, $NH_2(CH_2)_4CH$-) 4.13 (t, CH_2CH_2O-), 3.73 (br, NH_2CHCH_2S-), 3.55 (t, CH_2CH_2OH), 2.94 (br, CH_2CH_2N, $NH_2CH_2(CH_2)_3CH$-), 2.83 (dd, $-CH_2SCH_2$-), 2.57 (br, -NCH$_2CH_2$COO-), 1.86 (m, $NH_2(CH_2)_3CH_2$CH-), 1.73 (br, $-OCH_2CH_2CH_2CH_2O$), 1.69 (m, $NH_2CH_2CH_2(CH_2)_2$CH-), 1.54 (br, $-CH_2CH_2CH_2CH_2OH$), 1.37 (br, $-N(CH_2)_2CH_2(CH_2)_2OH$).

^{1}H-NMR of H (Tri-histidine end-modified PBAE polymer, H3C-C32-CH3) (400 MHz, CD_3OD, TMS), δ (ppm): 8.0-7.0 (br, $-NCH$NHCCH-), 4.60-4.36 (br, $-CH_2CH$-), 4.17 (t, CH_2CH_2O), 3.56 (t, CH_2CH_2OH), 3.05 (dd, $-CH_2$CH-), 2.88 (br, OH(CH_2)_4CH_2N-), 2.83 (dd, $-CH_2SCH_2$-), 2.72 (br, -NCH$_2CH_2$COO), 1.65 (m, $NH_2CH_2CH_2(CH_2)_2$CH-), 1.56 (br, $-CH_2CH_2CH_2CH_2OH$), 1.39 (br, $-N(CH_2)_2CH_2(CH_2)_2OH$).

^{1}H-NMR of D (Tri-aspartic acid end-modified PBAE polymer, D3C-C32-CD3) (400 MHz, CD$_3$OD, TMS), δ (ppm): 4.44-4.55 (br, NH$_2$COC*H*NHCOC*H*NH- and COC*H*NHCOC*H*CH$_2$-4.11 (br, NH$_2$C*H*CH$_2$S–), 3.9-4.03 (t, –N(CH$_2$)$_2$COOC*H$_2$*CH$_2$–), 3.36 (t, –N(CH$_2$)$_4$C*H$_2$*OH), 2.95(dd, -C*H$_2$*SC*H$_2$*-), 2.64–2.78 (m, –COOCH$_2$C*H$_2$*N–), 2.47–2.49 (t,– CHC*H$_2$*COO-), 1.62 (br, – N(CH$_2$)$_2$COOCH$_2$C*H$_2$*– and CH$_2$CHCOOCH$_2$C*H$_2$*–), 1.23–1.4 (br, –NCH$_2$(C*H$_2$*)$_3$CH$_2$OH).

^{1}H-NMR of E (Tri-glutamic acid end-modified PBAE polymer, E3C-C32-CE3) (400 MHz, CD$_3$OD, TMS), δ (ppm): 4.22-4.36 (br, NH$_2$COC*H*NHCOC*H*NH- and COC*H*NHCOC*H*CH$_2$-4.13 (br, NH$_2$C*H*CH$_2$S–), 4.04 (t, –N(CH$_2$)$_2$COOC*H$_2$*CH$_2$–), 3.38 (t, –N(CH$_2$)$_4$C*H$_2$*OH), 2.95(dd, – C*H$_2$*SC*H$_2$*–), 2.64–2.78 (m, –COOCH$_2$C*H$_2$*N–), 2.47–2.49 (t,–C*H*CH$_2$CH$_2$COO–, -CHC*H$_2$*CH$_2$COO–, –CHCH$_2$C*H$_2$*COO–), 1.62 (br, –N(CH$_2$)$_2$COOCH$_2$C*H$_2$*– and CH$_2$CHCOOCH$_2$C*H$_2$*–), 1.25–1.4 (br, –NCH$_2$(C*H$_2$*)$_3$CH$_2$OH).

4.3.2.2. Chitosan-thioglycolic acid conjugates

The covalent attachment of thioglycolic acid (TGA) to chitosan was achieved by the formation of amide bonds between the primary amino groups of the polymer and the carboxylic acid group of TGA (Friedl *et al.,* 2013). Briefly, 500 mg of chitosan was dissolved in 2% of acetic acid and then adjust to pH 5 with 5 M sodium hydroxide. Additionally, 500 mg of TGA was dissolved in demineralized water and TGA was chemically treated with ethyl(dimethylaminopropyl)carbodiimide (EDAC) in a final concentration of 50 mM in order to activate the carboxylic acid moieties. Afterward, activate TGA solutions were slowly added in chitosan solution and adjust to pH 5. The mixture solution was vigorously stirred at room temperature for 3 h and dialyzed (MWCO 12 kDa) for 3 days at 10 ºC. The resulting solutions were lyophilized and stored at 4 ºC until further use.

The degree of modification was determined with Ellman's reagent quantifying free thiol groups, as described by Friedl et al (Friedl *et al.,* 2013). In brief, 0.5 mg each conjugate was hydrated in 250 µl of demineralized water. Then, 250 µl of 0.5 M phosphate buffer at pH 8 and 500 µl of Ellman's reagent (3 mg of and 5,5'-dithiolbis(2-nitrobenzoic acid) dissolved in 10 mL of 0.5 M phosphate buffer at pH 8) was added and the mixture was incubated for 2 h at 37 ºC in dark. 150 µl of each sample was then transferred into a 96-well plate and the absorbance was measured at 450 nm using a microplate reader (TECAN infinite M200 spectrophotometer, Austria). The amount of free thiol groups was calculated using a standard curve obtained by chitosan solutions with increasing concentration of L-cysteine prepared in exact the same way as the samples. The disulfide content was evaluated after reduction with NaBH$_4$ and determined by Ellman's reagent. The total amount of these moieties is represented by the summation of reduced thiol groups and oxidized thiol groups in form of disulfide bonds (Sakloestusakun *et al.,* 2009).

4.3.2.3. Poly(acrylic acid)-bromelain conjugates

Poly(acrylic acid)-bromelain (PAA-BRO) conjugates were synthesized as previously described (Pereira de Sousa *et al.,* 2015). Briefly, 3.26 g of PAA solution (0.01 mmol) was dissolved in 1 L of demineralized water and adjust to pH 6. Then, 5g of EDAC and 3 g of NHS dissolved in 100 mL of demineralized water were added to the PAA solution and stirred for 1 h. Thereafter, 1.42 g of BRO (0.043 mmol) dissolved in 500 mL of demineralized water was slowly added to the reaction solution and stirred for 24 h at 10 ºC. The mixture solutions were dialyzed for 3 days at 10 ºC, lyophilized and stored at 4 ºC until further use.

The amount of enzyme conjugated to polymers was determined by micro BCA protein assay as described earlier (Pereira de Sousa *et al.,* 2015). Briefly, the conjugates were dissolved in 0.1 M NaOH solution containing 1.5 wt% of sodium dodecyl sulfate to obtain a concentration of 0.1 mg/mL. The mixtures were incubated at room temperature in a thermomixer (Thermomixer Conform; Eppendorf, Hamburg, Germany) under constant shaking, 1000 rpm for 2h. Finally, 150 µl of each sample was transferred into a 96-well plate and the absorbance was measured at 562 nm using the microplate reader. The amount of enzyme was extrapolated by fitting the data to a calibration curve obtained via analyzing solution with different concentration of bromelain. The enzyme content of polymers was reported on a weighted base as the ratio between the amount of conjugated enzyme and the amount of polymers.

4.3.3. Formulation of complexes

4.3.3.1. PBAE/DNA complexes with CS-TGA

Complexes were formulated by mixing polymer and pGFP (plasmid green fluorescent protein) in a weight ratio of 50:1. The PBAE solutions and pGFP solutions were diluted to 25 mM sodium acetate (NaAc, pH 5.2) to a final concentration of 6 mg/ml and 0.06 mg/ml, respectively. The chitosan-TGA conjugates (CS-TGA or CT) were dissolved in the same buffer (1.6 mg/ml) and filtered through 0.2 µm. The CT stock solution was diluted with 25 mM NaAc in a proportional ranging from 0.17 to 2.67 wt% relative to the wt% of PBAE solutions when mixed with the PBAE solution. Briefly, 50 µl of diluted CT solution was added to 50 µl of diluted PBAE solution, and vigorously mixed with vortex. 100 µl of diluted pGFP was then added to the mixture PBAE/CT solutions, mixed with vortex and incubated at room temperature for 10 min. The formulation of mixture PBAE polymers was prepared with lysine-histidine (K/H) or arginine-histidine (R/H) at 1:1 weight ratio.

4.3.3.2. PBAE/DNA complexes with PAA-BRO

Nanocomplexes were formulated by mixing polymer and pGFP (plasmid green fluorescent protein) in a weight ratio of 50:1. The R polymer solution and pGFP solution were diluted to 25 mM sodium acetate (NaAc, pH 5.2) to a final concentration of 6 mg/ml and 0.06 mg/ml, respectively. The PAA-BRO was dissolved in the same buffer (0.8 mg/ml) and filtered through 0.2 μm. The PAA-BRO stock solution was diluted with 25 mM NaAc in a proportion ranging from 0.17 to 1.33 wt% relative to the wt% of PBAE solutions when mixed with the PBAE solution. Briefly, 100 μl of diluted pDNA was added to 50 μl of diluted R solution, and gently mixed with vortex. 50 μl of diluted PAA-BRO was then added to the mixture solution, mixed vigorously with vortex and incubated at room temperature for 10 min. As control, R/DNA complexes were formulated by same process as described for complexes coated with PAA-BRO above. In this case, 0.06 mg/ml of pDNA was mixed into 3 mg/ml of R solution.

4.3.3.3. Coating the complexes labeled with Lumogen

For permeation study, 6.1 μl of Lumogen solution (0.5 mg/ml in DMSO) was mixed into R solution and incorporated into complexes. The resulting labeled particle suspension was used for further particle diffusion and tracking analysis.

4.3.4. Characterization of complexes

The particle size, zeta potential, and stability of complexes were determined, diluted in phosphate-buffered saline (PBS) at pH 7.4, by DLS using a Zetasizer Nano ZS (Malvern Instruments, Ltd., UK) at 25 °C. Each experiment was carried out in triplicate and the means ± SD result was reported.

Complex formulation was evaluated by agarose gel electrophoresis. PBAE/DNA complexes modified with or without coating agents were loaded onto a 0.8% agarose gel in Tris-Acetate-EDTA (TAE) buffer containing ethidium bromide (1μg/ml). The samples were run on the gel at 120 V for 80 min (Apelex PS305, France) and visualized using UV irradiation.

4.3.5. In vitro transfection and flow cytometry

Cellular transfection was carried out using pDNA plasmid in COS-7 cells. Cells were seeded on 96-well plates at a density of 1 x 10^5 cells/well in 150 μl of DMEM medium and incubated overnight to reach 80% confluence. PBAE/DNA incorporated with or without coating agents such as CT or PAA-BRO were prepared as described above (polymer/DNA = 50/1, wt/wt). Complexes were diluted in serum-free DMEM medium and added to cells at a final

plasmid concentration of 0.3 µg DNA/well. Briefly, 33 µl of complexes were diluted into 450 µl of serum-free DMEM medium and cells were washed once with PBS. Then, 150 µl of the resulting solutions were added to each well, achieving a final concentration of 0.3 µg DNA/well. Cells were incubated for 3 h and washed once with PBS, and incubated in complete DMEM. After 48 h, cells were imaged using fluorescence microscopy and then prepared for analysis by flow cytometry (BD LSRFortessa cell analyzer) to look for GFP expression. Untreated cells were used as a negative control. The non-coating PBAE/DNA complexes without the coating agents were used as a positive control.

4.3.6. Cytotoxicity assay

MTS assay (CellTiter 96® AQueous One Solution Cell Proliferation Assay, Promega Corporation, USA) was used to assess the viability of COS-7 cells transfected with complexes. Cell viability was evaluated 48 h after transfection using MTS assay as instructed by the manufacturer. At 48 h after transfection, the medium was removed, cells were washed with PBS and complete medium supplemented with 20% MTS reagent (v/v) was added. Cells were incubated at 37 °C and the absorbance was measured at 490 nm using a microplate reader (Elx808 Biotek Instruments Ltd, USA). Cell viability was expressed as a relative percentage compared with untreated cells.

4.3.7. Diffusion study

To investigate the transport of nanocomplexes across the mucus barrier, a quantitative permeation study in PImucus was performed following a method described previously by Köllner et al. (Köllner *et al.,* 2015). In brief, 200 µl of PImucus was slowly filled in a silicon tube with a length of 30 mm and a diameter of 3 mm and closed on one end with a silicon cap. 50 µl of each labeled particle suspension was added into the other open end and closed with another silicon cap. As blank value, 50 µl of diluted Lumogen solution in NaAc without particles was prepared by same process as described above for labeled particle suspension. All tubes were incubated at 37 °C for 4 h under continuous rotation. Thereafter, the tubes were frozen at -80 °C for 1 h and cut into 10 slices of 2 mm length. Each slice was treated with 200 µl of DMSO, and vigorously vortexed and ultrasonicated for 1 h. Afterwards it was left at room temperature for 24 h. Fluorescence was determined in order to assess the depth of diffusion into the mucus. The resulting fluorescence was determined using 100% value of each particle suspension.

4.3.8. Multiple particle tracking

Nanoparticle diffusion through intestinal mucus was assessed by multiple particle tracking (MPT) (Hanes and Lai 2007). The MPT technique can track particle displacement with a resolution to within 5 nm (Apgar *et al.*, 2000). Samples (0.5 g) of mucus were incubated in glass-bottom MatTek imaging dishes at 37 °C. The fluorescently labelled NPs were inoculated into each 0.5 g mucus sample in a 25 µl aliquots. To ensure effective particle distribution within the matrix a 2 hr period of equilibration was allowed following inoculation and prior to video microscopy capture of NP movement within the mucus. Video capture involved 2-dimensional imaging on a Leica DM IRB wide-field epifluorescence microscope (x63 magnification oil immersion lens) using a high speed camera (Allied Vision Technologies, UK) running at a frame rate of 33 ms i.e. capturing 30 frames sec^{-1}; each completed video film comprised 300 frames. For each 0.5 g mucus sample approximately 120 NPs were simultaneously tracked and their movements captured. For any distinct NP species, e.g. a particular polyelectrolyte mass ratio, a minimum of three distinct mucus samples were analysed, i.e. minimum of 360 individual NP trajectories assessed.

Videos were imported into Fiji ImageJ software which converts the movement of each NP into individual NP trajectories across the full duration of the 10 videos. However, for the analysis of particle diffusion only a 30 frame video period (1 sec) was used where the respective particle must have displayed a continuous presence in the X-Y plane for the 30 sequential frames. Limiting the period of analysis to 30 frames minimises the impact of mucin movement upon the particle diffusion calculations (Lai *et al.*, 2007). The individual particle trajectories were converted into numeric pixel data (Mosaic Particle Tracker within Fiji ImageJ). This data was then converted from pixels into metric distance based on the microscope and video capture settings. The distances moved by each particle over a selected time interval (Δt) in the X-Y trajectory were then expressed as a squared displacement (SD). The mean square displacement (MSD) of one particle represents the geometric mean of the particle's squared displacements throughout it's entire trajectory (Griessinger *et al.*, 2014).

MSD was determined as follows (Macierzanka *et al.*, 2014):

$$MSD_{(n)} = (X_{\Delta t})^2 + (Y_{\Delta t})^2 \qquad\qquad\text{(equation 4.1)}$$

In any single experiment an MSD was calculated for at least 120 individual droplets with the experiment replicated a further two times, i.e. 360 droplets studied in total. For each droplets species under study an "ensemble mean square displacement" (defined by ‹MSD›) was determined for each of the three replicate studies. The effective diffusion coefficient (‹Deff›) for a particular droplets species was then calculated by:

$$‹Deff› = ‹MSD›/(4 * \Delta t) \qquad\qquad\text{(equation 4.2)}$$

where 4 is a constant relating to a 2-dimensional mode of video capture and Δt is the selected time interval.

Proportion of diffusive droplets: Measuring droplet diffusion across various time intervals allows description of the proportion of droplets that are diffusive through the mucus matrix (Lai *et al.*, 2007). Equation 3 was used to determine a diffusivity factor (DF) which expresses the effective diffusion coefficient for each individual droplet (Deff) across the time intervals (Δt) of 1 s and 0.2 s

$$DF = Deff_{\Delta t=1\,s} / Deff_{\Delta t=0.2\,s} \hspace{3cm} \text{(equation 4.3)}$$

where the individual droplet $Deff = MSD/(4 * \Delta t)$. Droplets with a DF value of 0.9 and greater were defined as diffusive. The proportion of diffusive droplets within a given droplets type was then calculated and expressed as % Diffusive droplets.

Heterogeneity in droplet diffusion: Profiling the diffusive properties of each droplet within an entire population provides information on the heterogeneity of droplet movement and the presence of outlier sub-populations indicative of distinctive pathways of diffusion through the matrix. Here the effective diffusion coefficient for each individual droplet (Deff) was calculated at the time interval (Δt) of 1 s, and for any droplets type all 360 $Deff_{\Delta t=1\,s}$ were then ranked to allow comparison of the highest (90th) and lowest (10th) percentiles, where for example the 90th percentile is the Deff value below which 90% of the Deff observations may be found.

Droplet diffusion in water: The droplets' diffusion coefficient (D°) in water was calculated by the Stock-Einstein equation at 37 C°(Philibert 2005):

$$[D° = \kappa T / 6\pi\eta r] \hspace{3cm} \text{(equation 4.4)}$$

where κ is Boltzmann constant, *T* is absolute temperature, η is water viscosity, r is radius of the droplet. The diffusion of all droplets was also expressed as the parameter, % ratio [Deff] /[D°].

4.4.   Results and discussion
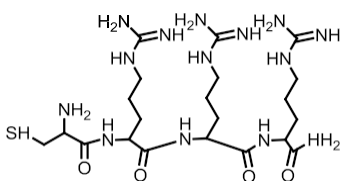
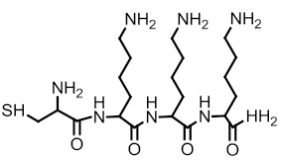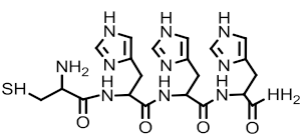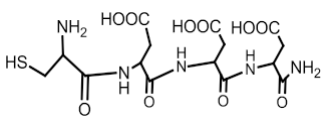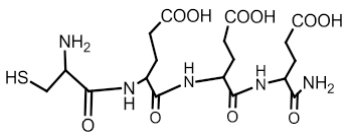### 4.4.1. Synthesis and characterization of polymers

4.4.1.1. Oligopeptide-terminated PBAEs

In Chapter 3.4.1, the synthesis of both acrylate-terminated C32 intermediate polymers was described in detail. This C32 polymer was applied for synthesis of all oligopeptide-terminated poly(β-amino ester)s (PBAEs). Synthesis of oligopeptide-terminated PBAEs was followed via two-steps procedure (Scheme 4.2). Oligopeptide end-modified PBAEs were obtained via addition of the thiol group of cysteine-oligopeptide moieties consisting of basic amino acids, i.e. arginine, lysine, histidine, glutamic acid and aspartic acid, to the acrylate-terminated end-groups of C32 polymer (Table 4.1). Oligopeptide-terminated PBAEs were characterized in terms of molecular structure by ^{1}H-NMR spectroscopy. The chemical structure of oligopeptide-modified PBAEs was confirmed by the disappearance of acrylate signals and the presence of signals typically associated with amino acid moieties. All polymers were obtained from the same C32 precursor. PBAEs bearing with glutamic acid and aspartic acid were used in Chapter 2.4.2.
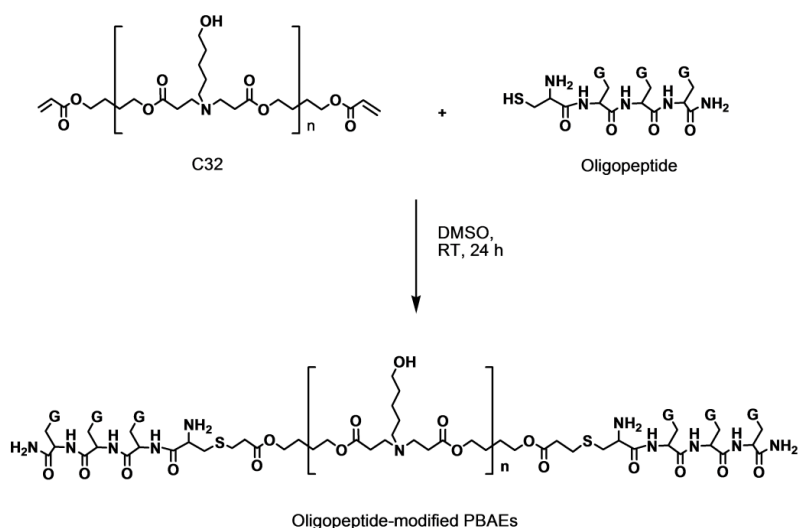
Scheme 4.2. Synthesis of oligopeptide-modified poly(β-amino ester)s. Terminal groups (G): arginine-, lysine-, histidine-, glutamic acid- and aspartic acid- oligopeptide.

Table 4.1. Synthesized oligopeptide-modified PBAE polymers and corresponding end-capping moieties.

Oligopeptide-modified PBAEs	Cysteine-oligopeptide moieties
Arginine-modified PBAEs, R or CR3-C32-CR3	
Lysine-modified PBAEs, K or CK3-C32-CK3	
Histidine-modified PBAEs, H or CH3-C32-CH3	
Aspartate acid-modified PBAEs, D or CD3-C32-CD3	
Glutamate acid-modified PBAEs, E or CE3-C32-CE3	

4.4.1.2. Chitosan-thiolglycolic acid conjugates

As it has been described before, in this Chapter, we have chosen two promising candidates as coating agents for the surface-modification of PBAE/DNA complexes. Thiolated chitosan is one of them. Scheme 4.3 shows the chemical structure of an immobilization of thiol groups on chitosan. The amount of free and total thiol groups was quantified according to the method described above (Friedl *et al.,* 2013). CS-TGA exhibited 402.15 ± 26.32 µmol free thiol groups and 408.87 ± 26.32 µmol disulfide bonds per gram polymer. A control was prepared in the same way as the CS-TGA conjugate but without the carbodiimide (EDAC) during the coupling reaction. This polymer displayed a negligible amount of remaining trace of TGA. After freeze-drying, the final products were obtained white powder of fibrous structure.
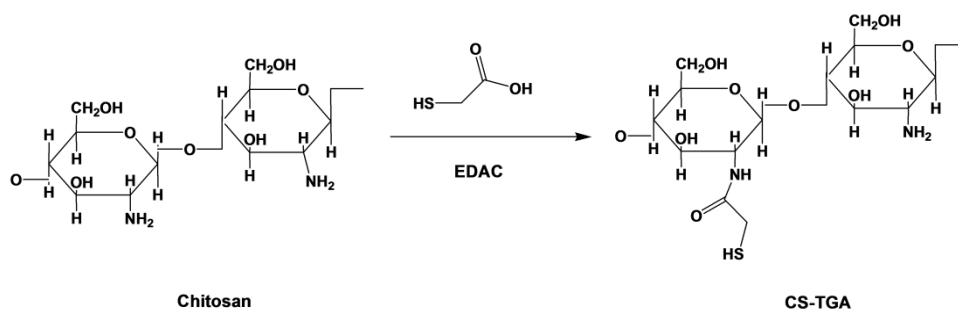
Scheme 4.3. Synthesis of chitosan-thiolglycolic acid conjugates.

4.4.1.3. Poly(acrylic acid)-bromelain conjugates

Poly(acrylic acid)-bromelain (PAA-BRO) conjugates is the other candidate chosen for the surface-modification of nanocarriers. The covalently attachment of PAA-BRO conjugates were performed via the formation of amide bond between carboxylic group of poly(acrylic acid) and amine group of bromelain. EDAC and NHS were used to improve the coupling rate of the enzyme (Köllner *et al.*, 2015). Compared with free forms, immobilized enzymes are more stable and easier to handle (Homaei *et al.*, 2010). The amount of enzyme conjugated to PAA was determined via micro BCA protein assay to be 789.31 ± 4.5 µg of enzyme per milligram of polymer. After freeze-drying, the final products appeared as white powder of fibrous structure.

4.4.2. PBAE/DNA complexes coated with CS-TGA

4.4.2.1. Formulation and characterization of complexes

In this Chapter, we have investigated the design and development of surface-modification formulation of PBAE/DNA with CS-TGA capable of enhancing stability, transfection efficiency with low cytotoxicity, and crossing the mucus layer. With thiolated-chitosan coating formulations, the mixtures of PBAE bearing lysine/histidine (K/H) and arginine/histidine (R/H) were selected for this study because they showed higher gene expression relatively to other oligopeptide-modified polymers (Segovia *et al.,* 2015). The formation of PBAEs with DNA having different weight ratios of CS-TGA was confirmed by agarose gel electrophoresis (Fig. 4.1). In comparison with the mobility of the naked pDNA, the movement of DNA was completely retarded in all test complexes. In other words, there was observed no significant DNA release when the PBAE/DNA complexes were coated with CS-TGA. These indicate that the addition of CS-TGA did not alter the formation ability of the PBAE/DNA complexes.
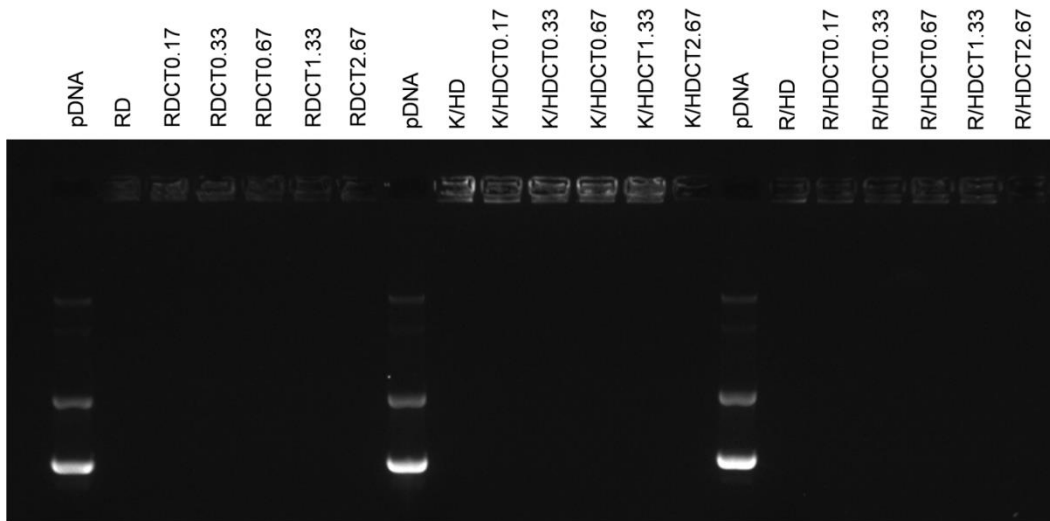

Fig. 4.1. Gel retardation assay of R/DNA coated with CS-TGA. Complexes were formulated by mixing polymers and GFP in a weight ratio of 50:1 and loaded onto an agarose gel containing ethidium bromide to assess DNA mobility by electrophoresis.

The particle size and zeta potential of the novel complexes comprising PBAEs and thiolated chitosan at 0.17 to 2.67 wt% were determined using a Zetasizer and the results are shown in Fig. 4.2. As control, unmodified R/DNA (RD) complexes were performed and had a mean size of 133 nm with a positive zeta potential of 20.5 mV (Fig. 4.2A). The RD complexes coated with differing amount of CS-TGA ranged from 130.4 to 192.6 nm in particle size and from 17 to 7.6 mV in zeta potential. The size of each sample is smaller than 200 nm and the smallest size was obtained when modified with 0.67 wt% of CS-TGA. There were small differences in size observed between complexes with or without CS-TGA. However, zeta potential values show a noticeable decrease with the small amount of the coating agents. These results indicate that the CS-TGA was completely covered on the surface of complexes. Moreover, they suggest that a range of amount of CS-TGA had an influence on the particle size and the surface charge of complexes. In the case of K/H mixtures of PBAEs, the particle size and zeta potential of K/H/DNA (K/HD) complexes were 237.8 nm and 17 mV, respectively (Fig. 4.2B). Compared to RD complexes, larger size was obtained, but similar zeta potential. The mean diameter of the resulting CT-coated K/HD complexes was found in a range of 185-198 nm with a zeta potential of about 13-10 mV. All coated K/HD complexes showed slightly smaller size but a significant decrease in zeta potential when compared to non-coated K/HD complexes, indicating that the surface of complexes were perfectly formulated with the coating agents. Moreover, the size and zeta potential of complexes were dependent on the weight ratio of thiolated chitosan. In the case of R/H mixtures of PBAEs, R/H/DNA (R/HD) complexes showed notably larger size (504.6 nm) and lower zeta potential (16.2 mV) compared to RD and K/HD complexes (Fig. 4.2C). There were obtained a decrease in particle size with increased amount of CS-TGA. In particular, a coating 0.17 and 0.33 depicted the appreciable decrease in size while the others showed little differences in the diameter of 231-247 nm. Moreover, R/HDCT complexes showed a significant decrease in zeta potential when coated with CS-TGA. The zeta potential of all coated R/HD complexes varied from 11 to 8 mV. These results confirmed that the size and zeta potential of the mixtures of PBAE/DNA complexes were affected by the amount of CS-TGA, resulting in more compact complexes. Interestingly, RD, K/H and R/H complexes coated with 0.67 wt% of thiolated chitosan exhibited the smallest size among all testing complexes.
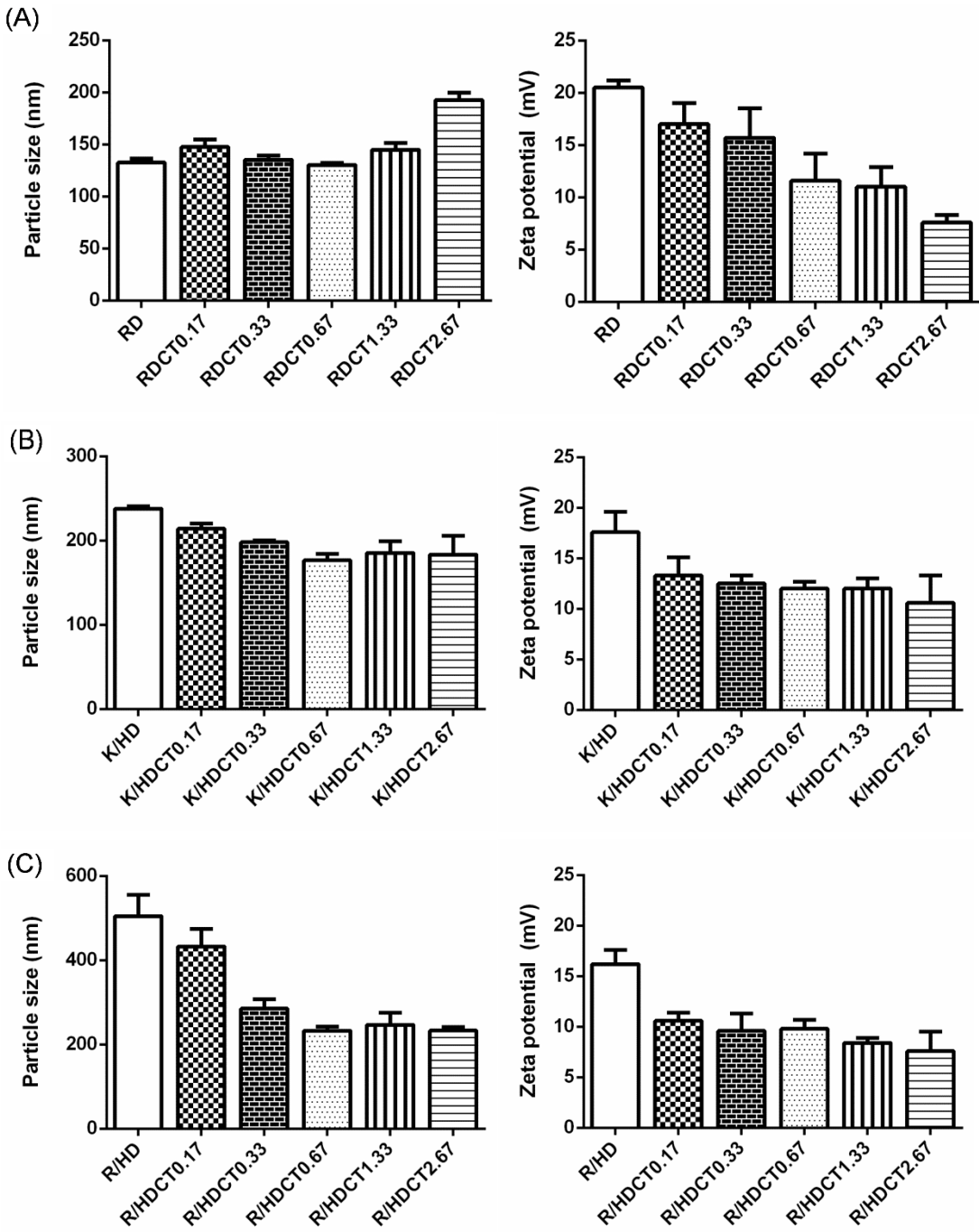
Fig. 4.2. The particle size and zeta potential of R/DNA (A), K/H/DNA (B) and R/H/DNA (C) complexes coated with or without 0.17, 0.33, 0.67, 1.33 and 2.67 wt% of CS-TGA. Each bar represents the mean ± SD (n ≥ 3).

4.4.2.2. Stability of PBAE/DNA coated with thiolated chitosan

In the previous Chapter, we found that chitosan-coated PBAE/DNA formulations significantly enhanced the stability compared to non-coated one. According to this, we expect that thiolated chitosan may influence the stability. In order to know the effect of thiolated chitosan on the stability, all the testing complexes were incubated for 4 h in PBS and analysed every hour and monitored changes in the particle size. The results of complexes comprising PBAE/DNA in combination with differing amount of CS-TGA are shown in Fig. 4.3. In the case of RDCT complexes, the size of all coated complexes except a coating 0.17 was displayed to be nearly constant over time (Fig. 4.3A). However, the particle size of RDCT0.17 was still less than 600 nm, indicating that all the coating RDCT complexes noticeably enhanced the stability. This observation supports that CS-TGA could affect to maintain the formulation of the RD complexes. All RDCT complexes showed the highest stability compared to the mixtures of PBAE/DNA coated with coating agents.

In the case of the mixtures of PBAEs, the stability of complexes in PBS within 4 h improved with increasing the amount of CS-TGA (Fig. 4.3B and C). In other words, there was obtained the significant enhanced stability when prepared with the higher amounts of thiolated chitosan. The particle size of both K/HD and R/HD complexes coated with 1.33 and 2.67 wt% of CS-TGA was less than 600 nm. Moreover, a coating of 0.67 wt% for R/HD complexes showed an improvement of stability. On the other hand, the complexes with lower amount of coating agents seemed to be aggregated. These results confirm that the amount of CS-TGA leads to high stability of PBAE/DNA complexes. Both K/H/DNA and R/H/DNA complexes coated with 1.33 wt% of CS-TGA showed the highest stability among all testing complexes, indicating that 1.33 wt% of coating agents might be an optimal weight content for improving the stability of the mixtures of PBAE-based complexes. Interestingly, there was obtained the constant particle size within 3 h (near 1000 nm) when the R/HD complexes were coated with 0.17 wt% of coating agents while the particle size of the coating of 0.17 wt% for K/HD complexes increased from 500 to 2600 nm. It had been already found that both unmodified and thiolated chitosan can clearly enhance the stability of the complexes based on PBAE bearing with arginine oligopeptides with DNA. As the arginine-histidine mixtures showed higher stability compared with the lysine-histidine mixtures, PBAE bearing with arginine may be favourably incorporated into thiolated chitosan. Although the initial particle size of R/HDCT complexes was larger than that of K/HDCT, there was obtained higher the stability of R/HD complexes coated with tholated chitosan relative to that of K/HDCT.
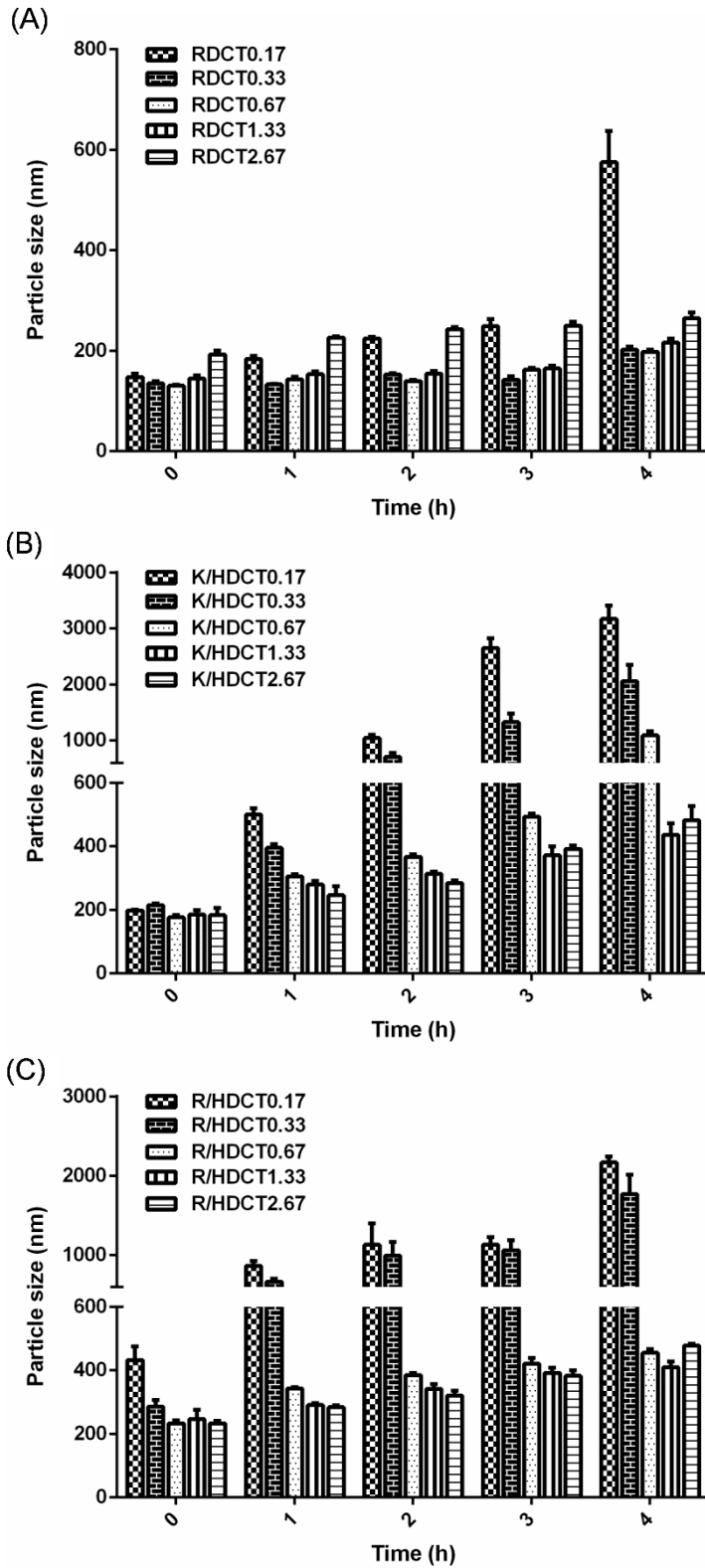
Fig. 4.3. Time-dependent changes in the size of R/DNA (A), K/H/DNA (B) and R/H/DNA (C) coated with or without 0.17, 0.33, 0.67, 1.33 and 2.67 wt% of CS-TGA. Complexes were incubated for 4 h in phosphate buffer saline at pH 7.4 and were analyzed by DLS every hour. Each bar represents the mean ± SD (n ≥ 3).

4.4.2.3. In vitro transfection efficiency

As described in Chapter 3, non-coated R/DNA complexes showed higher gene expression efficiency compared to a commercial transfection agents. Thus, the RD complexes were used here as a positive control instead of the commercial one. The transfection efficiency of PBAE/DNA complexes having different amount of CS-TGA were evaluated in COS-7 cells, using pGFP plasmid DNA, and the gene expression was determined by flow cytometry at 48 h post-transfection as shown in Fig. 4.4. In the case of RDCT complexes, a coating with 0.17 wt% of CS-TGA slightly improved the transfection efficiency while the other RDCT complexes maintained as high efficiency of gene transfer as the control. In the case of the mixtures of PBAEs, surprisingly, K/H and R/H-based complexes exhibited a 2.1- and 2.5-fold increase in transfection efficiency, respectively, compared to the control. In addition, all coated complexes except a coating of 2.67 wt% showed at least a 1.4-fold more effective than the RD complexes. The results showed that the transfection efficiency of the mixture of PBAEs coated with or without CS-TGA is even higher than that of RD complexes with or without coating agents. On the other hand, the transfection efficiency decreased noticeably when K/HD and R/HD complexes were prepared with above 1.33 and 0.67 wt% of CS-TGA, respectively, compared with non-coated K/HD and R/HD complexes. It should be noted that the non-coated complexes showed considerably enhanced stability when started to be prepared with above these amount of CS-TGA. These results are in agreement with the results obtained in Chapter 3. The coating agents may help PBAEs tightly bind to DNA, resulting in decreasing transfection due to the impaired DNA release in the cells. On the other hand, the other coated complexes exhibited sustained or improved transfection efficiency. Interestingly, R/HD complexes with 0.33 wt% of CS-TGA showed superior transfection efficiency among all tested complexes. Moreover, there was observed high stability in physiological conditions for 4 h. Thus, a coating 0.33 wt% of CS-TGA for R/HD complexes was considered to be an optimal formulation among their series. Thus, this formulation of R/HDCT0.33 may be the best candidate for gene delivery systems due to the highest transfection efficiency among all the complexes tested so far. Above all results indicate that transfection efficiency of the complexes is dependent on the amount of CS-TGA. More importantly, these results supported our hypothesis that the coating formulation may allow the synergistic effect of PBAE/DNA and the coating agents.
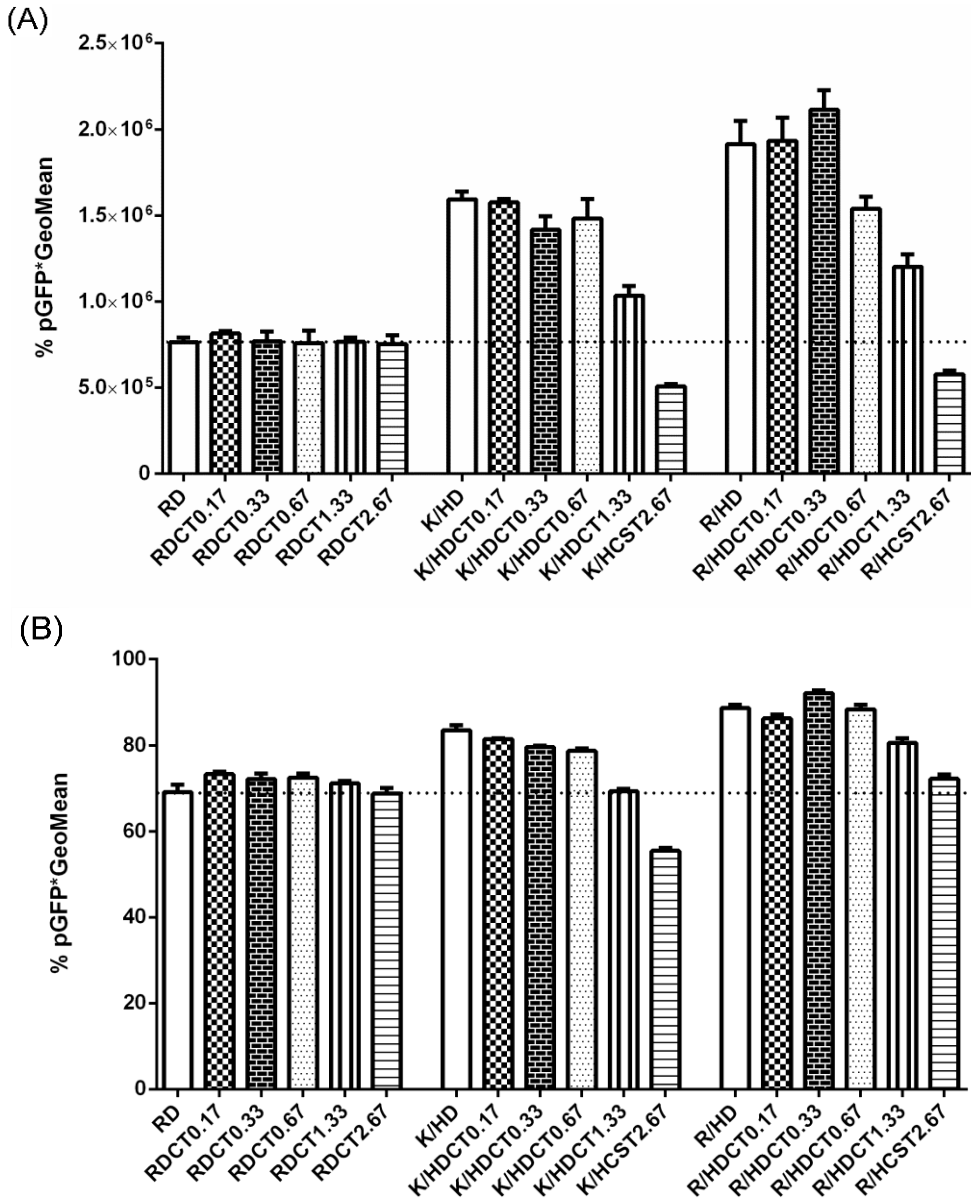
Fig. 4.4. Transfection efficiency of thiolated chitosan-modified PBAE/DNA complexes in COS-7 cells was determined by flow cytometry. (A) Bars represent a percentage of GFP positive cells multiplied by the GeoMean fluorescence of the positive population. (B) GFP expression was determined after 48 h by flow cytometry and bars represent percentage of cells positively transfected and the normalized total gene expression. Each bar presents the mean ± SD (n ≥ 3). NC: negative control (the group without any treatment).

4.4.2.4. Cell viability

To investigate the cytotoxicity of the novel coating carriers, the cell viability was determined by MTS assay. The viability of the cells treated with the non-coated K/HD and R/HD was even lower than the non-coated RD complexes (75%). We previously reported that PBAE bearing histidine termination induced high cell toxicity compared to the other oligopeptide-terminated PBAE polymers (Nat 2014), thus limiting their practical use despite their high transfection efficiency. However, the viability of complexes increased appreciably when prepared with CS-TGA (Fig. 4.5). Indeed, the level of cell viability increased with increasing the amounts of the coating agents. These indicate that a coating of CS-TGA led to reduce cell toxicity. All coating the complexes except K/HDCT0.17 showed over 80% of cell viability. These results support that the PBAE/DNA/CT complexes can be safer carriers.
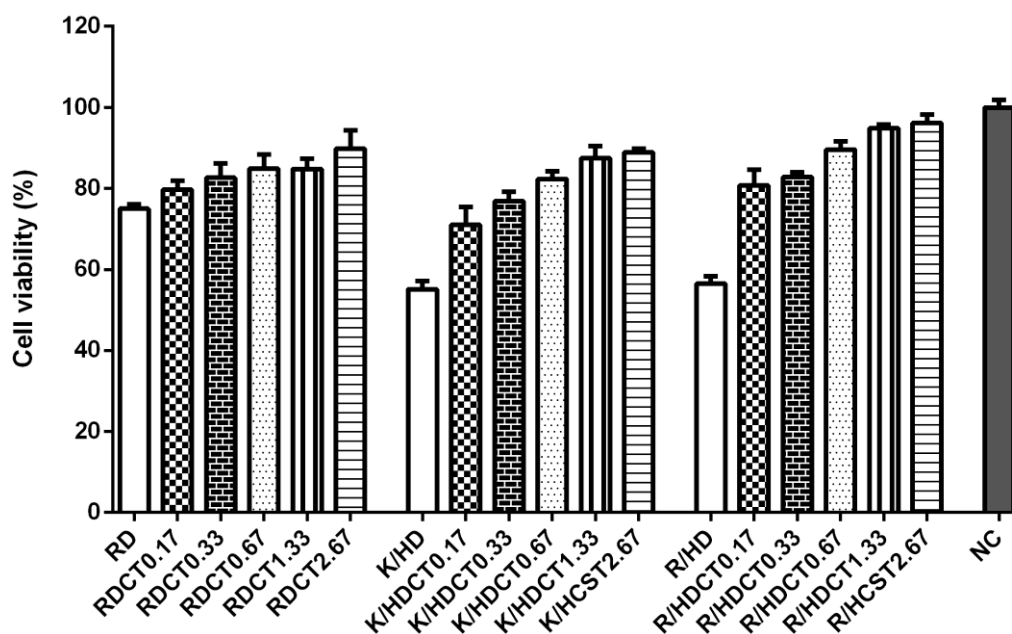

Fig. 4.5. Cell viability of cells after transfection, measured using the MTS assay. Viability was determined at 48 h post-transfection. Bars represent a percentage of viable cells relative to a control of untreated cells (NC). Each bar represents the mean ± SD (n ≥ 3).

4.4.2.5. Particle diffusion studies through mucus

The main aim of this Thesis is to develop the mucosal gene delivery systems capable of crossing the mucus gel layer. Prior to achieve this aim, we have evaluated and studied the physicochemical properties, the gene expression level and the viability of the PBAE/DNA/CS-TGA formulations. The complexes based on the mixture polymers coated with 0.33 and 1.33 wt% of CS-TGA have been chosen for particle diffusion study as they have showed relatively either higher stability or higher transfection efficiency among the particles tested.

In Chapter 2, we have developed the quartz crystal microbalance with dissipation (QCM-D) technique in order to study the interaction of the mucosal delivery systems with the mucin layer. The results supported that the developed QCM-D technique can be used as a simple and effective screening model for the development of efficient mucosal nanocarriers. As stated before, the method has allowed us to choose the different strategies that we are following in this Chapter for designing nanocarriers with high mucus permeation. This permeation behaviour of the nanoparticulate delivery systems developed in this section, the rotating silicon tube technique has been utilized. A diffusion system relating to the depth of particle diffusion through porcine intestinal mucus (PImucus) was studied using the rotating silicon tube. Recently, it was reported that thiolated particles improved particle diffusion rate through PImucus barrier due to the thiol groups (Köllner *et al.,* 2015). As shown in Fig. 4.6, non-coated K/HD and R/HD complexes diffusion through PImucus reached segment of 6 and 7, respectively. These results indicate that complexes without coating agents showed the lowest diffusion rate. In other words, thiolated chitosan coatings could facilitate particle diffusion through mucus. Interestingly, non-coated R/HD complexes were detected higher amount in the segment of 1 and 2 relative to non-coated K/HD despite bigger particle size with similar zeta potential. We may expect that PBAE bearing arginine oligopeptide could help particles transport into mucus although this mechanism has not been defined yet. In the case of K/H-based complexes, K/HDCT0.33 was detected the highest amount between the segment 1 and 4, which correspond to 2-8 mm. On the other hand, 1.33 wt% coating the complexes were detected up to the last segment 10, indicating the highest diffusion rate relative to non-coated K/HD or K/HDCT0.33. In addition, 1.33 wt% of CT was detected the higher amount between the segment 7 and 10, which is equivalent to 14-20 mm, compared to0.33 wt% of CT. This may be due to the stability of the complexes. Both coated complexes had nearly the same particle size and zeta potential, but K/HDCT1.33 showed much higher stability than K/HDCT0.33. Thus, mucus permeability of particles can be enhanced by the formulations which are more compact particles. In the case of complexes based on the mixtures of R/H, there were small changes in particle diffusion through PImucus for the R/HD complexes with or without thiolated chitosan in the first segment. On the other hand, the particle diffusion rate of all R/HD complexes showed a similar trend with K/HD complexes between the segment 2 and10. Although lower amount of R/HDCT complexes between the

segment 3 and 10 were obtained relatively to K/HDCT complexes, all the coating complexes enhanced mucus permeability. It might be expected that thiolated chitosan used as coating agents would lead to facilitate diffusion of the novel formulations through mucus.
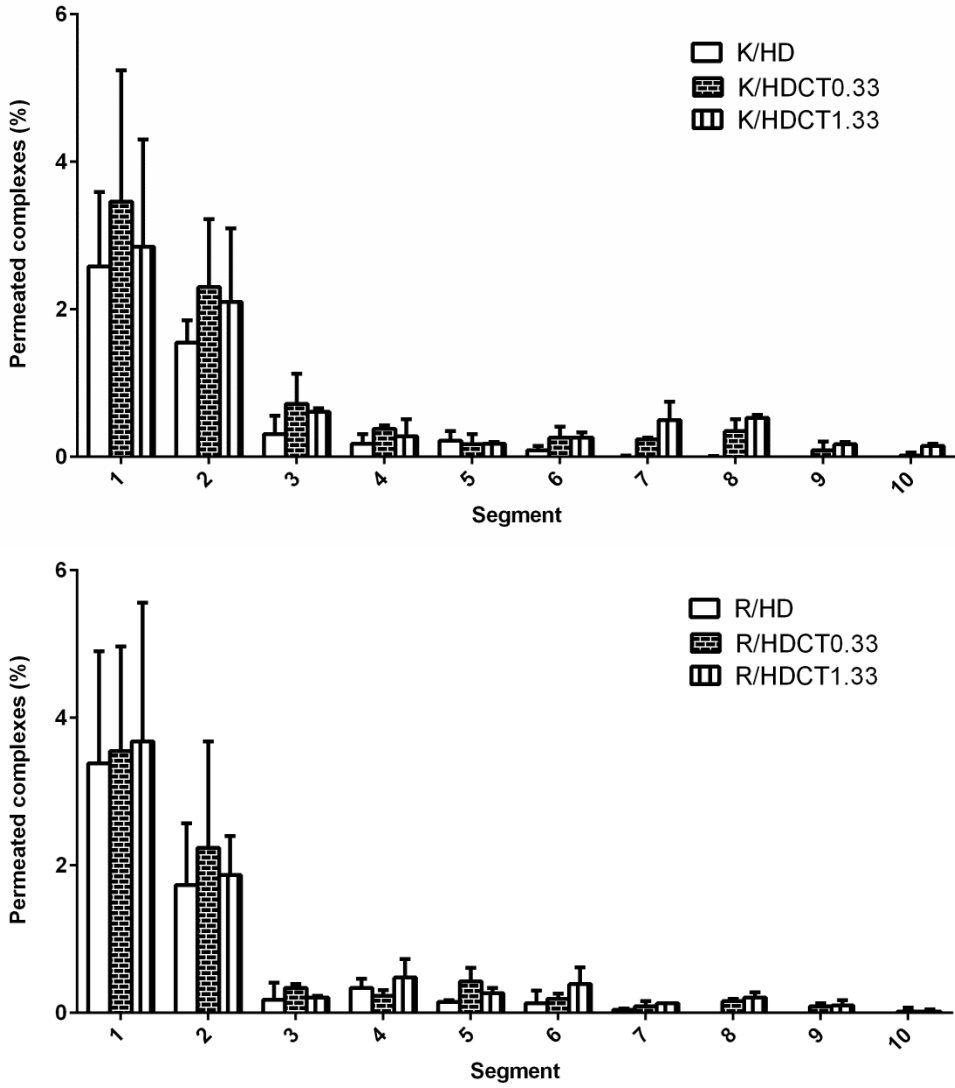

Fig. 4.6. Diffusion studies of Lumogen labeled PBAE/DNA complexes coated without or with thiolated chitosan through PImucus at 37 ºC for 4 h. Each bar represents the mean ± SD (n ≥ 3).

4.4.3. PBAE/DNA complexes coated with PAA-BRO

4.4.3.1. Formulation and characterization of complexes

The second objective of this Chapter was to develop the surface-modified formulation of PBAE/DNA with proteolytic enzyme. As described previously, poly(acrylic acid)-bromelain (PAA-BRO) conjugates were chosen as coating agents since it showed high mucus permeability. In 4.4.3, PBAEs bearing with arginine (R) were firstly chosen among the other oligopeptide-terminated PBAEs such as lysine or Histidine. After pre-screening of this study, it will be attempted to develop the formulations based on the other PBAEs for further investigation.

The condensation ability of PBAE with DNA complexes having 0.17, 0.33, 0.67, and 1.33 wt% of PAA-BRO was evaluated using agarose gel electrophoresis. The binding capability of PBAE towards DNA without PAA-BRO (RD complex) at a weight ratio of 50:1 was evaluated in our previous research (Segovia *et al.*, 2014). As shown in Fig. 4.7, DNA was completely retained at all differing weight ratios. These indicate that the addition of PAA-BRO did not affect the PBAE/DNA complex formation ability.
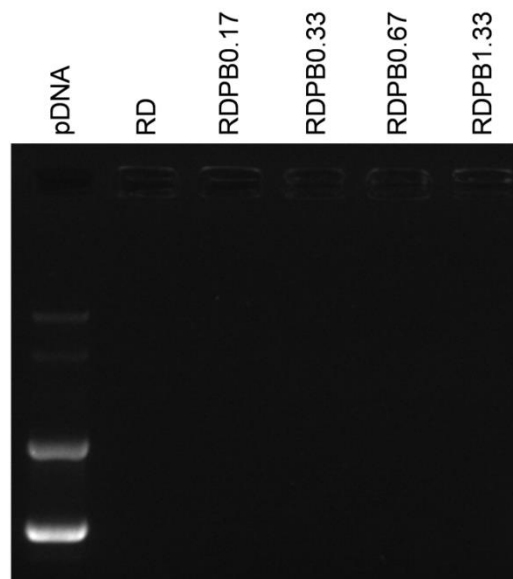

Fig. 4.7. Gel retardation assay of R/DNA coated with CS-TGA. Complexes were formulated by mixing polymers and GFP in a weight ratio of 50:1 and loaded onto an agarose gel containing ethidium bromide to assess DNA mobility by electrophoresis.

Self-assembled PBAE/DNA complexes in the presence/absence of PAA-BRO were simply prepared via electrostatic interaction between the positively charged PBAE/DNA complexes and the negatively charged PAA-BRO in NaAc buffer at pH 5.2. The particle size, polydispersity index and zeta potential of PBAE/DNA complexes with or without a coating of 0.17, 0.33, 0.67, and 1.33 wt% of PAA-BRO in PBS were measured by DLS and the results are presented in Table 4.2. The particle size and zeta potential of non-coated RD complex, analyzed as control, were 143 nm and 20.2 mV, respectively. The RD complex coated with differing amount of PAA-BRO ranged from 121.3 to 318 nm in diameter and from 18.6 to 12.6 mV in zeta potential depending on the weight ratio. These results indicate that a range of the amount of PAA-BRO had a noticeably effect on the particle size and the surface charge of complexes. With an increase in the amount of PAA-BRO among coating the complexes, the size of complexes increased appreciably while zeta potential value decreased considerably. These results suggest that the surface of complexes were completely covered with PAA-BRO. Compared to RD complex, smaller size and lower zeta potential were obtained when modified with both 0.17 and 0.33 wt% of PAA-BRO, resulting in more compact complexes. On the other hand, there was shown a significant increase in size and noticeable decrease in zeta potential with 1.33 wt% of PAA-BRO coating. This might be explained that some of the excessive PAA-BRO might shield onto the surface of complexes via the weak interaction, which would increase the particle size and reduced zeta potential of complexes. The complexes with 0.17 and 0.33 wt% of PAA-BRO was considered to be an optimum formulation due to their small size, and high stability as described below.

Table 4.2 Composition, particle size, polydispersity index (PI), and zeta potential of R/DNA complexes coated with PAA-BRO added in a proportion ranging from 0 to 1.33 wt% of the R polymer. Results are mean ± SD (n ≥ 3).

Formulation	Weight ratio R/DNA/PAA-BRO	Particle size (nm)	PI	Zeta potential (mV)
RD	100/2/0	143.0 ± 5.5	0.140 ± 0.015	20.2 ± 2.5
RDPB0.17	100/2/0.17	121.3 ± 2.0	0.153 ± 0.015	18.6 ± 1.5
RDPB0.33	100/2/0.33	137.9 ± 5.0	0.158 ± 0.010	18.2 ± 2.0
RDPB0.67	100/2/0.67	195.5 ± 13.5	0.169 ± 0.035	17.1 ± 2.5
RDPB1.33	100/2/1.33	318.0 ± 27.5	0.251 ± 0.080	12.6 ± 2.0

4.4.3.2. Stability of PBAE/DNA coated with PAA-BRO

The stability of the novel formulation is one of the main issues in this Thesis. Thus, we studied their stability against particle aggregation in phosphate-buffer saline buffer (PBS) at pH 7.4. Complexes comprising PBAE/DNA in combination with differing amount of PAA-BRO were incubated for 4 h in PBS and analyzed every hour in order to monitor changes in the size of the complexes. The results of RD, RDPB0.17, RDPB0.33, RDPB0.67 and RDPB1.33 are shown in Fig. 4.8. Surprisingly, there was obtained no significant increase in the particle size of RDPB0.17 and RDPB0.33 within 4 h in PBS, while a coating 0.67 and 1.33 depicted an extensive increase in the size every hour. Particularly, the size of RDPB0.17 was shown to be nearly constant over time. These results confirmed that 0.17 wt% of PAA-BRO could be an optimal weight content to sustain the formulation of the complexes. Complexes having 0.67 or 1.33 wt% PAA-BRO were not seen to be particularly resistant to agglomeration. When the PBAE/DNA complexes were not completely covered with the coating materials, these nanoparticles were formulated with loose binders, resulted in the larger size and lower stability than non-coated complexes. Interestingly, the particle size and zeta potential of complexes coated with 0.33 wt% PAA-BRO are similar to those of non-coated complex, but much higher stability in PBS. These results support the stability of complexes is dependent on the coating of PAA-BRO.
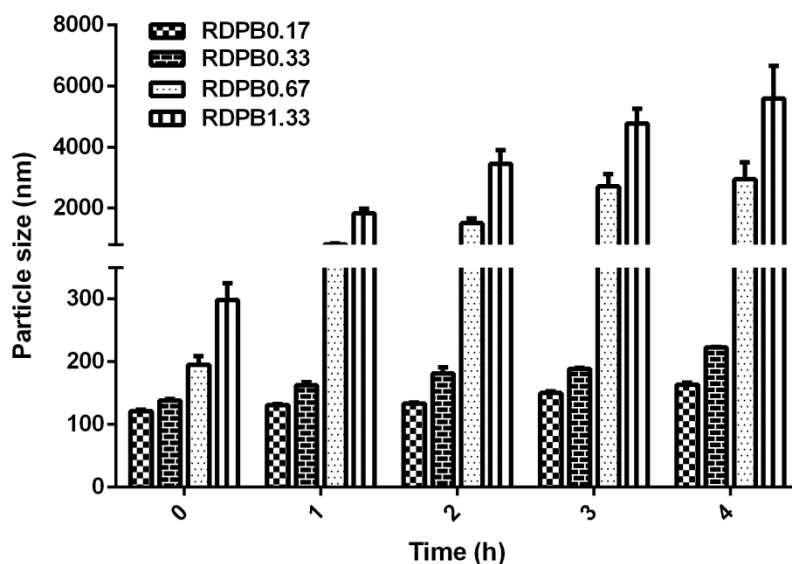

Fig. 4.8. Time-dependent changes in the size of R/DNA coated without or with 0.17, 0.33, 0.67 and 1.33 wt% of PAA-BRO. Complexes were incubated for 4 h in phosphate buffer saline at pH 7.4 and were analyzed by DLS every hour. Each bar represents the mean ± SD (n ≥ 3).

4.4.3.3. In vitro transfection efficiency

We have demonstrated in Chapter 3 that oligopeptide-modified PBAE/DNA complexes formed by mixing PBAEs, especially bearing arginine termination, with plasmid DNA were reported higher gene expression in cell-type-specific manner and better cellular viability compared to the commercial transfection agents. Thus, non-coated RD was used here as a positive control to compare the effect of coating agents on the transfection efficiency. The aim of this section was to maintain high transfection efficiency of complexes bearing mucolytic agent while enhancing the mucus permeability. In order to achieve this objective, the transfection efficiency of PBAE/DNA complexes having differing amount of PAA-BRO were evaluated in COS-7 cells, using pGFP plasmid DNA. The pGFP expression was determined by flow cytometry analysis at 48 h post-transfection. Results of flow cytometry and fluorescence microscopy are illustrated in Fig. 4.9. All complexes with surface coating demonstrated higher transfection efficiency compared to non-coated complex. With 0.17 and 0.33 wt% of PAA-BRO, complexes showed more cells expressing GFP than non-coated control. In particular, a coating with 0.17 wt% of PAA-BRO, which showed the smallest size, the highest stability and mucus permeability among all tested complexes, induced a 1.4-1.5 and 2-fold evaluation in the transfection efficiency compared to other coated complexes and non-coated one, respectively. These results indicate that transfection efficiency is dependent on a specific relative amount of coating agents. This may be considered due to the surface of PBAE/DNA/PAA-BRO complexes exhibiting free thiol groups, which would improve transfection efficiency. These results indicate that coating agents seems to contribute a potential DNA delivery. 0.17 wt% of PAA-BRO was considered to be the optimum weight for coating the PBAE/DNA complexes due to their relatively small size, higher stability, and even higher particle permeability and transfection efficiency compared to those of other coated complexes and non-coated one.

(A)

(B)
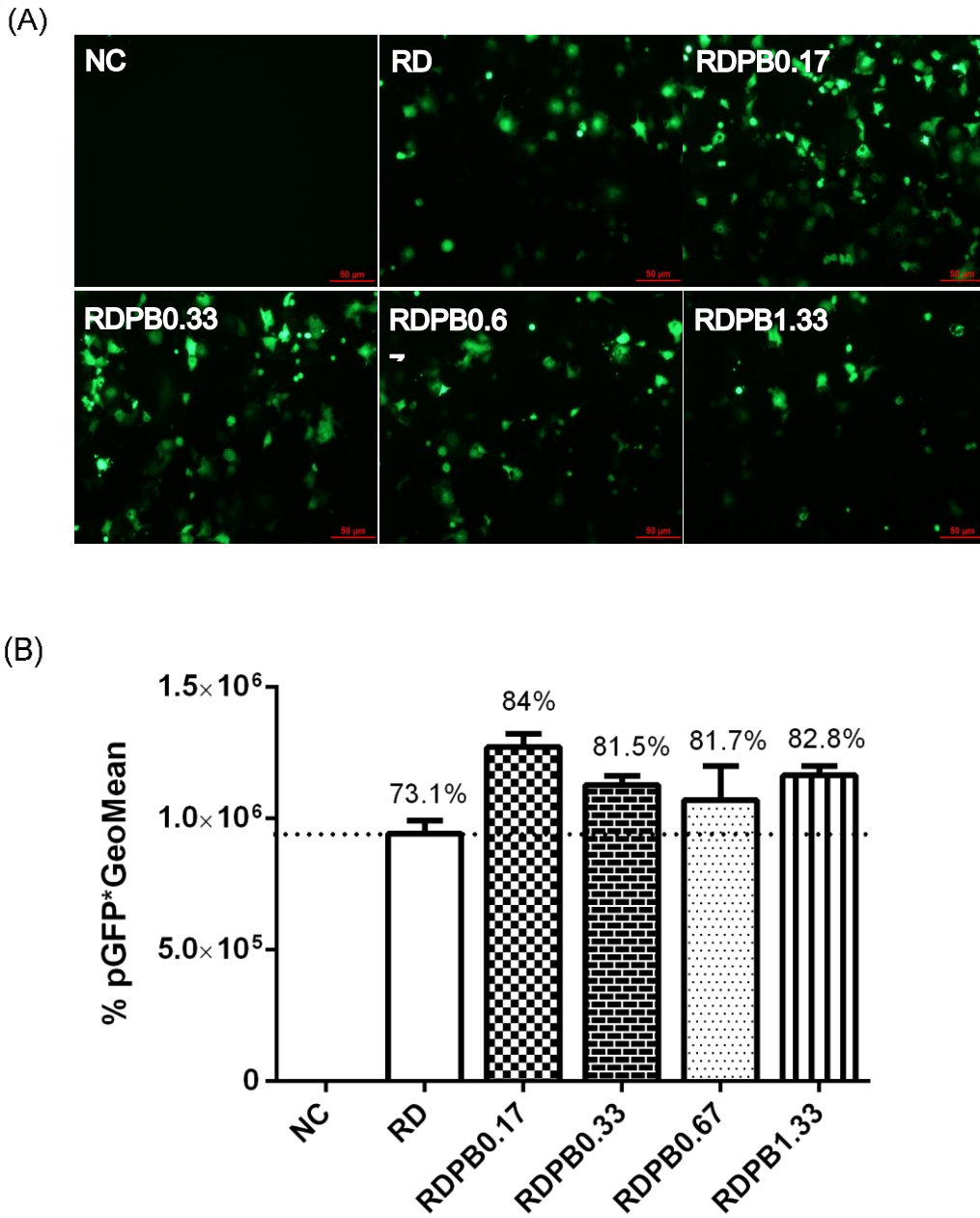
Fig. 4.9. Transfection efficiency of complexes with or without coating agents in COS-7 cells was determined by flow cytometry. (A) Fluorescent images of GFP expression in COS-7 cells at 24 h. (B) Bars represent a percentage of GFP-positive cells multiplied by the GeoMean fluorescence of the positive population at 48 h. Percentage numbers above each bar represent percentage of transfected cell (%). Each bar represents the mean ± SD (n ≥ 3). NC: negative control (the group without any treatment).

4.4.3.4. Cell viability

It has been reported that many cationic delivery vehicles although the polymers are effective at improving DNA delivery and expression, the same mechanism that results in this improvement also causes toxicity (Hunter *et al.*, 2010, Fields *et al.*, 2012, Gu, *et al.*, 2012). However, as described above, we recently reported that oligopeptide-modified PBAE/DNA complexes showed high transfection efficiency with low cytotoxicity. We expected that low amount of coating agents might not influence the cytotoxicity of coating PBAE/DNA complexes. The study was done with PBAE/DNA complexes having differing amount of PAA-BRO used in transfection study and the viability of cells cultured in the media treated with distinct complexes (Fig. 4.10). All the complexes coated with PAA-BRO showed slight decrease in cellular toxicity when compared to non-coated PBAE/DNA complexes. Over 80% average cell viability was observed for all coated complexes. These results indicate that coating the PBAE/DNA/PAA-BRO complexes should be safe carriers.
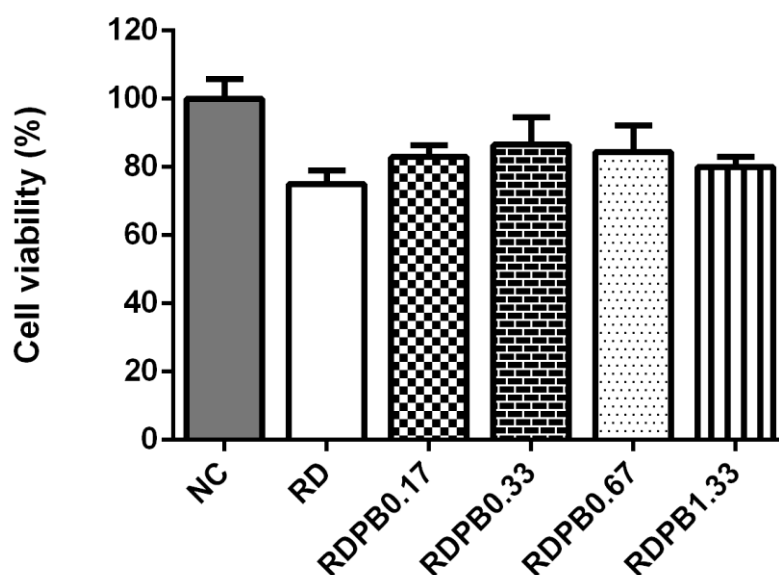

Fig. 4.10. Cell viability of cells after transfection, measured using the MTS assay. Viability was determined at 48 h post-transfection. Bars represent a percentage of viable cells relative to a control of untreated cells (NC). Each bar represents the mean ± SD (n ≥ 3).

4.4.3.5. Particle diffusion studies through mucus

Complexes transported through PImucus were studied using the rotating silicon tube method, which is related to the depth of mucus penetration. It is well known that mucolytic properties of enzyme facilitate particle diffusion through mucus. Thus, the effect of coating the complexes having PAA-BRO ranging from 0.17 to 1.33 wt% on mucus permeation was evaluated using silicon tube and results of complexes transported through PImucus are shown in Fig. 4.9. As control, non-coated RD complexes diffusion through PImucus reached segment of 5, indicative of the lowest diffusion rate. As a result of their lack to cleave mucoglycoprotein substructure, non-coated one stopped their diffusion earlier. Complexes coated with 0.17 and 0.33 wt% of PAA-BRO were detected the highest amount in the segment 1 and 2, respectively.   Moreover, in the both cases, higher diffusion rate and amount were demonstrated compared to other coated complexes and non-coated one. RDPB0.17 and RDPB0.33 complexes were detected up to the last segment 10, which is equivalent to 20 mm, while other tested complexes were not detected in the last few segment of 8-10, which correspond to 16-20 nm. These indicate that the amount of PAA-BRO seems to relate the capability of mucus diffusion. Furthermore, in the case of all coated complexes, these results except a coating of 0.67 wt% support the strong correlation with the stability of complexes. Reason for the lower diffusion rate could be particle aggregation or disassembly, which may lead to stability problem overtime and thus these complexes might be lost their ability of mucolytic properties of enzyme.

As can be seen in Table 4.2, surprisingly, all complexes showed highly positive zeta potential, which could be expected an interaction with negative charge of mucus and get trapped. However, the very small amount of enzyme seems to be sufficient to facilitate particle diffusion through mucus although the complexes showed even highly positive charge when found in a small particle size (≤140 nm). On the other hand, it is interesting to notice that the complexes coated with 0.67 wt% exhibited lower capability to diffuse through mucus compared to 1.33 wt%, which were shown the largest size, lowest zeta potential and stability. It might be expected that zeta potential would lead to particle transport when the particles are not small enough. However, the mechanism of the coating formulation is still remained to further investigate.
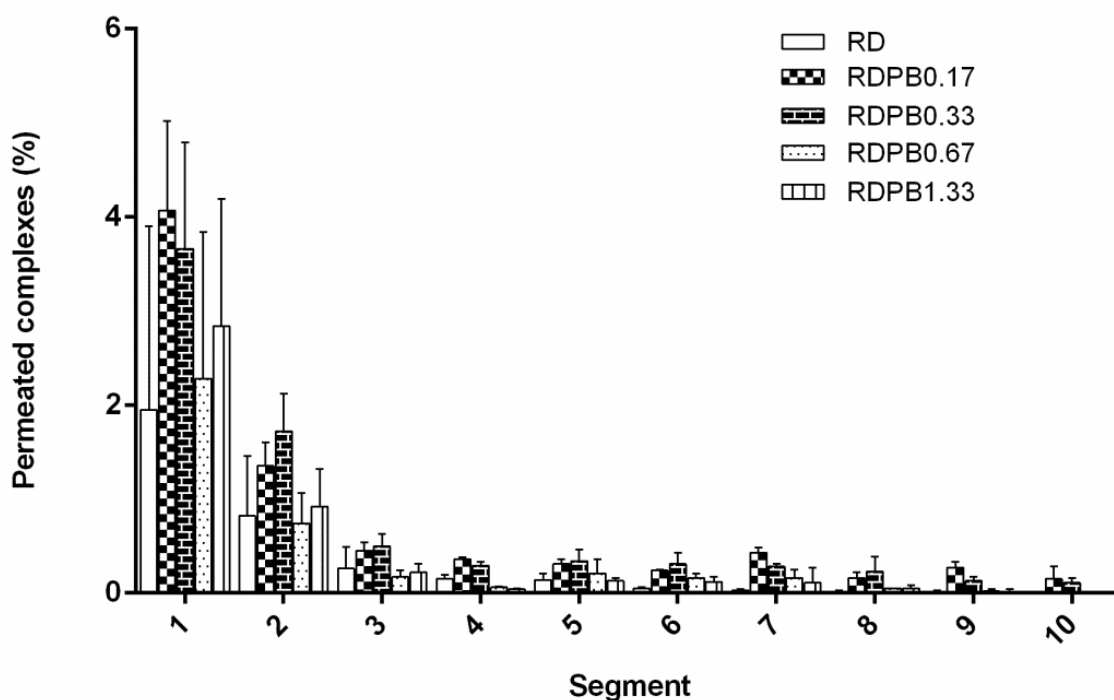
Fig. 4.9. Diffusion studies of Lumogen labeled R/DNA complexes coated without or with PAA-BRO through NPIM at 37 ºC for 4 h. Each bar represents the mean ± SD (n ≥ 3).

4.5.   Concluding remarks

In the first work of this Chapter, we have developed surface-coating complexes formed by simply mixing PBAE/DNA with CS-TGA via electrostatic interaction. These coatings considerably enhanced both stability and cell viability whilst maintaining high transfection efficiency. In addition, especially, thiolated chitosan coating led to facilitated K/HD complexes transport through PImucus. We found that physicochemical properties and mucus permeability of complexes were dependent on the specific amount of coating agents. Regarding the safety concerning of the K/HD and R/HD complexes, which showed much higher transfection efficiency with high cytotoxicity compared to RD complexes, these complexes were formulated with the different weight percent of CS-TGA, resulting in a reduction of toxicity. Most of complexes bearing thiolated chitosan maintained high transfection efficiency with low cytotoxicity.

Thereafter, we have developed surface-coating complexes formed by simply mixing PABE/DNA with PAA-BRO via electrostatic interaction. The platform consists of a non-viral gene carrier created by combining the benefits of PBAE and mucolytic agents. Coated

complexes showed the synergistic effects of PBAEs and PAA-BRO, resulting in enhanced transfection and particle diffusion through mucus. We found that all coating PBAE/DNA complexes exhibited higher particle transport through PImucus and transfection efficiency with better cell viability compared to non-coated complexes. In particular, 0.17 wt% of mucolytic agent was adequate for coating PBAE/DNA complexes, which showed the smallest size and highest stability, to enhance noticeably mucus permeability and gene expression with low cytotoxicity. Thus, these novel surface-modified nanocarriers may be applicable for non-viral gene therapy to mucosal tissue.

4.6.   References

Anderson, D.G.; Akinc, A.; Hossain, N.; Langer, R. *Mol. Ther.* **2005**, *11*, 426-34.

Anitha, A.; Deepa, N.; Chennazhi, K.P.; Nair, S.V.; Tamura, H.; Jayakumar. R. *Carbohydr. Polym.* **2011**, *83*, 66-73.

Bernkop-Schnürch, A.; Brandt, U.M.; Clausen. A.E. *Sci. Pharm.***1999**, *67*, 196–208.

Bernkop-Schnürch, A.; Hornof, M.; Zoidl, T. *Int. J. Pharm.* **2003**, *260*, 229–37.

Bernkop-Schnürch, A.; Hornof, M.; Guggi, D. *Int. J. Pharm.* **2004**, *57*, 9–7.

Bernkop-Schnürch, A. *Adv. Drug Deliv. Rev.* **2005**, *57*,1569–1582.

Borrelli, F.; Capasso, R.; Severino, B.; Fiorino, F.; Aviello, G.; de Rosa, G.; Mazzella, M.; Romano, B.; Fasolino, I.; Izzo, A.A. *Neurogastroenterol. Motil.* **2011**, *23,* 745-e331.

Bravo-Osuna, I.; Vauthier, C.; Farabollini, A.; Palmieri, G.F.; Ponchel, G. *Biomaterials* **2007**, *28,* 2233-2243.

de la Fuente, M.; Csaba, N.; Garcia-Fuentes, M.; Alonso, M.J. *Nanomedicine* 2008, *3*, 845-57.

Dawson, M.; Krauland, E.; Wirtz, D.; Hanes, J. *Biotechnol. Prog.* 2004, *20*, 851-57.

Dosta, P.; Segovia, N.; Cascante, A.; Ramos, V.; Borrós, S. *Acta Biomater.* **2015**. *20*, 82-93.

Elfinger, M.; Pfeifer, C.; Uezguen, S.; Golas, M.M.; Sander, B.; Maucksch, C.; Stark, H.; Aneja, M.K.; Rudolph, C. *Biomacromolecules* **2009**, *10*, 2912-20.

Edelstein, M.L.; Abedi, M.R.; Wixon, J.; Edelstein, R.M. *J. Gene. Med.* **2004**, *6*, 597-602.

O. Felt, P. Buri, R. Gurny, *Drug Dev. Ind. Pharm.***1998,** *24*, 979–993.

Fields, R.J.; Cheng, C.J.; Quijano, E.; Weller, C.; Kristofik, N.; Duong, N.; Hoimes, C.; Egan, M.E.; Saltzman, W.M. *J. Controll. Release* **2012**, 1*64*, 41-8.

Friedl, H.E.; Dunnhaupt, S.; Waldner, C.; Bernkop-Schnurch. A. *Biomaterials* **2013**, *34*, 7811-8.

Fogg, F.J.J.; Hutton, D.A.; Jumel, K.; Pearson, J.P.; Harding, S.E.; Allen, A. *Biochem. J.* **1996**, 316, 937–42.

Guang, W.; Liu, K.; de Yao, *J. Controlled Release* **2002**, *83.* 1–11.

Galindo-Rodriguez, S.A.; Allemann, E.; Fessi, H.; Doelker, E. *Crit. Rev. Ther. Drug Carr. Syst.* **2005**, *22*, 419–64.

Green, J.J.; Shi, J.; Chiu, E.; Leshchiner, E.S.; Langer, R.; Anderson, D.G. *Bioconjug. Chem.* **2006**, 1*7,* 1162-9.

Green, J.J.; Zugates, G.T.; Tedford, N.C.; Huang, Y.H.; Griffith, L.G.; Lauffenburger, D.A.; Sawicki, J.A.; Langer, R.; Anderson, D.G. *Adv. Mater.* **2007**, *19,* 2836-42.

Green, J.J.; Zugates, G.T.; Langer, R.; Anderson, D.G. *Methods Mol. Biol.* **2009**, *480*, 53-63.

Gao, Y.; Xu, Z.; Chen, S.; Gu, W.; Chen, L.; Li, Y. *Int. J. Pharm.* **2008**, *359,* 241-6.

Gu, J.; Wang, X.; Jiang, X.; Chen, Y.; Chen, L.; Fang, X.; Sha, X. *Biomaterials* **2012**, *33*, 644-58.

Harris, T.J.; Green, J.J.; Fung, P.W.; Langer, R.; Anderson, D.G.; Bhatia, S.N.*Biomaterials* **2010**, *31*, 998-1006.

Homaei, A.; Sajedi, R.; Sariri, R.; Seyfzadeh, S.; Stevanato, R. *Amino Acids* **2010**, *38,* 937–942.

Hornof, M. D.; Kast, C.E.; Bernkop-Schnürch, A. *Eur. J. Pharm. Biopharm.* **2003**, *55*, 185–190

Hunter, A.C.; Moghimi, S.M. *Biochim. Biophys. Acta* **2010**, *1797*, 1203–9.

Kafedjiiski, K.; Hoffer, M.; Werle, M.; Bernkop-Schnürch. A. *Biomaterials* **2006**, *27*, 127-35.

Kaparissides, C.; Alexandridou, S.; Kotti, K.; Chaitidou, S. *J. Nanotechnol.* **2006,** *2*, 1-11.

Kast, C.E.; Bernkop-Schnurch. A. *Biomaterials* **2001**, *22*, 2345–52.

Keeney, M.; Ong, S.G.; Padilla, A.; Yao, Z.; Goodman, S.; Wu, J.C.; Yang, F. *ACS Nano* **2013**, *7,* 7241-50.

Köllner, S.; Dünnhaupt, S.; Waldner, C.; Hauptstein, S.; Pereira de Sousa, I.; Bernkop-Schnürch, A. *Eur. J. Pharm. Biopharm.* **2015**, *97*, 265-72.

Kursa, M.; Walker, G.F.; Roessler, V.; Ogris, M.; Roedl, W.; Kircheis, R.; Wagner, E. *Bioconjug. Chem.* **2003**, *14*, 222–31.

Lai, S.K.; Wang, Y.Y.; Hanes, J. *Adv. Drug Deliv. Rev*. **2009**, *61*, 158-71.

Lee, D.; Zhang, W.; Shirley, S.A.; Kong, X.; Hellermann, G.R.; Lockey, R.F.; Mohapatra. S.S. *Pharm. Ref.* **2007**, *24*, 157-67.

Li, C.; Guo, T.; Zhou, D.; Hu, Y.; Zhou, H.; Wang, S.; Chen, J.; Zhang, Z. *J. Controlled Release* **2011**, *154*, 177-188.

Liao, Z.X.; Peng, S.F.; Hong, Y.C.; Mi, F.L.; Maiti, B.; Sung, H.W. *Biomaterials* **2012**, *33*, 3306-15.

Lichen, Y.; Jieying, D.; Chunbai, H.; Liming, C.; Cui, T. *Biomaterials* **2009**, *30,* 5691–5700.

Loretz, B.; Thaler, M.; Schnurch, A.B. *Bioconjug. Chem.* **2007**, *18,* 1028–1035.

Luo, X.; Feng, M.; Pan, S.; Wen, Y.; Zhang, W.; Wu, C. *J. Mater. Sci. Mater. Med.* **2012**, *23,* 1685-95.

Majima, Y.; Inagaki, M.; Hirata, K.; Takeuchi, K.; Morishita, A.; Sakakura, Y. *Arch. Oto.RhinoLaryngol.* **1998**, *244*, 355–359.

Mao, S.; Leong, K. *Adv. Drug Deliv. Rev.* **2010**, *62,* 12-27.

Martien, R.; Loretz, B.; Thaler, M.; Majoob, S.; Bernkop-Schnurch. A. *J. Biomed. Mater. Res. A.* **2007**, *82*, 1-9.

Mastorakos, P.; de Silva, A.L.; Chisholm, J.; Song, E.; Choi, W.K.; Boyle, M.P.; Morales, M.M.; Hanes, J.; Suk, J.S. *Proc. Nati. Acad. Sci. USA.* **2015**, *112*, 8720-5.

Mintzer, M.A.; Simanek, E.E. *Chem. Rev.* **2009**, *109*, 259-302.

Miyata, K.; Gouda, N.; Takemoto, H.; Oba, M.; Lee, Y.; Koyama, H.; Yamasaki, Y.; Itaka, K.; Nishiyama, N.; Kataoka, K. *Biomaterials* **2010**, *31*, 4764-70.

Müller, C.; Leithner, K.; Hauptstein, S.; Hintzen, F.; Salvenmoser, W.; Bernkop-Schnürch, A. *J. Nanopart. Res.* **2013**, *15,* 1–13.

Müller, C.; Perera, G.; König, V.; Bernkop-Schnürch, A. *Eur. J. Pharm. Biopharm.* **2014**, *87*, 125–31.

Lee, K.Y.; Kwon, I.C.; Kim, Y.H.; Jo, W.H.; Jeong, S.Y. *J. Controlled Release* **1998**, *51*, 213–220.

Lee, M.K.; Chun, S.K.; Choi, W.J.; Kim, J.K.; Choi, S.H.; Kim, A.; Oungbho, K.; Park, J.S.; Ahn, W.S.; Kim, C.K. *Biomaterials* **2005**, *26*, 2147–2156.

Luo, X.; Feng, M.; Pan, S.; Wen, Y.; Zhang, W.; Wu, C. *J. Mater. Sci. Mater. Med.* **2012,** *23,* 1685-1695.

Peng, S.F.; Yang, M.J.; Su, C.J.; Chen, H.L.; Lee, P.W.; Wei, M.C.; Sung, H.W. *Biomaterials* **2009**, *30*, 1797-808.

Pereira de Sousa, I.; Cattoz, B.; Wilcox, M.D.; Griffiths, P.C.; Dalgliesh, R.; Roger, S.; Bernkop-Schnürch, A. *Eur. J. Pharm. Biopharm.* **2015,** *97*, 257-64.

Sakloetsakun, D.; Hombach, J.M.R.; Bernkop-Schnürch, A. *Biomaterials* **2009**, *30*, 6151-6157.

Samaridou, E.; Karidi, K.; Pereira de Sousa, I.; Cattoz, B.; Griffiths, P.; Kammona, O. *Nano LIFE* **2014**, *4,* 1441013-1-11.

Schmitz, T.; Bravo-Osuna, I.B.; Vauthier, C.; Ponchel, G.; Loretz, B.; Bernkop-Schnürch, A. *Biomaterials* **2007**, *28*, 524–531.

Segovia, N.; Dosta, P.; Cascante, A.; Ramos, V.; Borrós, S. *Acta Biomaterialia* **2014,** *10,* 2147-58.

Stephenson, J. *J. Am. Med. Assoc.* **2001**, 285, 2864-2570.

Suh, W.; Han, S.O.; Yu, L.; Kim. S.W. *Mol. Ther.* **2002**, *6*, 664–72.

Suh, J.; Dawson, M.; Hanes, J. *Adv. Drug Deliv. Rev.* **2005**, *57*, 63-78.

Yamanaka, Y.; Leong, K. J. *Biomater. Sci. Polym. Ed.* **2008***, 19,* 1549-70.

Zhao, X.; Yin, L.; Ding, J.; Tang, C.; Gu, S.; Yin, C.; Mao. Y.. *J. Control. Release* **2010**, *144*, 46-54.

Zheng, H.; Tang, C.; Yin, C. *Biomaterials* **2015**, *70,* 126-37.

Zugates, G.T.; Peng, W.; Zumbuehl, A.; Jhunjhunwala, S.; Huang, Y.H.; Langer, R.; Sawicki, J.A.; Anderson, D.G. *Mol. Ther.* **2007**, *15*, 1306-12.

Zugates, G.T.; Tedford, N.C.; Zumbuehl, A.; Jhunjhunwala, S.; Kang, C.S.; Griffith, L.G.; Lauffenburger, D.A.; Langer, R.; Sawicki, J.A.; Anderson, D.G. *Bioconjug. Chem.* **2007**, *18*, 1887-96.

GENERAL CONCLUSIONS

➢ A quartz crystal microbalance with dissipation (QCM-D) technique was developed for mucin-relevant investigations, especially mucosal drug delivery systems. As important as this work, in this Thesis, we have developed the novel mucosal nanocarriers of biopharmaceutics that can enhance the stability and transfection efficiency, and facilitate mucus penetration.

➢ For the first time, this technique was used for evaluating the viscoelastic behaviour of the mucoadhesive polymers with native porcine gastric mucin (NPGM) at pH 4, and the results were compared with commercially available porcine gastric mucin (CPGM). We revealed that higher viscosity and shear modulus values were obtained for the NPGM layer, thus selecting NPGM for further studies. In addition, among mucoadhesive polymers tested, thiolated chitosans (TC) showed the highest mucoadhesion.

➢ It was firstly found that the developed QCM-D technique can be evaluated two different properties of mucoadhesion and mucus permeability of polymers or particles. Mucoadhesive thiolated chitosans with low (TCL), medium (TCM) and high (TCH) contents of free thiol groups were assessed mucus permeability properties at pH 4 and 6.8, and TCL showed the highest permeation through the mucin layer, thus chosen for further formulating mucosal nanocarriers. The positively charged TCL can interact the negatively charged both poly(β-amino ester)s (PBAEs) and DNA to form polyelectrolyte complexes (TCD/DNA and TCE/DNA). These particles showed higher mucoadhesion than mucus permeation, indicating that most particles were immobilized onto the NPGM layer, therefore needed to develop the novel formulation.

➢ To better understand how particles interact with the mucin layer using QCM-D, both the calculated data of the changes in thickness, viscosity and shear modulus as well as the monitoring data of the changes in frequency and dissipation were evaluated and studied in order to select the useful nanoparticulate delivery systems. Thus, the developed QCM-D method can be used as a simple and effective screening model for developing efficient mucosal drug delivery systems.

➢ We have developed a surface-modified formulation of DNA delivery systems consisting of biodegradable PBAEs, which recently demonstrated high buffering capacity and transfection efficiency, but required their stability in physiological conditions and mucus penetration. Sugars such as mannitol, sucrose or trehalose, unmodified chitosans with 22

a 22 kDa (CS) or 60-120 kDa (CSM), CS-thioglycolic acid (CS-TGA) conjugates, and poly(acrylic acid)-bromelain (PAA-BRO) conjugates were applied as the additives or coating agents for the novel formulation of mucosal systems of DNA delivery. In all the formulations of PBAE/DNA delivery systems, the physicochemical properties, stability, transfection efficiency, viability and mucus permeability are dependent on the amount of the coating agents. Therefore it is important to find the suitable coating agents and their specific amounts for the novel formulations. All formulations are compared with unmodified PBAE/DNA formulations.

➢ A sugar-modified formulation of PBAE/DNA delivery systems was developed in order to enhance its stability with high transfection efficiency. A sugar coating formulation improved the stability and maintained high transfection efficiency compared with non-coated PBAE/DNA nanocarriers. On the other hand, DNA complexes based on a novel polymer blending of PBAEs and mannitol (MntR) and sucrose (SucR) considerably enhanced stability and gene expression level.

➢ A chitosan-coated formulation of PBAE/DNA delivery systems exhibited noticeably enhanced stability compared to non-coated one. However, CSM seemed to inhibit the release of DNA from its complexes when using COS-7 cells, indicating of low transfection efficiency. On the other hand, CS showed slightly decreased transfection efficiency with increasing the amount of CS. Consequently, CS may be more efficient coating agent for surface-modified formulations compared with CSM. Nevertheless, further an enhancement of transfection efficiency is required for mucosal nanocarriers of DNA delivery.

➢ CS-TGA conjugates were synthesized and applied as coating agents for the PBAE/DNA formulations. All coatings considerably enhanced stability and cell viability whilst maintain high transfection efficiency. In addition, especially, thiolated chitosan coating led to facilitated K/HD and R/HD complexes transport through porcine intestinal mucus (PImucus). Regarding the safety concerns of K/HD and R/HD complexes, which showed much higher transfection efficiency with high cytotoxicity compared to RD complexes, the coating formulations of these formulations exhibited high cell viability. Thus, PBAE/DNA coated with CS-TGA may be useful for mucosal delivery systems of macromolecular drugs.

➢ PAA-BRO conjugates were synthesized, surface-coating complexes formed by simple mixing R/DNA with PAA-BRO via electrostatic interaction. Coated complexes showed the synergistic effects of PBAEs and PAA-BRO, resulting in enhanced transfection and particle diffusion through mucus. All coating PBAE/DNA complexes exhibited higher particle transport through mucus and transfection efficiency with better cell viability compared to non-coated complexes. In particular, 0.17 wt% of mucolytic agent was adequate for coating PBAE/DNA complexes, which showed the smallest size and highest

stability, to enhance noticeably mucus permeability and gene expression with low cytotoxicity. Thus, these novel nanocarriers may be applicable for non-viral gene therapy to mucosal tissue.